Optimizing Total Hip Arthroplasty using Predictive Dynamic Simulation of Human Sit-to-Stand Movement and Deep Learning for Flexible Spinopelvic Model Identification

by

AliAsghar MohammadiNasrabadi

A thesis
presented to the University of Waterloo
in fulfillment of the
thesis requirement for the degree of
Doctor of Philosophy
in
Systems Design Engineering

Waterloo, Ontario, Canada, 2023

© AliAsghar MohammadiNasrabadi 2023

Examining Committee Membership

The following served on the Examining Committee for this thesis. The decision of the Examining Committee is by majority vote.

External Member:	Maxime Raison Professor, Dept. of Mechanical Engineering, Polytechnique Montréal University
Supervisor(s):	John McPhee Professor, Dept. of Systems Design Engineering, University of Waterloo
Internal Member:	Eihab Abdel-Rahman Professor, Dept. of Systems Design Engineering, University of Waterloo
Internal Member:	Bryan Tripp Associate Professor, Dept. of Systems Design Engineering, University of Waterloo
Internal-External Member:	Andrew Laing Associate Professor, Dept. of Kinesiology and Health Sciences, University of Waterloo

Author's Declaration

This thesis consists of material all of which I authored or co-authored: see Statement of Contributions included in the thesis. This is a true copy of the thesis, including any required final revisions, as accepted by my examiners. I understand that my thesis may be made electronically available to the public.

Statement of Contributions

Chapters 2, 3, 4, and 5 include content from three multi-author papers with me as the lead author. My responsibilities encompassed study conceptualization, conducting all models, experiments, simulations, and code development, as well as manuscript preparation and submission. Contributions from my co-authors, including guidance and manuscript feedback from my supervisor Prof. McPhee, and annotation work on 10% of our X-ray dataset (the test dataset) for validation purposes by Dr. Gemah Moammer, Dr. Ahmed Quateen, and Dr. Kunal Bhanot from Grand River Hospital, were instrumental. References for these papers are listed below:

1. **AliAsghar MohammadiNasrabadi**; John McPhee. "Preliminary optimization of cup-implant orientation in total-hip arthroplasty using a parametric predictive analysis of lower-limb dynamics influenced by spine stiffness". *Multibody System Dynamics*, (2023). DOI: 10.1007/s11044-023-09951-3

2. **AliAsghar MohammadiNasrabadi**; John McPhee. "The effects of spine stiffness, spinal fusion, and spinopelvic parameters on lower limb motion and total hip arthroplasty outcomes: A review of clinical and experimental research". Submitted to *the Orthopedic Review Journal*, (2023).

3. **AliAsghar MohammadiNasrabadi**; Gemah Moammer; Ahmed Quateen; Kunal Bhanot; John McPhee. LanDet: "An efficient physics-informed deep learning approach for automatic detection of anatomical landmarks and measurement of spinopelvic alignment". Submitted to *the Journal of Orthopaedic Surgery and Research*, (2023).

Abstract

Recent studies have highlighted the significance of spine stiffness and spinopelvic measures in the analysis of lower limb dynamics during human motion. These factors are essential for optimizing surgical planning, especially in total hip arthroplasty (THA) procedures. Their critical role is particularly evident in individuals who have prior spine fusion surgery undergoing THA. However, the mechanism through which these parameters impact human movement remains to be fully elucidated.

This thesis aims to bridge this knowledge gap by introducing a novel approach to optimizing THA. It involves integrating an innovative deep learning model, LanDet—an anatomical landmark detection algorithm—with a predictive human dynamic model for surgical planning. This integration is crucial in considering the often-neglected aspects of spine stiffness, pelvic tilt, and spinopelvic measures, especially in patients with previous spine fusion surgery. The LanDet model streamlines the extraction of spinopelvic metrics, thus improving the efficiency and accuracy of surgical planning. It also provides essential data to assign suitable stiffness parameters for the predictive simulation model. The predictive model is then utilized to optimize hip cup implant orientation, tailored for each specific spinopelvic condition. This approach ensures a more refined patient categorization system than currently exists, and enables surgeons to optimize hip implant orientation, thereby minimizing the risk of implant impingement and potential dislocation post-surgery.

The first part of the thesis introduces LanDet, explaining its role in enhancing surgical planning efficiency and precision. LanDet not only expedites the extraction of spinopelvic metrics using a physics-informed deep learning model but also supports a refined patient categorization system. It provides necessary data for assigning suitable stiffness parameters in the predictive model, which is critical for individualizing THA procedures. LanDet demonstrates performance improvements and addresses current challenges in anatomical landmark detection, such as the misdetection of adjacent or similar landmarks.

Building on LanDet's capabilities, the second part of the thesis concentrates on optimizing the orientation of the cup implant. This includes an analysis of factors like

spine stiffness and pelvic tilt, vital in evaluating the risk of implant impingement and dislocation after THA surgery. Through two case studies involving motion capture and radiographic analysis, the research illustrates the impact of varying spinopelvic conditions on lower limb motion during daily activities, such as the sit-to-stand movement. A significant achievement of this research is the development of a dynamic human model incorporating detailed spine elements. This research pioneers the use of predictive dynamic modeling in this context, refining cup implant orientation by considering patient-specific spinopelvic conditions. It establishes a direct correlation between spine stiffness, pelvic tilt, and the risk of implant impingement, providing guidance and insights for surgeons in pre-operative planning.

In summary, this research introduces an end-to-end approach to optimize THA surgery outcomes, which can be extended to investigate the impact of diverse pathological conditions, not addressed in this specific research, on optimized implant positioning. This can advance THA and other surgical procedures, contributing to increased patient satisfaction and delivering possible time and cost savings to healthcare systems.

Acknowledgements

My heartfelt thanks go to Prof. **John McPhee**, my advisor, for his exceptional guidance, patience, and generosity during my PhD journey. His steadfast support, prompt and eager provision of resources and expertise, significantly contributed to navigating complex challenges. Prof. McPhee's deep knowledge and insightful advice have been instrumental, and I am profoundly grateful for his guidance. His endless patience and absence of frustration, even in times of my shortcomings, have been remarkable. It is an honor to be his student, and I cherish the opportunity to have been under his guidance.

I am deeply indebted to my parents, **Naser** and **Fatemeh**, for their endless love and support in every stage of my life and academic endeavors. Their unwavering encouragement and faith in my capabilities have been the backbone of my achievements. They selflessly prioritized my education, providing all necessary resources for my excellence. I also extend heartfelt thanks to my sister, **Fahimeh**, for her encouragement in my pursuit of a PhD and her enduring kindness and support throughout my life.

I also extend my gratitude to my peers and friends at the Motion Research Group (the **MoRG**). Their collective knowledge and fellowship have immensely supported me.

Lastly, I express my deepest love and profound appreciation to my wife, **Zohreh**, for her unwavering support, countless sacrifices, and relentless encouragement. Her influence has been a cornerstone of the success I have achieved throughout my PhD journey. Her boundless love and resilience have left an indelible mark on both my life and my academic pursuits.

Dedication

In gratitude to those whose dedication and enduring sacrifices have been the wind beneath my wings.

Table of Contents

Examining Committee ii

Author's Declaration iii

Statement of Contributions iv

Abstract v

Acknowledgements vii

Dedication viii

List of Figures xiv

List of Tables xx

1 Introduction 1

1.1 Spine, Pelvis, and Hip Relationship and Measures 1

1.2 Total Hip Arthroplasty (THA) and Spine Stiffness 3

1.3 Automatic Extraction of Spinopelvic Measures and Patient Categorization 5
1.4 Research Overview 6
1.5 Thesis Outline 8

2 Background **11**

2.1 Chapter Overview 11
2.2 Automatic Extraction of Anatomical Landmarks 12
2.2.1 Deep Learning Approaches 13
2.2.2 Key-point Detection Methods 14
2.2.3 Object Detection 16
2.2.4 Discussion 19
2.3 Clinical Studies on the Effects of Different Spine Geometries and Stiffnesses on Lower Limb Motion 20
2.3.1 Introduction 20
2.3.2 The Importance of Spinopelvic Measures and Considering Hip and Spine Relationship 22
2.3.3 Patient Categorization towards Patient-specific THA Surgery . 25
2.3.4 Spine Stiffness and Fusion Surgery 29
2.3.5 Summary and Discussion 31
2.4 Musculoskeletal Modeling and Simulation of Human Motion 40
2.4.1 Approaches to Spine Modeling 41
2.4.2 Predictive Human Musculoskeletal Simulations 46
2.4.3 Sit-to-Stand Motion Simulations 48

2.4.4 Hip Biomechanics and Impingement Analysis 49
2.4.5 Conclusion 52

3 Automatic Extraction of Anatomical Landmarks using Deep Learning Approaches and Patient Categorization Based on Spinal Conditions 54

3.1 Chapter Overview 54
3.2 Introduction 55
3.3 Materials and Methods 56
3.3.1 Spinopelvic Geometric Measurements 56
3.3.2 Detection Using Landmarks as Constraint Objects 58
3.3.3 Dataset and Data Preparation 60
3.3.4 Model Architecture 61
3.3.5 Experiments 66
3.3.6 Model Performance and Evaluation Metrics 67
3.4 Results and Discussion 68
3.4.1 Model Performance and Accuracy of Automated Measurements 69
3.4.2 Model Reliability and Level of Agreement Between the Model and Surgeons 75
3.4.3 Limitations and Advantages 77
3.5 Conclusion 78

4 Motion Capture Experiment and Radiographic Analysis **81**

4.1 Chapter Overview . . . 81

4.2 Case-Study Experiments: Motion Capture and Radiographic Analyses of Human Sit-to-stand Movement . . . 82

4.2.1 Radiographic Analysis . . . 83

4.2.2 Motion Capture Analysis . . . 88

4.2.3 Different Spinopelvic Motions . . . 88

4.3 Discussion and Conclusion . . . 93

5 Predictive Human Model of Sit-to-Stand Motion Influenced by Spine Stiffness to Optimize Cup Implant Orientation in THA **96**

5.1 Chapter Overview . . . 96

5.2 Introduction . . . 97

5.3 Method . . . 101

5.3.1 Overview . . . 101

5.3.2 Biomechanical Modeling of a Functional Spine Unit Considering Non-linear Passive Spine Elements . . . 102

5.3.3 Multibody Dynamics Human Skeletal Model . . . 106

5.3.4 Optimization and Predictive Simulation . . . 108

5.3.5 Effects of Different Spinal Conditions . . . 110

5.3.6 The Effect of Anterior and Posterior Pelvic Tilt . . . 111

5.3.7 Impingement Analysis and Implant Positioning Optimization . . . 114

5.4 Results and Discussion . . . 117

5.4.1 Validation of Lumbar Spine Functional Unit and Predictive Dynamic Model . . . 117
5.4.2 Prior Spine Fusion Surgery and the Risk of Hip Dislocation in a THA Surgery . . . 119
5.4.3 Impingement Analysis Results: Is The "Lewinnek safe zone" Really Safe? . . . 122
5.4.4 Cup Implant Orientation Optimization . . . 123
5.4.5 Anterior and Posterior Pelvic Tilt and Optimal Implant Placement 130
5.5 Conclusion . . . 133

6 Conclusion **136**

6.1 Summary of Contributions . . . 139
6.2 Limitations of Current Study and Future Work Recommendations . . . 142

References **145**

APPENDICES **190**

A Motion Capture Experiment Data Processing **191**

A.1 Calibration . . . 191
A.2 Standard Coordinate Systems . . . 193
A.2.1 Local Coordinate System Equations . . . 193
A.2.2 Intersegmental Angles . . . 195

List of Figures

1.1 Main pelvis and spine measures 2

1.2 Replacing damaged hip joint with implant in a THA surgery 4

1.3 Thesis workflow 7

2.1 U-Net architecture 16

2.2 Comparison of fundamental deep learning-based object detection model designs 18

2.3 Classification of spine and acetabulum according to mobility definition 26

2.4 Classification of hip-spine according to spinal alignment and mobility whereas ΔSS is defined as the change in SS slope from standing to sitting position 29

2.5 A break down on the reported spinopelvic metrics and spinal fusion factors that cause spine stiffness in the literature 38

3.1 Main spinopelvic measures in lateral X-ray images, considering both femoral heads to calculate the center of rotation for the pelvis 57

3.2 A: Manual labeling of landmarks and specifying bounding boxes. B: Extracted landmarks as objects with different confidences, trained model output, evaluated with the test set. C: choosing the highest confidence for each landmark as the prediction results and calculation of the spinopelvic measures 59

3.3 ***LanDet*** utilizes a dense detection network denoted as DN that is trained with the multi-task loss $LanDet_{loss}$. The purpose of this network is to transform an input image represented by I into a collection of output grids denoted as $\hat{G}$. These grids contain the predicted landmark objects represented by $\hat{O}_l$. To obtain candidate detections, a technique called non-maximum suppression (NMS) is employed for $\hat{O}_l$. The geometrical constraints are applied on these candidate detections to generate the final predictions for $\hat{O}_l$, which then be used to calculate desired measures. 62

3.4 Comparison of model performance: ***LanDet*** model with physics-informed constraint versus landmarks as objects model (before constraint) for two datasets. Additionally, the figure presents the performance of the ***LanDet*** model on the combined dataset, allowing for a comparison of its performance on each dataset. 71

3.5 ICC metric results for the evaluation of model reliability by comparing the extracted results from the model with manual annotation by three surgeons (Reviewer1: senior spine surgeon, Reviewer2: senior neurosurgeon, and Reviewer3: senior orthopedic surgeon). 76

3.6 Challenging cases successfully addressed by the model in the datasets: A) Partially cut-off images, B) Images with obstacles in the hip region, C) Images from patients with hip implants, D) Images from patients with spinal implants. 77

3.7 The advantage of applying physics-informed constraints, which improved the accuracy of localization of some similar and adjacent landmarks. The superior posterior corner of S1 is not detected before applying constraints, P1 (without constraints), which is solved by LanDet that incorporate geometrical constraints (P1 LanDet). Also, a mis-detection of L5 superior posterior (P2 without constraint) instead of S1 superior posterior is resolved by LanDet (P2 LanDet). 79

4.1 Spinopelvic measures changing between standing (left) and sitting (right) postures for patient with no prior fusion surgery. The pelvis is tilted effectively, with a change of 15 ° ($\Delta PT = 15°$), and the spine has contributed to the motion with a change in LL ($\Delta LL = 25°$). . . 84

4.2 Spinopelvic measures changing between standing (left) and sitting (right) postures for a patient with prior fusion surgery. Because of the stiffer spine ($\Delta LL = 9°$), the pelvis has lost the ability to tilt through a large angle ($\Delta PT = 3°$), increasing the patient's risk of dislocation after THA. 86

4.3 Data distribution and patient categorization 87

4.4 A comparison of spinopelvic measures for the category of stationary pelvis and all patients. The box and whisker plots indicate the mean, minimum, maximum, lower quartile, and upper quartile of the data. . 87

4.5 Marker placement on the subject 89

4.6 Joint angle results from the motion capture experiment, with dashed lines representing mean values and shaded areas denoting standard deviation across trials. 90

4.7 Motion capture experiment results: A comparison between hip joint angle, pelvic tilt, and lumbar lordosis changes during motion for two subjects with different spinal stiffnesses. 92

5.1 The framework of evaluating the effect of different spine conditions on lower limb motion and obtaining optimal cup orientation to avoid implant impingement after THA. 101

5.2 Lumbar spine functional unit with the pelvis and connecting nonlinear ligaments and IVDs 103

5.3 Definition of joint angles in the model. Five DoF is considered for the lumbar spine (γ_{L5}, γ_{L4}, γ_{L3},γ_{L2},γ_{L1}), two for the thoracic spine (γ_{T12}, γ_{T6}), and three for lower body (γ_{hip}, γ_{knee}, γ_{ankle}). 107

5.4 Definitions of neutral (left), anterior (center), and posterior (right) pelvic tilt conditions. 113

5.5 The simulation model (center), including detailed spine model (left) and AID impingement definition (right). 115

5.6 Radiographic anteversion (β_{Ant}) and inclination (β_{Inc}). The International Society of Biomechanics (ISB) standard is used to define the pelvis local coordinate frame 116

5.7 Validation of the predictive model using the results from motion capture experiment for subject 2. 119

5.8 A comparison of the predictive model results for the normal, stiff, and fused spine in different levels. 121

5.9 Comparison of predictive model motion results for the spine and pelvis in normal (solid shape and lines) and stiff-fused (worst-case scenario, anatomically stiff spine along with a long fusion including S1-L5-L4-L2) (transparent shape and dashed lines) conditions during two phases of sit-to-stand motion: A) Lift-off phase, B) Standing phase. 122

5.10 Impingement analysis results evaluating Lewinnek safe zone for the predicted motion of healthy (A) and stiff spine (B) subjects. The 3D contour graph (left) shows all possible combinations of anteversion and inclination angles and calculated AID values during the motion. To provide a better insight, some instances of motion are shown as 2D contour graphs (right). The lower the values of AID, the more risk of impingement ($AID = 0$ means the impingement occurred). While healthy spines (graphs above the line) have no close-to-zero AID values, the stiff spine subject (bottom) has some zero or sub-zero values ($t = 0.6s$) indicating a potential moment of impingement. . . . 124

5.11 Impingement analysis for healthy and fused spine subjects, showing that AID could be less than zero for a fused spine subject (impingement occurred), at critical values for inclination and anteversion that are within the Lewinnek safe zone. 125

5.12 Implant impingement analysis for A: recommended values of β_{Inc} and β_{Ant} in the literature for normal spine subjects and B: optimized values for each spinal condition to avoid impingement; the more distance the trajectories have from the solid circular impingement area (higher AID values), the safer patients are from implant impingement. 127

5.13 A new categorization of patients who are possible candidates to be preoperatively monitored using predictive simulation for an optimal cup anteversion positioning; **N**: normal stiffness and mobility, **S**: stiff spine, which has three sub-groups: $\mathbf{S_A}$: spine stiffness due to aging or anatomical parameters (i.e. $\Delta SS < 10$), $\mathbf{S_{F1}}$: one or two levels of lumbar spine fusion, and $\mathbf{S_{F3}}$: three or more levels of lumbar spine fusion. In the spine fusion condition, the sacrum engagement affects the results. 128

5.14 AID trajectories for a normal spine (not stiff or fused) with anterior or posterior pelvic tilt conditions. The left polar figure illustrates scenarios where identical orientation values are applied, treating each case as a healthy subject. The right graph displays AID trajectories using the optimized cup implant orientation. 131

5.15 AID trajectories for a fused spine (S1-L5-L4) with anterior or posterior pelvic tilt conditions. The left polar figure illustrates scenarios where identical orientation values are applied, treating each case as a healthy subject. The right graph displays AID trajectories using the optimized cup implant orientation. 133

List of Tables

2.1 Overview of clinical research on spinal stiffness 32

3.1 The comparison of mean values of manual measurements (MA) and automatically predicted measures (PR) 70

3.2 Comparison of LanDet Model Estimation Errors with Literature Reports 72

3.3 ***LanDet*** model results (PR) for the combined dataset compared to MA 74

4.1 Spinopelvic measures and their changes from standing to sitting position for patients with prior fusion surgery 85

4.2 Volunteer participant information 89

4.3 Anatomical marker placement 90

5.1 Ligament insertion points 103

5.2 Parameter values describing nonlinear behavior of ligaments and IVDs 104

5.3 Anthropometric data for participant 2. 108

5.4 Parameter values describing nonlinear behavior of ligaments and IVDs (Eq.5.2 and Eq.5.5) for stiff spine 112

5.5 Validation of the functional spine dynamic model using in-vitro experiment performing different loading condition and comparing resulting range of motion (ROM) between the model and literature 118

5.6 RMS error for each joint angle for subject 2 119

5.7 Implant Parameters Used in Simulation Studies 126

5.8 Comparison of the optimized (model) cup anteversion values for different spinopelvic mobility and stiffness compared to 1 year post-operative evaluation in the literature (lit). The results of fusions with (S1✓) and without (S1×) sacrum involvement are presented. 129

5.9 Comparison of clinically recommended implant placement orientation values with optimal values from our predictive model. Upward ↑ (increase) and downward ↓ (decrease) arrows indicate the necessary adjustments in implant orientation compared to a healthy condition without anterior or posterior pelvic tilt. 131

5.10 Clinically recommended values versus optimal values from predictive model for cases with spinal fusion (S1-L5-L4) and anterior/posterior pelvic tilt. Upward ↑ (increase) and downward ↓ (decrease) arrows indicate the necessary adjustments in implant orientation compared to a healthy condition without anterior or posterior pelvic tilt. 132

Chapter 1

Introduction

1.1 Spine, Pelvis, and Hip Relationship and Measures

There are several measures in the spine and pelvis by which the shape and function of the spine-pelvic complex is defined [1, 2, 3]. The Main pelvic measures are Acetabulum Anteversion (AA), Pelvic Incidence (PI), Pelvic Tilt or Pelvic Version (PT or PV) and Sacrum Slope or Sacrum Tilt (SS or ST). These measures are shown in Figure 1.1.

Acetabulum Anteversion (AA), in the radiographic definition [4], is defined as the angle between acetabular axis and coronal plane, which is sometimes called planar anteversion. Pelvic Incidence (PI) is a morphologic parameter defined as the angle between the perpendicular line ($\hat{n}$) to the upper end plate of last vertebra of the sacrum (S1) at the mid-point (Q), and the connecting line of this point to the center (C) of femoral head [3]. This parameter is strictly related to the shape of the pelvis

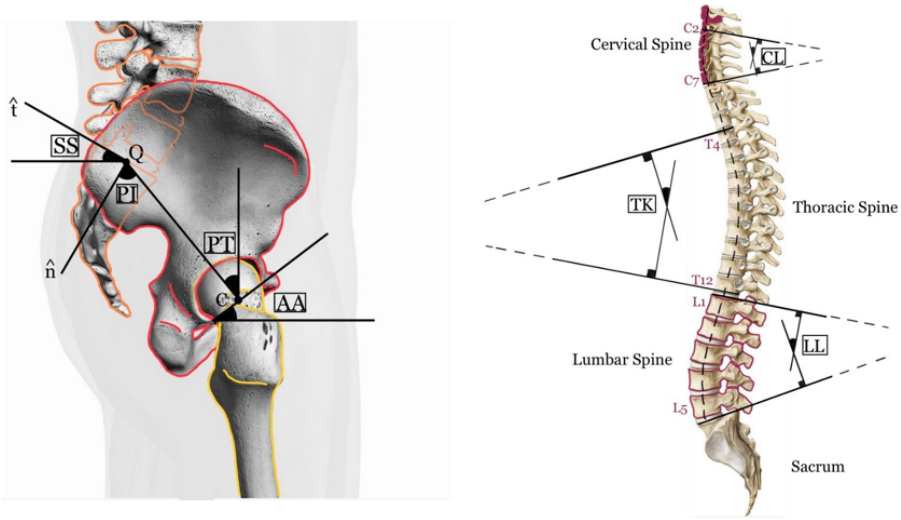


Figure 1.1: Main pelvis and spine measures

[5]. This parameter remains constant in each pelvic posture and it is equal to the sum of two measures (PT and SS) [6]. Pelvic tilt or pelvic version (PT or PV) is the angle between the vertical reference line and the connecting line between Q and C. Sacrum Slope (SS) is the angle between the tangent ($\hat{t}$) to the upper end plate of S1 and the horizontal reference line. The normal ranges for PT and SS are $13° \pm 6°$ and $42° \pm 8.5°$, respectively [7, 8]. More detailed information on the normal values for the pelvic measures in standing and sitting positions are discussed by Ike et al. [9]. Researchers have delved into the impact of spinopelvic measures on total hip arthroplasty, exploring various aspects of the spinopelvic relationship [6, 10, 11, 12, 13, 14, 9]. Lumbar Lordosis (LL), Thoracic Kyphosis (TK) and Cervical Lordosis (CL) are the main measures of the spine. LL is the angle between the tangent to the lower plate of L5 and upper plate of L1. Thoracic Kyphosis (TK) indicates the curvature of the thoracic part of the spine and is defined as the angle between the tangent to the lower plate of T12 and upper plate of T4 [15]. Cervical Lordosis (CL)

represents the cervical curvature and is defined as the angle between the tangent to the lower plate of C7 and upper plate of C2.

1.2 Total Hip Arthroplasty (THA) and Spine Stiffness

Total Hip Arthroplasty (THA) is a surgical procedure employed to excise damaged portions of the hip joint. This anatomical structure, often likened to a "ball and socket" joint, comprises the femoral head (or an artificial stem) as the ball and the pelvic cavity (or an artificial cup) as the socket (Figure 1.2). During THA, the femoral head and the spherical pelvic bone cavity are excised and substituted with artificial implants. The global prevalence of THA is estimated at 87 cases per 100,000 individuals and is projected to increase by 40% by 2030 [16]. In Canada, there were approximately 59,000 hip replacements conducted during the 2016–2018 period. A comparative analysis of reports from 2016 and 2018 revealed a notable 17.4% increase in hip replacement surgeries. It has been reported that 8.2% of patients who had THA surgery, requiring revisions to address issues like complete dislocations hip dislocation (occurs when the femur's head is displaced from the cup), leg length disparities, and implant loosening [17, 18].

It has been reported that patients with fixed spinopelvic alignment (i.e., in whom less PT change occurs when they move from standing to sitting posture) are at higher risk of dislocation [19]. Some researchers have clinically studied the effects of spinal fusion and disorders on the risks of hip impingement (contact between the femoral neck and the cup) and dislocation [10, 20] using medical imaging before and after the surgery. Considering patient-specific spinopelvic mobility, which is thought to

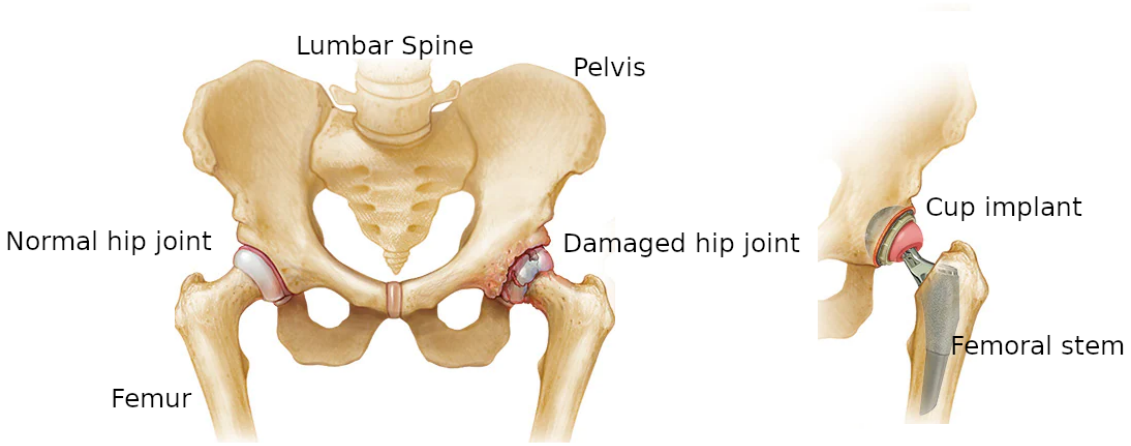


Figure 1.2: Replacing damaged hip joint with implant in a THA surgery

be because of different spine anatomy and stiffness [21], helps surgeons identify the optimal cup positioning and orientation during the surgery. The contribution of the spine in postural changes during certain motions depends on the stiffness of the spine, and can affect spinopelvic motion if stiffness or deformity are present [13]. In combination, reduced spinal flexion, decreased pelvic tilt range, and more hip flexion when moving from standing to sitting positions increase a patient's risk of hip dislocation after THA surgery [22]. It can be assumed that this relationship affects the success of the surgery, but the exact mechanisms involved and their influence on an operation's outcome have not yet been clarified [6], motivating this research on the effects of spinal geometry, kinematics, and stiffness on spinopelvic motion. The stiffness of the spine is influenced by a range of factors, including anatomical characteristics, spinopelvic measures, age-related changes, and the effects of spinal fusion surgery. In Chapter 2, we conduct a review on each of these factors to gain an understanding of how they collectively impact spine stiffness and, ultimately, the outcome of THA procedures.

One of the primary contributing factors to hip dislocation occurs when there is contact between the femoral neck and the cup, a condition known as impingement [23]. This contact can result in the femur being levered out of the cup. Currently, there is a notable dearth of mechanistic models within the existing literature that explain the intricate relationship between implant positioning, design parameters, patient-specific characteristics, and impingement during the dynamic motions encountered in daily activities. Proper cup positioning and orientation are critical factors in reducing the risk of impingement or hip dislocation during THA surgery [24]. Traditionally, the widely-accepted standard for cup orientation has been the Lewinnek safe zone [25]. However, recent research has cast doubt on the efficacy of this metric in predicting hip dislocation risk. Additional factors, such as pelvic tilt (PT) and spine flexibility, which are not considered by the Lewinnek guidelines, have been shown to influence the likelihood of hip dislocation [13, 26, 27, 21]. However, there is an absence of detailed mechanistic models in the literature to explore the factors mentioned above. Therefore, there is a need for such research to investigate the impact of subject-specific factors like spinopelvic measures or spinal stiffness on lower limb motion. Such studies can shed light on whether incorporating these considerations into THA surgery planning can effectively mitigate the risk of impingement or dislocation post-surgery.

1.3 Automatic Extraction of Spinopelvic Measures and Patient Categorization

To achieve the optimal results in THA surgery, surgeons should take into account a patient's unique characteristics and the stiffness of their spine. Researchers in clinical practice have taken this into consideration by classifying patients according

to their spinopelvic measures and spine stiffness levels. For each category, they have suggested tailored surgical strategies [13, 14, 22]. Surgeons use spinopelvic measures for preoperative evaluation and diagnosis of spinal and pelvic malalignment disorders. For the analyses, they prefer to use X-ray images, which impose lower doses of radiation than CT-scans, taken in standing position to reflect true alignment under the effect of the physiological axial loads on the spine. The most important measures to be evaluated are the Sacral Slope (SS), Pelvic Tilt (PT), Pelvic Incidence (PI), Lumbar Lordosis (LL), and Sagittal Vertical Axis (SVA). Certain anatomical landmarks are used to extract these measures from lateral X-ray images. Manual annotation of these landmarks is time-consuming and the accuracy of this process is dependent on the annotator and image quality. To improve consistency, there has been a growing interest in automatic approaches that extract these measures. Deep Learning (DL) techniques have achieved the highest levels of accuracy in landmark prediction so far [28]. The prevailing approach for landmark detection in recent studies, known as heatmap-based regression [29, 30, 31], comes with certain inherent limitations. In this thesis research, we introduced LanDet, a novel deep learning model that detects landmarks as objects and incorporates anatomical constraints directly into the model, enhancing its accuracy and efficiency."

1.4 Research Overview

As discussed in Section 1.2, a gap exists between clinical investigations and engineering approaches, particularly mechanistic models, in the pursuit of optimizing THA surgical outcomes. This motivates us to integrate engineering techniques into THA pre-operative planning to enhance and optimize its overall outcome. To gain a deeper

understanding of the influence of various spinal conditions on lower limb motion, a literature review along with two case-study experiments were conducted. These encompassed a motion capture study involving sit-to-stand motion, as well as a pre-operative radiographic analysis utilizing X-ray images of patients in both sitting and standing postures. This comparison of spinopelvic measures was crucial in elucidating the necessity for a dynamic human model in achieving optimal surgical planning.

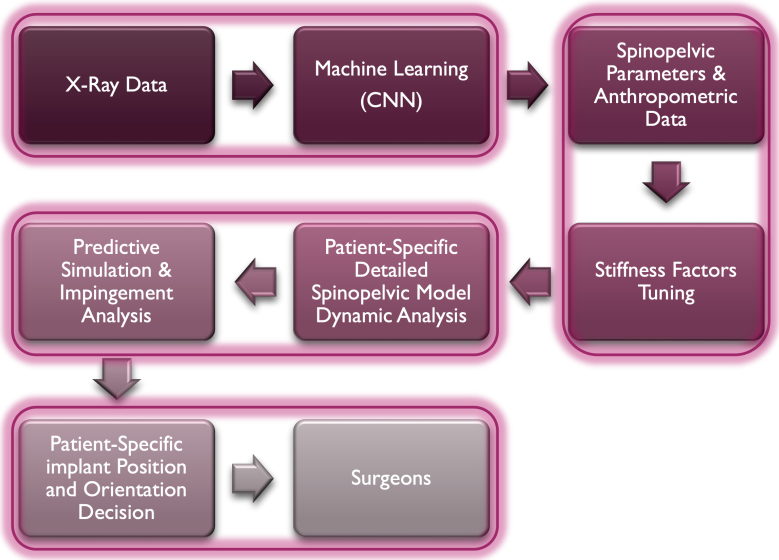


Figure 1.3: Thesis workflow

The primary goal of this research is to introduce an end-to-end approach for optimizing THA surgery, taking into account the influence of spine stiffness and spinopelvic measures to address potential surgical challenges (Figure 1.3). This is particularly crucial in scenarios where surgeons may not fully consider the impact of subject-specific factors such as spine stiffness, pelvic tilt, and spinopelvic measures. To achieve this, two key steps are involved. Firstly, we employ a deep learning approach to overcome the complexities associated with automatically extracting spinopelvic measures and utilizing them for patient categorization. Subsequently, a

subject-specific multibody dynamic musculoskeletal human model, complete with intricate spinal elements, will be constructed. This model will enable a detailed investigation into how spine stiffness affects lower limb motion and, notably, the outcomes of THA surgery. Furthermore, we utilize predictive simulations utilizing this dynamic model with the aim of determining the optimal implant configuration that minimizes the risk of dislocation following THA.

The outcomes of this study are expected to have a significant positive impact on THA surgical planning, ultimately reducing the risks of hip impingement or dislocation post-THA. These improvements are likely to enhance patient satisfaction and minimize post-surgical complications. Moreover, the anticipated positive outcomes are expected to translate into time and cost savings within healthcare systems.

1.5 Thesis Outline

Chapter 2 offers a detailed literature review, organized into three sections. In Section 2.2, the current state-of-the-art in automatic extraction of spinopelvic measures is discussed, along with associated challenges and potential avenues for improvement. Section 2.3 provides an overview of clinical studies examining the impact of spine stiffness, spinopelvic measures, and spinal fusion on THA surgery. This section discusses the disparity between clinical observations and the engineering techniques required to bridge this gap. Finally, Section 2.4 delves into a review of the literature concerning spinal modeling approaches, predictive musculoskeletal simulations, specifically focusing on sit-to-stand motion, as well as hip biomechanics and computational models aimed at optimizing implant positioning.

Chapter 3 introduces a novel physics-informed deep learning methodology devel-

oped for extracting anatomical landmarks crucial for computing essential spinopelvic measures, pivotal in patient categorization. This approach leverages anatomical constraints, treating landmarks as objects, to enhance the accuracy of the landmark detection algorithm. Additionally, within this chapter, a novel single-stage landmark detection method is introduced, named ***LanDet***. This approach is founded on the aforementioned innovative principles and serves the dual purpose of eliminating the requirement for computationally-intensive heatmaps while simultaneously enhancing the accuracy of landmark detection through the incorporation of anatomical constraints. Categorizing patients based on spinopelvic measures is essential for fine-tuning spine stiffness parameters in the predictive dynamic simulation, a topic that will be elaborated on in the later chapters.

Chapter 4 delves into two case-study experiments designed to provide an understanding of how various spinal conditions impact hip movements. The initial experiment involves a motion capture study, where subjects engage in a sit-to-stand motion, enabling the capture of joint angles. The second experiment entails a radiographic analysis utilizing X-ray images from patients considering THA surgery. This analysis entails a comparison between the traditional method, which focuses solely on spinopelvic measures in standing and sitting postures, and an approach incorporating a continuous trajectory of joint angles and measures. This chapter emphasizes the significance of dynamic motion analysis as opposed to relying solely on stationary X-ray imagery (i.e., worst position for dislocation is neither sitting nor standing, but in between the 2). This pivotal shift sets the stage for Chapter 5, where we delve into how a predictive simulation can address various "what if" scenarios.

Chapter 5 addresses a previously-mentioned gap in the literature regarding implant positioning recommendations for patients seeking THA with a history of spinal fusion

or stiff spine conditions. To address this, we employ a novel predictive simulation approach, developing a multibody human model with detailed spinal elements, including nonlinear ligaments and Intervertebral Discs (IDs). This model is utilized to assess the influence of spine stiffness on lower limb dynamics, specifically emphasizing the sit-to-stand motion. We consider diverse spinal conditions, including instances of stiff or fused spines across various levels of lumbar vertebrae. In each patient-specific scenario, we ascertain the optimal cup implant orientation by using the Angular Impingement Distance (AID) metric, precisely measuring the proximity to potential implant impingement. This pioneering and fully predictive simulation approach marks a significant milestone, as it enables us, for the first time, to mathematically recommend cup implant orientations customized to each patient's specific spinal condition. This tailored approach can effectively minimize the risk of implant impingement following THA.

Chapter 6 serves as the concluding section of this thesis, offering a summary of the research endeavors and the significant contributions made in the area of automatic anatomical landmark detection and predictive human motion simulation. It also addresses limitations and provides recommendations for potential future work. Additionally, this chapter explores avenues for refining musculoskeletal modeling and predictive simulations, aiming to improve implant placement in future studies.

Chapter 2

Background

2.1 Chapter Overview

In this chapter we focus on providing a literature review, structured into three main sections according to the objectives of this thesis research. In Section 2.2, it delves into the most current advancements in the automatic extraction of spinopelvic metrics. This section also highlights the challenges associated with this process and proposes potential avenues for enhancement. Moving on to Section 2.3, a thorough examination of clinical studies investigating the effects of spine stiffness, spinopelvic metrics, and spinal fusion on THA surgery is provided. The objective here is to clarify the existing gap between clinical observations and the engineering methodologies needed to bridge it. Finally, Section 2.4 scrutinizes the literature pertaining to spinal modeling approaches, predictive musculoskeletal simulations with a specific focus on sit-to-stand motion, hip biomechanics, and computational models designed to optimize implant positioning.

2.2 Automatic Extraction of Anatomical Landmarks

The assessment and prediction of the geometric characteristics of the spinopelvic complex have garnered significant interest among both the clinical and research communities [32, 33, 34]. Radiological examination of the spine and pelvis plays a crucial role in both surgical and non-surgical treatments of spinal disorders [35]. Understanding the sagittal balance of the spine and pelvis, which entails the interplay between spine and pelvic measures, is crucial for maintaining postural equilibrium. Initially, measurements of sagittal balance were conducted manually using conventional radiographs and later assisted by computer-based tools [30]. However, the inherent limitations of radiographic imaging and subjectivity in manual measurements introduced errors [36].

To address these challenges, machine learning techniques, a subset of artificial intelligence (AI), were employed, allowing computer models to recognize patterns in data [37]. With the advancement of deep learning (DL), a specialized branch of machine learning that emulates the information processing of neural systems, performance in automated image analysis significantly improved. DL methods excel in learning optimal features and feature compositions without human-designed feature extraction. Consequently, DL has found extensive application in various domains, including radiology, musculoskeletal radiology, and spinal disorders [32].

The concept of sagittal spinopelvic balance has gained widespread recognition among radiologists and spine professionals, as it is essential for understanding the etiopathogenesis of spinal deformities and selecting appropriate treatment options [30]. Evaluating sagittal balance typically involves radiographic measurements of geometric

relationships among specific anatomical landmarks in sagittal X-ray images. Measures such as Sacral Slope (SS), Pelvic Tilt (PT), Pelvic Incidence (PI), Lumbar Lordosis (LL), and Sagittal Vertical Axis (SVA) are commonly used to assess sagittal balance [38]. However, manual measurements can be subjective, time-consuming, and prone to inaccuracies due to the complexity of accurately identifying anatomical landmarks. To overcome these challenges, various computer-assisted tools and software have been developed, but they still rely on observer input [39].

2.2.1 Deep Learning Approaches

Recent advancements in artificial intelligence and deep learning techniques have provided promising avenues for automating the process of extracting anatomical measures from radiographic images of the spine [40]. These technologies offer the potential to enhance efficiency, reduce the burden on healthcare professionals, and improve the accuracy of measurements [41]. Additionally, they enable the analysis of a wide range of clinical scenarios, including sagittal and coronal deformities, degenerative phenomena, and images acquired with varying fields of view [40].

Machine learning approaches also have been utilized to classify the severity of spinal disorders in a radiation-free method [42]. In this context, several studies have proposed innovative methods leveraging machine learning algorithms to automate the measurement of spinal alignment parameters without using images. Samadi et al. developed machine learning algorithms to classify the spinal disorders and the Cobb angle in adolescents with idiopathic scoliosis based on the lumbosacral joint (L5-S1) efforts during gait as the input data [42, 43].

Other innovative approaches encompass techniques ranging from fully convolu-

tional neural networks with differentiable spatial to numerical layers (DSNT) to fine-tuned Mask R-CNN models for vertebral segmentation [40, 28]. The results of these studies have shown promising outcomes, with accurate predictions of vertebral locations and sagittal alignment parameters, despite inherent challenges and limitations [31, 28].

While these automated methods demonstrate significant potential, it is essential to critically assess their performance and address the associated challenges. These include potential variations in image quality, noise, and the presence of different spinal pathologies [31, 28]. Moreover, it is imperative to evaluate the reliability and reproducibility of automated measurements in comparison to manual assessments performed by experienced clinicians [30].

Heatmap-based regression, the most common method used for landmark detection in recent studies [29, 30, 31, 44], has some inherent drawbacks including issues with overlapping heatmap signals and post-processing requirements.

2.2.2 Key-point Detection Methods

To assess sagittal spinopelvic measures, two primary methods are generally employed. The first approach involves landmark detection [45, 39, 30, 40, 46, 47, 29, 31, 48, 44], often complemented by preliminary structure detection, followed by direct geometric measurements using the identified landmarks. The second approach utilizes structure segmentation [49, 41, 50, 51, 52], followed by landmark and/or inclination detection from the segmented structures. Some studies have also reported measurements based on shape model matching or direct feature embedding [53, 47]. While recent solutions tend to combine both approaches, earlier studies mostly relied on landmark

detection alone. Notably, convolutional neural networks (CNNs) were frequently used, where input images underwent convolutional and pooling layers for feature extraction and fully connected layers for feature classification [54]. However, the trend is now shifting towards segmentation with CNNs, incorporating encoder-decoder architectures. Consequently, landmarks are often transformed into segmentable heatmaps using various techniques, including Gaussian or exponential functions [29, 31, 44], spinal curvature constraints [55], or the differentiable spatial to numerical transform (DSNT) in combination with network architectures like a fully convolutional network (FCN) [40, 56], cascaded pyramid network (CPN) [31], or dense neural network (DenseNet) [28]. A recent approach involves initial structure segmentation followed by vertebral endplate and/or landmark identification [32].

The U-Net architecture, known for its "U"-shaped layer arrangement (Figure 2.1), has gained popularity due to its skip connections, enabling the preservation of fine image details through skip connections from early to late layers. This allows for the retention of small-scale features that might otherwise be lost, while still capturing large-scale features [32]. The U-Net architecture [30, 49, 57, 58, 44], along with its variations like the Residual U-Net (ResUNet) [29], Multi-Dilated Recurrent Residual U-Net (MDR2-UNet) [59], and Stacked Hourglass Network (SHN) [55] has been widely utilized in deep learning applications. These models have proven effective in tasks like spine segmentation, demonstrating adaptability to limited training data and maintaining class balance. They have been employed for both structure segmentation and landmark detection. Other deep learning architectures have been used for sagittal spinopelvic parameter measurement, including region-based CNN (R-CNN) [41] for landmark detection, RetinaNet [30], residual neural network (ResNet) [56], and bidirectional feature pyramid network (BiFPN) [44] for structure detection, mask

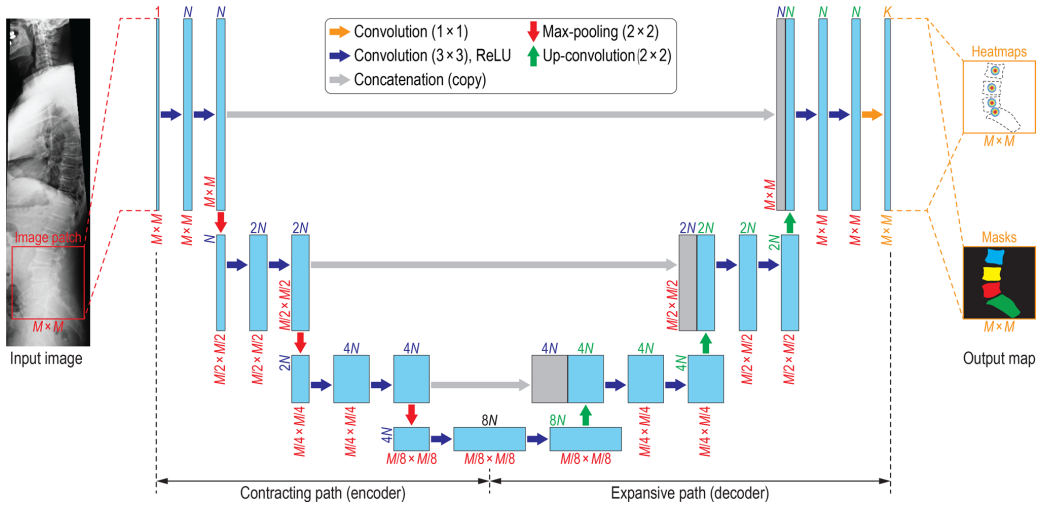


Figure 2.1: U-Net architecture [32]

R-CNN [41] for structure segmentation, and cascaded amplifier regression network (CARN) [53] for direct feature embedding. Some architectures have benefited from the implementation of the Wing or focal loss functions, as well as multi-view feature fusion in anteroposterior and lateral X-rays [48]. Notably, structure segmentation has primarily been applied to either cervical or lumbar X-ray images, suggesting that current state-of-the-art DL architectures may still have room for improvement in whole spine image analysis [32].

2.2.3 Object Detection

Object Detection involves identifying objects in images and categorizing them by estimating bounding boxes around them. There's significant overlap between object detection and anatomical landmark detection, as body segments and keypoints can be treated as objects. This approach has been previously used for the purpose of human pose estimation while using object detectors for body part detection, and modern

approaches have extended this to keypoint detection [60]. Traditional methods before deep learning involved sliding windows and extracting features like HOG [61], SIFT [62], or Haar-like features [63, 64], classified using SVMs [65] or AdaBoost [66]. Deep learning-based approaches, utilizing CNNs, have largely replaced traditional methods.

These deep learning-based object detection methods can be categorized into single-stage and two-stage algorithms. Single-stage detectors perform both object localization and classification simultaneously across a dense grid, exemplified by detectors like YOLO [67], SSD [68], and RetinaNet [69]. Two-stage detectors, popularized by R-CNN family networks (e.g., R-CNN [70], Fast R-CNN [71], Faster R-CNN [72]), first generate a sparse set of candidate object locations (region proposals) and then classify them. Figure 2.2 illustrates the architectural components in modern CNN-based object detectors, depicting single-stage and two-stage models. The architecture typically includes a backbone CNN feature extractor (e.g., VGG [73], ResNet [74], MobileNetV2 [75]), a "neck" that integrates feature maps, and a network head for dense or sparse prediction. Single-stage detectors provide bounding box and class predictions for all locations in multi-scale output grids. In contrast, two-stage detectors extract a sparse set of region proposals and classify them in a separate stage [76].

The two-stage algorithms, including R-CNN, Fast R-CNN, and Faster R-CNN, initiate with region proposals generated by selective search. They use features extracted by networks like AlexNet [77] and employ classifiers and bounding box regression to refine object localization. Although these methods showed improvement in performance, they had drawbacks such as fixed input size and separate component training. Fast R-CNN combined feature extraction and classification, achieving both speed and accuracy. Ren et al. [72] integrated region proposals using a Region

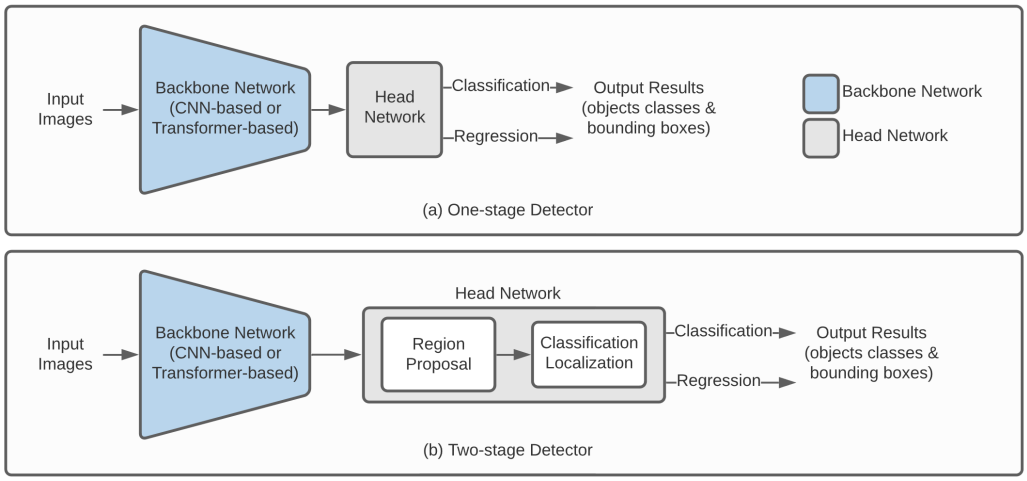


Figure 2.2: Comparison of fundamental deep learning-based object detection model designs: Single-stage versus dual-stage architectures. The foundational network may be either a convolutional neural network (CNN) or a transformer-based network, and its classification depends on whether the head network is structured as a one-stage or two-stage model. In (a), the one-stage detector accomplishes object localization and classification concurrently within the head network. Conversely, for the two-stage detector, localization and classification occur after region proposals have been generated, as illustrated in (b). [76]

Proposal Network (RPN), significantly enhancing speed. This led to Faster R-CNN [72], which was considerably faster than its predecessors. Several improvements followed, including fully-convolutional classification (R-FCN) [78], feature pyramid networks (FPN) [79], Cascade R-CNN [80], and Libra R-CNN [81], addressing various challenges in training and detection.

One-stage algorithms, like YOLO [67], SSD [68], and RetinaNet [69], perform both classification and regression over a dense grid. YOLO, for instance, directly converts feature maps to a dense output grid, associating each cell with objectness, class probabilities, and bounding box estimates. This approach provides a commendable balance between speed and accuracy. SSD, inspired by YOLO, introduced anchor

boxes and adjustments to better match object shapes. It also utilized multi-scale output grids, achieving similar speed as YOLO but with higher accuracy.

YOLOv2 [67] refined the anchor box strategy using k-means clustering and incorporated other techniques, further enhancing performance. Despite outperforming SSD on some metrics, it exhibited less precise bounding box localization. The introduction of RetinaNet, utilizing Focal Loss to address class imbalance, revolutionized single-stage detectors. This dense detector surpassed the accuracy of existing two-stage detectors while maintaining the speed of single-stage detectors. Recent iterations of YOLO have also achieved high accuracy without using Focal Loss, indicating their inherent robustness. Although single-stage human pose estimation methods have the potential to be faster than two-stage methods, current state-of-the-art single-stage estimators struggle with the processing of large heatmaps [82], impacting their speed.

2.2.4 Discussion

When considering the choice between object detection using a one-stage algorithm like YOLO and keypoint detection for anatomical landmark detection, several compelling reasons favor the utilization of the one-stage approach. One of the primary advantages lies in its efficiency. YOLO and similar one-stage detectors perform both classification and regression over a dense grid, enabling real-time processing of images. This speed is crucial in applications where prompt feedback or continuous monitoring of anatomical landmarks is essential, such as in medical interventions or sports analysis.

Further more, one-stage detectors eliminate the need for complex post-processing steps that are often required in keypoint detection methods. Keypoint detection involves additional processing to identify and localize specific points of interest,

which can introduce computational overhead. In contrast, the direct object detection approach of YOLO streamlines the process and reduces the computational burden.

In summary, the adoption of a one-stage object detection algorithm, such as YOLO, for anatomical landmark detection offers a compelling solution characterized by its speed, simplicity, and efficiency. These attributes make it particularly well-suited for applications where real-time processing and accurate identification of landmarks are paramount. While keypoint detection approaches have their merits, the one-stage object detection methodology stands out as an effective and efficient choice for this specific task. Further details on our application of this approach for anatomical landmark detection and the automatic extraction of spinopelvic measures will be discussed in Chapter 3.

2.3 Clinical Studies on the Effects of Different Spine Geometries and Stiffnesses on Lower Limb Motion

2.3.1 Introduction

Analyzing the spine's role in lower limb motion may initially seem labor-intensive for seemingly marginal gains. However, the surge in patient complaints post-Total Hip Arthroplasty (THA) surgeries [18], sepcially from patients who have had prior spinal surgery [21], underscores the significance of incorporating spinal dynamics into the lower limb motion analysis. While the widely-adopted Lewinnek safe zone [25] sets the standard for cup orientation, recent studies have revealed its limited

correlation with the risk of hip dislocation [13, 26, 27]. This risk, it turns out, is also influenced by factors like pelvic tilt (PT) and spine flexibility—variables overlooked by the Lewinnek guidelines. This chapter delves into clinical research exploring the impact of the spine on lower limb motion. By doing so, we aim to gain insight into whether accounting for these effects in THA surgery planning can mitigate the risk of impingement or dislocation post-operation.

Patients with a fixed spinopelvic alignment, characterized by minimal pelvic tilt variation when transitioning from standing to sitting, face an increased risk of dislocation. Researchers have conducted thorough investigations into the effects of spinal fusion and associated disorders on hip impingement and dislocation risks, utilizing both pre- and post-surgery imaging techniques [20, 10]. Considering individual spinopelvic mobility, influenced by spinal anatomy and rigidity, provides crucial guidance for surgeons in determining the optimal cup positioning and orientation during surgery. The spine's influence on postural shifts during specific movements is contingent on its rigidity, potentially impacting spinopelvic motion in cases of stiffness or deformity. Reduced spinal flexion, alterations in pelvic tilt patterns, and increased hip flexion during position changes all amplify the risk of hip dislocation after THA surgery. While this relationship likely plays a pivotal role in surgical outcomes, the exact mechanisms and their impact on results remain a subject of ongoing investigation [6]. This underscores the need for research with an engineering perspective, focusing on spinal geometry, kinematics, and stiffness in spinopelvic motion.

To bridge the gap between clinical findings and potential engineering solutions, we conducted a review of pertinent research concerning spinopelvic measures, spine stiffness, spinal fusion surgery, and their impacts on lower limb motion and THA

outcomes. Our review encompassed three primary categories. Spinopelvic measures play a pivotal role as key factors in patient categorization. Section 2.3.2 provides an overview of studies in this category, emphasizing their significance. Moreover, understanding the interplay between various spinopelvic types and their effects on lower limb dynamics is crucial. Consequently, Section 2.3.3 explores studies focused on delineating the hip-spine relationship and establishing patient-specific surgery planning protocols.

The spine serves a crucial function in maintaining alignment and stability within the spinopelvic complex. Increased spine stiffness, often attributed to factors like fusion surgery, aging, and inherent anatomical variations [10, 9], can significantly alter the behavior of this complex and subsequently impact lower limb motion. This alteration in spine stiffness can, in turn, influence pelvic tilt, thereby affecting hip range of motion and impeding everyday activities such as sit-to-stand motion. These combined factors heighten the risk of post-surgery impingement or dislocation. Consequently, Section 2.3.4 presents our final review, which delves into studies assessing the effects of spine stiffness or fusion surgery.

All the studies we reviewed are summarized in Table 2.1, providing details on study criteria, methodologies, and the most noteworthy research findings.

2.3.2 The Importance of Spinopelvic Measures and Considering Hip and Spine Relationship

In this section, clinical investigations will be reviewed to gain understanding of their findings on any relationship between spinopelvic measures and different spinopelvic motions. Although hip-spine relationships and their relationship to THA were noticed

several years ago [83, 84], the topic has since grown in importance. Phan et al. [11] defined PI, PT, and SS as the main measures to be used in evaluating spinal sagittal balance. They divided patients into four groups according to their spinal flexibility and sagittal balance. Several previous studies had not considered spine effects like prior spinal fusion on lower limb motions and sagital balance [85, 86, 87, 88, 89], even though they influence spinopelvic measures like AA during THA. The lack of a treatment algorithm for patients who have had prior fusion surgeries was another challenge for researchers who considered these relationships [90, 89, 86, 85]. A treatment algorithm was proposed in recent research by Vigdorchik et al. [21], based on a hip-spine classification system that will be discussed in this section. A study by Phan et al. [11] introduced a conceptual framework for the estimation of hip range of motion (ROM) in standing and sitting positions. This analysis resulted in identifying possible limitations in the flexion and extension of the hip as a result of THA surgery with different spinopelvic measures. They concluded that sagittal imbalance of the lumbar spine, along with spinal fusion, influences AA during THA. But as the research mentioned, to assess the types and amount of influence, further screenings are needed as a clinical solution. Thus, these influences should be considered in future studies to avoid increasing the risk of impingement and dislocation.

According to different spinopelvic measures, some researchers have started to investigate the effects of the spinopelvic relationship on total hip arthroplasty [6, 10, 11, 12, 13, 14, 9]. Clarifying the evidence of any relationship between articular impingement or dislocation and types of spine-hip relation (SHR), was the main criterion of the research by Riviere et al. [13] to investigate the increased risk of articular impingement or dislocation. For the SHR, they proposed a new concept of "kinematically aligned THA". They also considered functional cup orientation in

comparison with the definition of the "safe zone" introduced by Lewinnek et al. [25]. Abdel et al.[26] reported that more than 58% of complaints about dislocation after THA surgeries are from those patients who had their implant placement according to Lewinnek's safe zone. The updated definition by Riviere et al., describes the effects of lumbar mobility and pelvic kinematics on hip biomechanics in contrast to the static safe zone defined by Lewinnek. The idea behind Lewinnek's work was that a general safe zone should be determined for every patient having THA surgeries. However, it turns out that considering patient-specific measures like PI, PT, SS, and LL can affect the outcome of this surgery, and this general static safe zone should be modified to cover these patient-specific measures. To achieve that, researchers must evaluate the relationship between these measures and their effects on lower limb dynamics. One of these evaluations, by Ochi et al. [91], investigated the effects of pelvic incidence during standing to sitting and changing LL and TK on the positioning of the acetabulum in THA. Their results indicate the importance of dynamic evaluation of sit-to-stand motion pre-operatively. After comparing two patients with the same PT and LL measures in a standing posture, who experienced different PT and LL in sitting postures, they concluded that this difference occurs because of differences in spinopelvic mobility. The importance of dynamic evaluations before and after THA was emphasized in this research, and the need to explore them further in future studies was stressed in [91].

Another factor that can affect hip and spinal stiffness is Osteoarthritis disease [92]. Osteoarthritis is a degenerative joint disease, in which the tissues in the joint break down over time (cartilage, tendons, ligaments, synovium, bone) and it is more common in older people [92]. The most common locations are hands, knees, hips, neck, and lower back [93]. Incorporating findings from the study Kim et al.

had on the impact of hip mobility on lumbar and pelvic mobility before and after THA, highlights the critical link between hip osteoarthritis and spinopelvic dynamics. This study provides empirical support for the biomechanical interplay between hip joint degeneration and alterations in pelvic and lumbar mobility, emphasizing the importance of considering these relationships in the management of THA [94]. In another study, Sultan et al. compared dynamic changes in pelvic position parameters between hip Osteoarthritis (OA) patients and non-arthritic subjects, revealing that OA patients exhibit significant alterations in pelvic tilt, obliquity, and rotation from standing to walking. The findings, demonstrating a three- to four-fold increase in dynamic change for the OA group, underscore the importance of considering these kinematic variations during THA to optimize implant positioning and enhance post-surgical outcomes [93].

2.3.3 Patient Categorization towards Patient-specific THA Surgery

In response to a patient's specific measures and levels of spine stiffness, surgeons should consider a variety of approaches to achieving the best outcome in THA surgery. Researchers focused on clinical applications categorized patients based on various spinopelvic measures and spine stiffnesses and proposed different surgery plans for each category [13, 14, 22]. Riviere et al. defined three categories for spinopelvic mobility and related them to four types of spinal shape. As can be seen in Figure 2.3, patients with spine types 1 or 2 (flat shape) are considered to have a stiff spinopelvic complex and tend to compensate with a greater hip range of motion for daily activities. On the other hand, for patients with more curvature in their spine, the PI factor becomes greater and their acetabula tend to have lower anteversion. Some practical

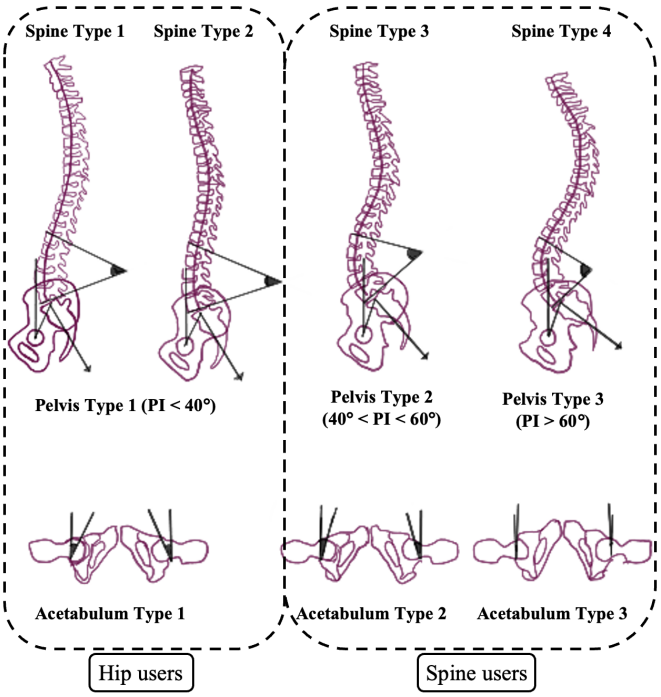


Figure 2.3: Classification of spine and acetabulum according to mobility definition [13]

solutions proposed in this research are said to lead to better outcomes in THA [13, 95].

Lum et al. defined another classification of spinopelvic motion by considering a relationship between acetabulum antiversion, pelvic tilt and lumbar lordosis. The classification includes six possible groups of patients: normal, stiff, hyper-mobile, fused, stuck standing and stuck sitting [14]. Other classifications have been proposed based on spinopelvic balance and degree of motion [4, 89, 12]. A Radiographic study, the method that the researchers used for evaluating the spinopelvic measures, is the most common preoperative method that has been used in other research as well. [10, 6, 12].

The definition of normal and abnormal spinopelvic motions and the way that these motions will cause impingement and ultimately dislocation should be clarified. The criteria for the classification of different types of spinopelvic relationships [4, 11, 89, 12, 14] rely on knowing the range of motion (ROM) in each part of this complex for different classes of patients with different types of spinopelvic motion. Consequently, any restriction or different behaviors of hip, pelvis, and spine can be considered as criteria for a categorization. In a normal stand to sit motion, the angle between the upper and lower part of the body will change from about 0 to 90°. This range of motion involves both hip and pelvis, so the hip joint may not flex to 90°. The motion becomes possible with a 20° posterior pelvic tilt and 55 to 70° hip flexion with a decrease in LL [84, 83]. This motion will lead to a decrease in SS while PT and AA increase. If for any reason, pelvic tilting is restricted, the hip joint must compensate for the lack of pelvic tilt in this motion. A person's ability to achieve an effective pelvic tilt may change for various reasons (e.g., aging, spinopelvic measures, spine stiffness, pain). This change will result in a different pattern of motion in the lower limbs, specifically in the hip joint, which can increase the risk of impingement or

dislocation.

According to the classification by Lum et al, if a patient has a normal spinopelvic motion in a stand to sit motion, the sacrum should have the ability to tilt posteriorly, followed by a simultaneous decrease in LL and increase in AA, which all together change the posture from standing to sitting [85]. If the spine becomes stiffer because of, for instance, spinal fusion surgery, then the sacrum loses its ability to tilt effectively, which may cause articular impingement or dislocation. In contrast, with a hypermobile spine, the risk of impingement decreases [6].

Sharma et al. defined the hip-spine relationship according to spinal mobility, deformity, stiffness, and range of pelvic tilt [96]. They have identified five categories of patients, and proposed a specific implant inclination and anteversion for each category. Their research suggests that patients with a spinal deformity characterized by a posteriorly tilted pelvis at standing posture have the highest risk of dislocation after THA.

In a more recent hip-spine classification for THA, Vigdorchik et al. described how to use this classification as a tool to improve the outcome of THA surgeries through preoperatively evaluating patients to determine their spinopelvic mobility [21]. They considered two major features of spinal alignment: spinal deformity and spine stiffness. The magnitude of "PI-LL" is used as the criterion to categorize patients with normal alignment or spinal deformity. In addition, the change in SS slope from standing to sitting position has been used to identify stiff spines (Figure 2.4). The outcome of this classification is the applicable treatment advice based on different spinal types. They have proposed functional anteversion and inclination, with different values than those of the "static safe zone" proposed earlier. Vigdorchik et al. reported a two-year post-surgery follow-up, in which 97% of patients experienced no dislocations

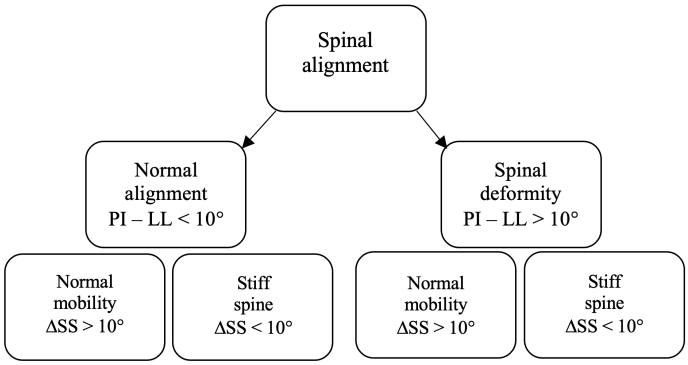


Figure 2.4: Classification of hip-spine according to spinal alignment and mobility whereas ΔSS is defined as the change in SS slope from standing to sitting position [21]

.

following THA adapted to meet their specific spinopelvic mobility in accordance with the new classification system. In the control group, 84% of patients experienced no dislocations [22].

2.3.4 Spine Stiffness and Fusion Surgery

The main reason reported for changes in spinal stiffness is spinal fusion surgery [10, 9, 97, 98, 99, 100]. Bedard et al. [101] investigated the high rates of hip dislocation following THA surgery after spinal deformity surgery. They reported abnormally high hip dislocation rates when THA was concurrent with spinal fusion surgery: in about 20% of patients in their institution and 8% in a national data base. Although they reported this higher rate, they did not identify the exact underlying mechanism. In another study, Eneqvist et al. [102] investigated the outcomes of THA surgeries for those with lumbar surgeries prior to THA. They concluded that a clear relationship exists between prior lumbar spine surgeries and less-favourable THA outcomes than expected, a fact that might be included in surgery planning for THA.

Not only have prior fusion surgery affects on THA been identified, as demonstrated in [102] and [101], but also the order of these surgeries is important as well. As the importance of the spine becomes clearer in THA surgeries, researchers have started to investigate the timing and order of fusion and THA surgeries as a source of insights into the as yet undetermined mechanisms of high hip dislocation rates in those with spinal fusion [103, 104]. When fusion results in a fixed spinal alignment [19] or involves the sacrum and some levels of the lumbar spine, the risk of impingement will increase as a result of this excessive spinal stiffness [105]. In addition, patients with spinal deformity are reported to be at higher risk of dislocation [106, 101, 21]. Besides spinal fusion surgery or deformity, different spinal shapes or spinopelvic measures affect spinal movement, as discussed in some research [13, 14, 10]

Patients can have a stiff spine even without fusion surgery. Vigdorchik et al. [98] included this category of patients as well, considering patients with limited lumbar flexion (stiff spines). With this criterion, they showed that the majority of patients with a stiffer spine have not had prior fusion surgery. This finding is not in contrast with the hypothesis of stiffer spine as a result of fusion surgery, but rather expands the definition of spine stiffness. In fact, patients with prior fusion surgery should be considered as certain candidates to have stiffer spines, but Vgdorchik et al. [98] have shone light on the previously ignored fact that a majority of patients found to have spinal stiffness have not had fusion surgery.

Individuals with stiffer spines for any of the reasons discussed (i.e., spinopelvic abnormalities, spinal fusion surgery, aging) will experience different spinal dynamic behaviors during daily activities such as sit-to-stand motions. For these cases, some surgeons will consider a modification in the implant position and orientation to include the effect of the stiffer spine. However, as yet, they have no numerical validation

as to how this modification will affect the final outcome. Even with the recent guidelines suggested by Vigdorchik et al. [21], patient-specific outcome prediction with a modification in the anteversion and inclination of hip implants can not be numerically accurate and must be evaluated experimentally. One possible solution for this knowledge gap is using a predictive model that can include all the parameters capable of altering the outcome of THA. The advantage of modeling approaches is their potential to provide numerical insights for surgeons in a predicted dynamic motion that go beyond the insights given by static X-rays alone. Also, FDA supports using computational models to improve medical devices performance [107]. In fact, with a patient-specific predictive model, surgeons may be able to change the stiffness factors and see their effects on lower limb dynamic motion instead of using general categorization and treatment advice as discussed in [98, 21]. We discuss this in details in Chapter 5.

2.3.5 Summary and Discussion

In summary, while research has explored the effects of spinopelvic relationship and spinal stiffness on total hip arthroplasty, the precise underlying mechanism remains unclear. Given the discussed parameters, each individual exhibits distinct hip range of motion and dynamic behavior during various motions, underscoring the critical need for dynamic motion and hip impingement analyses to enhance surgical planning effectiveness. This highlights the significance of surgeons having access to dynamic analysis rather than relying solely on static X-rays.

To offer a perspective on current clinical research and the various considerations addressed in the literature, we have compiled a summary of the reviewed material in Table 2.1. This table includes different spinopelvic measures, levels of spinal stiffness,

and examinations of spinal fusion surgeries from various studies. Additionally, we provide details about the methodology employed in each study along with its key highlights.

Table 2.1: Overview of clinical research on spinal stiffness and spinopelvic relationship effects on lower limb dynamics and THA surgery outcomes

Ref	Criteria	Methodology	Highlights
[11]	Spinal deformity, Spinal fusion, PT, PI-LL	Review	• Long spinal fusion (multiple levels) is considered. • Sagittal imbalance of the lumbar spine (PT>25°; PI-LL>10°) is clarified. • Patients are categorized based on sitting and standing lateral lumbar radiographs.
[108]	Spinal deformities, PT	Conceptual study and surgical recommendations	• Spinal deformities can restrict lumbar ROM and increase pelvic tilt. • Pelvic tilt caused by scoliosis should be measured. • In the case of deformity, spinopelvic measures are more important than the classic safe zone.
[91]	PI, PT, SS, LL, TK, SVA	Radiographic	• Lumbar spine mobility affects acetabular orientation during postural change. • Thoracic measures are not related to pelvic inclination changes. • Patients with low spinal mobility are identified as dislocation candidates.

Continued on next page

Table 2.1 – *Continued from previous page*

Ref	Criteria	Methodology	Highlights
[13]	PI	Systematic review	• Sagittal pelvic kinematics affect dislocation risk. • Patients are classified based on spine and hip relationships. • The correlation between PI and THA outcome is introduced.
[12]	Spinal fusion, Aging, Spinal imbalance, SS, Ante-inclination	Radiographic	• Pre- and post-operative X-ray images were compared. • Patients with biological or surgical spinal fusion are at higher risk for dislocation. • Dynamic movement analysis is recommended to validate the results.
[10]	Spinal fusion, Spinal imbalance	Review	• Spinal balance can change THA outcomes. • The exact mechanism of how spinal imbalance affects THA is still not answered. • A conceptual framework has been presented as a guideline for THA surgery.

Continued on next page

Table 2.1 – *Continued from previous page*

Ref	Criteria	Methodology	Highlights
[9]	SS, PI, Spinal imbalance, Ante-inclination, Pelvic femoral angle	Conceptual study and surgical recommen-dations	• Normal standing to sitting motion happens with 55° to 70° of hip flexion and 20° of posterior PT. • The main cause of abnormal standing to sit motions is decreased PT due to spinal or hip stiffness. • Ideal cup positioning is suggested for patients categorized as having normal, stiff, kyphotic, or hypermobile spinopelvic mobility.
[10]	Spinal deformity, Spinal fusion, PT, LL, SVA, PI-LL	Review	• Dislocation risk increases in patients with deformity or prior fusion. • Spinal alignment can change THA outcomes, but the exact mechanism remains uncertain.
[19]	Spinopelvic alignment, SS, LL, Proximal femoral angle, Acetabular inc and ant	Retrospective analysis	• Less spine flexion, less change in pelvic tilt, more hip flexion from standing to sitting were reported in patients who experienced dislocation after THA. • Fixed spinopelvic alignment increases the risk of hip dislocation.

Continued on next page

Table 2.1 – *Continued from previous page*

Ref	Criteria	Methodology	Highlights
[14]	Spinopelvic mobility, PT, LL, AA	Conceptual study and surgical recommendations	• A categorization has been proposed based on different spinopelvic mobilities: normal, stiff, hypermobile, fused, stuck standing, and stuck sitting. • Implant positioning based on spinopelvic mobility recommended.
[109]	SS, LL, APPt	Systematic review	• Common terminology and simplified spinopelvic relationships are summarized. • Patient-specific and functional safe zones using dynamic spinopelvic relationships are recommended.
[96]	SS, APPt, PT	Systematic preoperative work up	• Patients are categorized based on spinal mobility, deformity, stiffness, and range of pelvic tilt. • Patients with flat back deformity are determined to have highest risk of hip dislocation after THA

.

Continued on next page

Table 2.1 – *Continued from previous page*

Ref	Criteria	Methodology	Highlights
[110]	Functional component anteversion (FCA), PT	Retrospective analysis	• Relationships between severity of lumbar disk degeneration (not fusion) and PT and FCA are evaluated. • To maintain sagittal balance, PT changes differently in patients with severe lumbar spinal degeneration (more posterior tilt in standing and anterior tilt during gait). • This change in PT significantly changes the FCA, increasing the risk of impingement.
[111]	PT, SS, APPt, FPP	Conceptual study and surgical recommendations	• Simplified hip-spine relationship is introduced, and patients are categorized based on definitions of normal and abnormal hip-spine relationship. • A conceptual algorithm for THA is proposed, and fusion surgery timing is discussed.
[21]	SS, PI-LL, APP, Spinal fusion	Radiographic analysis and surgical recommendations	• A hip-spine categorization of patients is proposed considering spinal stiffness and alignment. • Different levels of fusion are considered. • Modified inclination and anteversion are suggested for four groups: normal mobility with normal alignment, stiff spine with normal alignment, normal mobility with spinal deformity, stiff spine with spinal deformity.

Continued on next page

Table 2.1 – *Continued from previous page*

Ref	Criteria	Methodology	Highlights
[112]	PT, PI-LL, LL	Radiographic analysis and surgical recommendations	• Anterior and posterior impingement are evaluated for patients with different lumbar flexion, PI-LL, and pelvic mobility. • The patients with highest risk of dislocation are those with degenerative spinal disease and adverse pelvic mobility.
[20, 97, 102, 105, 108, 113, 114, 115];	Spinal fusion	Retrospective analysis	• Spinal fusion surgeries increase THA complications and dislocation risk [113, 97, 108, 102]. • Dislocation rates are higher for those with 3 to 7 levels of fusion than those with 1 to 2 [97]. • Four spinal diseases are included: lumbosacral spondylosis; lumbar disk herniation; acquired spondylolisthesis; degenerative disk disease [108]. • The order of surgeries has not been studied [113, 97]. • Short and long fusions are included [113, 97]. • Surgery sequences are studied. Prior fusion surgery leads to more THA complications than fusion surgery after THA [104]. • Sacrum inclusion in fusion surgery increases the risk of dislocation in THA [105]. • Patients with prior fusion surgery had worse THA outcomes. Levels of fusion were not included in the study [115].

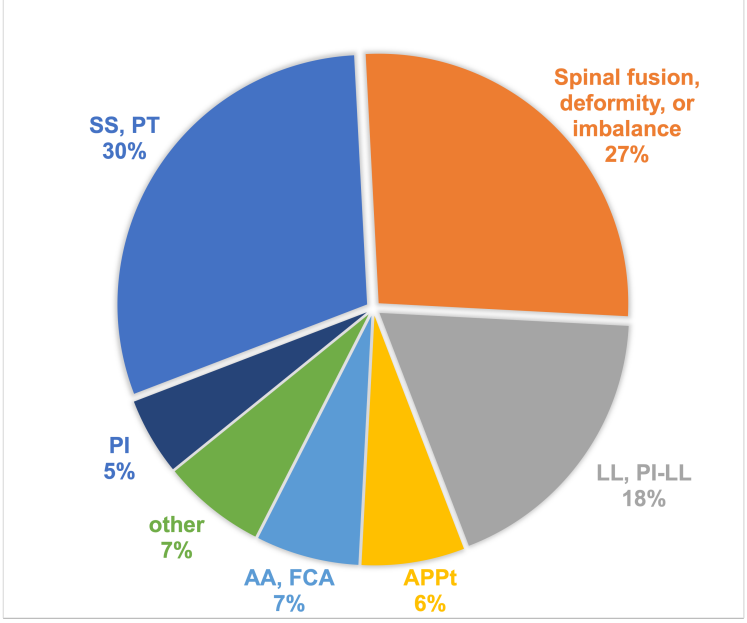


Figure 2.5: A break down on the reported spinopelvic metrics and spinal fusion factors that cause spine stiffness in the literature

Table 2.1 summarises spinopelvic measures, spinal fusion, method of study, contributions, claims, and highlights in the literature. As shown in Figure 2.5, here is the breakdown of reported factors for spine stiffness:

Spinopelvic Measures:

- Pelvic Tilt (PT) and Sacral Slope (SS): These are the most commonly cited metrics (30%) influencing spine stiffness. Surgeons typically assess the variation between standing and sitting values of these metrics to determine the rigidity of the spine. A change of less than 10 degrees (ΔPT or $\Delta SS < 10°$) suggests a potential instance of spinal stiffness.

- Pelvic Incidence (PI) and Lumbar Lordosis (LL): Pelvic Incidence itself is a biological individual constant and could not be a good indicator of a potential stiff spine case (only 5% citation). But the correlation of PI and LL ($PI - LL$) is an important metric evaluating the saggital balance and spinopelvic alignment.

The prevalence of these metrics are 18% in the literature.

Spinal Fusion Factors and Spine Stiffness:

Spinal fusion, deformity and imbalance are reported to play a crucial role in spine stiffness. There are several consideration that needs to be reviewed to understand the factors that are affecting spine stiffness for those who experience spinal fusion:

- Instrumentation and Fusion Levels: The choice of fusion levels and the type of instrumentation used in spinal fusion surgeries significantly affect spine biomechanics. Longer fusion constructs tend to alter the natural mobility of the spine.
- Implant Material and Design: The material and design of spinal implants play a crucial role in stabilizing the spine post-fusion. Factors like rod diameter, screw size, and interbody cages influence spinal stiffness.
- Degree of Fusion: Achieving solid fusion is essential for spinal stability. Incomplete fusion can lead to instability and contribute to spinal stiffness.
- Patient-specific Factors: Individual patient factors, such as age, bone density, and pre-existing spinal conditions, can influence the success of fusion and subsequent spine stiffness.
- Complications and Adjacent Segment Disease: Complications arising from fusion surgery and the development of adjacent segment disease can impact spinal biomechanics, potentially leading to stiffness.

Traditional approaches [25] often neglect these factors when optimizing implant positions, resulting in inadequate guidance for surgeons regarding safe implant positioning zones. While clinicians are beginning to recognize these factors [21], the precise mechanisms by which they influence spine stiffness remain unclear and warrant further investigation. To address this, a computational approach, particularly

predictive motion simulation, can prove invaluable in achieving optimized implant positioning while taking these factors into account. In the following section, we review the literature on musculoskeletal modeling approaches, detailed spine modeling, and computational methods for optimizing cup implant positioning.

2.4 Musculoskeletal Modeling and Simulation of Human Motion

In order to study the human musculoskeletal system, musculoskeletal simulations employ computer-generated models and mathematical models. These models include intricate depictions of bones, muscles, joints, and soft tissues, making it possible to replicate a variety of actions, from simple daily motions like reaching and walking to more difficult activities like playing sports or undergoing surgery [116, 117]. The aforementioned studies offer valuable perspectives on the biomechanical components that underlie human locomotion, encompassing muscle activation patterns, joint forces, and energy consumption. Through the study of the complex interactions that exist between the musculoskeletal system and its surroundings, scientists can create novel strategies that improve human health and function.

Musculoskeletal simulations can be classified into two main categories [117]. The first group includes experiment-driven models that depend on measurable external factors like ground reaction forces and experimental data like kinematic details. Fully-predictive simulations fall into the second group; they produce motion through an optimal control without requiring experimental data. According to predetermined optimization cost functions, such as decreasing energy consumption, lowering stress levels, or limiting fatigue, motion is predicted in fully-predictive simulations [118, 119].

The fully-predictive approach is the only one used in this thesis. Thus, we present a summary of previous studies in this field in this section. Furthermore, in order to make it easier to analyze how the dynamics of lower limbs are affected by a stiff spine, our human model has detailed spine components. We first briefly review the literature on spine modeling approaches (Section 2.4.1), and then we look at studies on full-body predictive models (Section 2.4.2) . In our investigation of human motion, we primarily concentrate on the sit-to-stand action, for which in Section 2.4.3 we present an analysis of sit-to-stand motion models followed by hip biomechanics and impingement analyses review in Section 2.4.4.

2.4.1 Approaches to Spine Modeling

Biomechanical modeling is pivotal in providing surgeons with predictive tools for surgical planning. In this section, we focus on spine modeling, which primarily involves two categories: Finite Element Method (FEM) models and multibody models. An understanding of the musculoskeletal intricacies of the spine is fundamental for accurate modeling. This encompasses knowledge of the vertebrae, muscles, ligaments, facet joints, and intervertebral discs—integral components that collectively determine spinal function throughout its diverse regions.

Spine Elements: Features and Modeling

Vertebrae, the rigid elements of the spine, exhibit diverse structures in different spinal segments, corresponding to their distinct functions [120]. These vertebral structures enable the spine to distribute weight effectively [121]. Facet joints connect adjacent vertebrae and govern spinal movements [122]. Intervertebral discs located

between vertebrae contribute to spinal flexibility, allowing bending and twisting in multiple directions [121, 122, 123]. While intervertebral discs primarily provide spinal mobility and flexibility, other components like ligaments and muscles also contribute. Ligaments serve as passive elements that maintain structural integrity and promote spinal stability [124].

Each segment of the spine can be modeled using various methods. For instance, vertebrae, as the fundamental units of the spine, can be modeled using the Finite Element Method (FEM) or musculoskeletal modeling [125]. In contrast to FEM, which focuses on stress relationships within segments, musculoskeletal modeling adopts a multibody approach that emphasizes motion and intersegmental loads. The lower number of degrees of freedom in multibody models leads to shorter computational times. In this method, each vertebra is treated as a rigid body [120]. The lumbar spine is modeled with individual vertebrae, while the thoracic and cervical regions can be modeled either as separate vertebrae or lumped together. If the thoracic part is considered a single rigid body [126], it may increase spine stiffness, potentially affecting upper spinal loading without significantly impacting lower spine load predictions [127, 128].

In multibody musculoskeletal modeling, intervertebral discs and facet joints, responsible for connecting vertebrae and facilitating spinal flexibility, are represented as joints. To capture all rotational degrees of freedom in the spine, spherical joints are commonly employed in the modeling. Muscles and ligaments, serving as active and passive elements, respectively, are included to enable the computation of reaction forces at spherical joints [125]. In the FEM approach, muscles are often omitted, but in the multibody approach, Hill-type modeling [129] is frequently used to represent muscles and ligaments. In this approach, muscles are modeled as active contractile

elements with passive elastic springs [120]. Nonlinear springs can accurately represent ligaments due to their property of exerting force only when stretched [125]. Another approach is to use deformable beams as connecting elements, which not only provide reaction forces and moments but also determine the overall stiffness of the spinal complex. All these modeling approaches have been developed to predict spinal loads, aiding surgeons in surgical planning.

Finite Element Method in Spine Modeling

There are two general approaches to modeling the spine: dynamic-based multibody modeling and Finite Element Method (FEM) modeling. FEM involves the analysis of structures, such as the spine. Both approaches yield outputs like disc pressures [130, 131] and facet joint contact forces [132]. Shojaei et al. [133] introduced an FEM model of the spine that includes a nonlinear finite element representing the spine, with thoracic vertebrae grouped together but each lumbar vertebra modeled individually. Lumbar stiffness is represented by six deformable beams, incorporating nonlinear stress-strain and moment-rotation relationships in all three directions. Additionally, 56 muscles were defined to model connections between vertebrae and between the spine and pelvis.

Some FEM models have been developed to enhance the efficiency of surgeries, such as spinal fusion and disc replacement, by simulating surgical options and evaluating their outcomes [134, 135]. While other FEM models exist, their high computational cost has sparked interest in using multibody approaches. However, combining both methods could offer an efficient model for predicting spinal loads and assessing the impact of spine stiffness on total hip arthroplasty (THA).

Multibody Modeling of the Spine

Multibody models of the spine have become increasingly precise and complex in recent years [136]. The predominant approach for spinal modeling has been inverse dynamics [137]. Analyzing the motion of different body segments and the intersegmental forces during human motion aligns well with the multibody modeling approach. Common software packages like OpenSim and Anybody are employed for multibody modeling of the human [126, 138, 139, 140, 141, 142, 143].

Ode et al. [144] developed a biomechanical model based on multibody dynamics to determine the forces exerted between the vertebrae in the spine. This model calculates these forces through inverse dynamics, utilizing kinematic data gathered from walking. To transform this data, which is initially captured in absolute coordinates by optical sensors, into relative joint coordinates, an optimization process is employed. This conversion is essential for estimating the forces and torques at the joints. De Zee et al [139] developed a lumbar spine model using Anybody, incorporating 154 muscles and 18 degrees of freedom. This model encompasses seven segments, with a 3-degree-of-freedom spherical joint connecting each vertebra. An artificial segment with zero mass and inertia was introduced to account for intra-abdominal pressure effects. The model, based on inverse dynamics, resolved the muscle redundancy problem through an optimization method. Certain muscles, like the intratransversarii and interspinalis, were excluded from the model. Additionally, force-length and force-velocity relationships for muscles were not included. The model could generate a maximum extension moment of 238 Nm, and it could calculate the pressure between L4 and L5. Han et al. [126] augmented the model by adding short muscles, while also incorporating ligaments and disc stiffness into the lumbar region. This model predicted the highest flexion force in the longissimus muscle, and in extension, the

rectus abdominis muscle generated the maximum force. For lateral bending and axial rotation, the psoas major was predicted to produce the maximum force. This study highlighted the significance of including a complete set of ligaments and muscles. Recognizing this importance, Bayoglu et al. [143] developed a more detailed musculoskeletal model of the spine, considering additional muscles. This model encompassed 60 segments and 193 degrees of freedom, accounting for vertebrae, ribs, sacrum, sternum, and pelvis in the spine. Additionally, it included segments like clavicle, hyoid, thyrohyoid, scapula, and humerus without mass properties. To represent the connections between the pelvis, spine, and upper limb, 351 muscle-tendon elements were used, representing 49 muscles. The model incorporated stiffness properties for intervertebral discs, facet joints, and ligaments using a lumped stiffness model with linear torsion springs. This model accurately predicted intervertebral pressure, aligning well with previous studies. Based on inverse dynamics, muscle forces were calculated to minimize muscle fatigue. However, some limitations existed, such as the exclusion of ligaments and the addition of their stiffness properties to the joints. Additionally, the use of spherical joints restricted translational degrees of freedom, which may impact joint reactions and muscle forces [145, 146]. Force-length and force-velocity relationships for muscles were not considered, and a simple muscle model was utilized. Furthermore, none of the previous detailed musculoskeletal models incorporated the lower limb and connecting elements, leaving a gap in understanding the effect of spine stiffness on lower limb dynamics.

Modeling Simplifications

Simplifications in modeling (e.g., characteristics of structural elements and lumped representations of different structures) impose constraints on detailed biomechanical

modeling of the human spine. Ghezelbash et al. described the impact of some simplifications in modeling and different joint positioning on the accuracy and validity of results [147]. Two types of spine modeling were considered in this research. The first model employed multibody modeling of the spine with spherical joints, including rotational springs between the joints representing spine stiffness. This model was also considered without springs. In the other model, deformable beams were employed as connection elements in spine modeling. This model included both linear and nonlinear beams for stiffness representation [148]. Both of these models were compared with a detailed FEM model [149], and the accuracy and validity of both were assessed. Results were evaluated by introducing an offset ranging from -2 to 4 mm in the joints. The kinematics of the models were compared with the FEM model, and the spinal loads were compared to in-vivo experimental data [150]. The results indicated that considering nonlinearity in models with spherical joints and deformable beams led to acceptable accuracy in predicting spinal loads and kinematics. However, the model with spherical joints could not accurately predict axial displacement due to limitations in that direction. Models with linear properties in connecting springs were unable to provide accurate results and imposed limitations, including excessive flexion angles beyond 30 degrees and high external loads. Additionally, some simplifications, such as neglecting rotational springs, led to overestimation of compression and shear forces [147].

2.4.2 Predictive Human Musculoskeletal Simulations

Predictive musculoskeletal simulation is a method that avoids depending on experimental data to predict motion. In such method, we assume that human motion naturally optimizes aspects like energy use, performance, or effort, or any combination

of these, as described by Norman et al. [151]. One advantage of predictive simulations is their ability to study "what-if" scenarios over a wide range of situations, as explained by [118, 152, 153, 154]. For example, prior to carrying out any real surgical procedures, these simulations allow studies into various implant placements and the optimal results, including reaching maximum joint stability.

In spite of this, predictive modeling is fraught with difficulties that are caused by restrictions on the data that can be used, such as the absence of essential inputs such as kinematic data and ground reaction forces. The lack of available data in this context makes the conclusions particularly susceptible to the assumptions used to determine optimality, as emphasized by Dembia et al. [155] in their study on OpenSim. It gets even more complicated when trying to define a suitable cost function; you have to choose one that fits each person's particular situation. The cost function used for an elderly senior, for example, can be very different from the one used for a young athlete performing the same exercise, like the sit-to-stand motion. Commonly used cost functions seek to decrease factors such as joint torque, muscle activation, produced power, reaction force, and jerk.

In the following part of this chapter, we narrow down the review to sit-to-stand motion, which is employed in this thesis to research the biomechanics of the hip joint after THA affected by spine stiffness by employing a predictive human model that incorporates a detailed spine. Readers interested in a more in-depth investigation of predictive simulations for human movement are encouraged to read the complete evaluation that was written by Febrer et al. [118].

2.4.3 Sit-to-Stand Motion Simulations

Sit-to-stand motion has diverse applications, from assistive robot design to addressing movement disorders [156, 157] and developing rehabilitation exoskeletons [158, 159, 160, 161, 162]. This thesis places particular emphasis on understanding the mechanics of hip joints and how spine stiffness influences lower limb biomechanics, given its crucial role in daily activities [163]. It is noteworthy that sit-to-stand motion has been identified as a routine activity that may pose a risk of hip dislocation in patients following THA surgery [164].

Modeling sit-to-stand motion often assumes symmetrical sagittal plane motion, leading to the development of multi-link systems. The three-link model, comprising segments for shanks, thighs, and the trunk connected via hip, knee, and ankle joints, is widely used for predicting sit-to-stand motion [151, 165]. However, for specific conditions, especially in older adults or those with a rigid spine, it has been demonstrated that incorporating more detailed upper limb components, such as the spine and arms, is crucial. As a result, more intricate models have been developed, encompassing upper and lower arms, the torso, thighs, shanks, and feet to account for the influence of lumbar and torso joints on sit-to-stand motion [136, 157, 166, 167].

Predictive simulations present challenges in defining an appropriate cost function that accurately represents human body optimization for a specific movement, along with establishing precise initial conditions. Researchers have explored various cost functions in predictive simulations. Some are based on kinetic metrics like torque, force, and energy, while others focus on minimizing kinematic factors like jerk and joint angular velocity. Typically, a combination of these factors is used in a cost function to achieve accurate predictions [168, 167]. These functions aim to achieve accurate predictions of sit-to-stand motion by considering factors like torque, force,

energy, jerk, and joint angular velocity.

While the majority of studies have focused on predicting sit-to-stand motion in healthy adults, limited research has been conducted for individuals with impaired conditions. Previous models predominantly employed torque-driven muscle models. Notably, recent work emphasizes the importance of incorporating nonlinear muscle and ligament properties [166], especially for older adults. Additionally, the impact of different spinal conditions, such as a stiff or fused spine, on lower limb mechanics was largely overlooked in prior models, representing additional limitations in this area of research.

2.4.4 Hip Biomechanics and Impingement Analysis

Research on the biomechanical aspects of the hip joint during various daily activities has been a subject of recent investigation, often employing computer simulations. Musculoskeletal models play a crucial role in quantifying the biomechanics of hip joint during daily tasks like walking and sit-to-stand motion. Studies have demonstrated that both scaled generic and subject-specific models [169, 170, 171, 172] have provided reasonably accurate predictions. It's important to note that factors like hip and implant shape and the choice of musculoskeletal model significantly influence the results. Incorporating more complex elements such as muscle wrapping and subject-specific data has demonstrated the potential to enhance prediction accuracy by approximately 30% [169].

Ensuring the correct placement of the cup is widely acknowledged as a crucial factor in reducing the risk of implant impingement and following hip dislocation [24]. However, the Lewinnek safe zone guideline [25], though widely accepted, has

shown limited correlation with the actual risk of hip dislocation, as indicated by several studies that we reviewed in Section 2.3.2. This discrepancy can be attributed to the guideline's failure to account for individual characteristics like pelvic tilt and spine stiffness. Therefore, it is imperative to prioritize the development of innovative, subject-specific approach that can effectively address post-THA challenges, ultimately improving THA outcomes. Existing literature has predominantly focused on investigating factors contributing to hip dislocation during sit-to-stand movements, given the frequency of this action in daily activities [163]. Additionally, it's worth noting that hip dislocations after THA often occur during sit-to-stand motion [164, 173].

Computational models have emerged as powerful tools in predicting impingement risks and optimizing implant orientations. Finite Element Analysis (FEA) has become a widely accepted method for examining implant impingement in THA. This analytical approach has been employed to study various aspects influencing THA outcomes, including acetabular component alignment and implant design [174, 175, 176]. Recent research has explored various aspects of impingement and dislocation in Total Hip Arthroplasty (THA) surgeries. One critical aspect involves predicting dislocation stability for different positions of prosthetic components across various activities. Three-dimensional finite element (FE) models have been proposed to evaluate the range of movement (ROM) and maximum resisting moment (RM) until dislocation, thereby establishing a "safe zone" for impingement and dislocation avoidance [177]. However, since these studies rely on FEA or force plate measurements, they may not be immediately suitable for clinical applications due to their time-consuming, complex, or expensive nature.

To gain an understanding of pelvic tilt and spine stiffnesss throughout the entire

range of motion, a dynamic simulation becomes essential. Various methods have been proposed to account for the variability in pelvic tilt when determining optimal orientations for impingement-free cups in functional cup alignment [178, 179, 89, 180]. These techniques allow for an examination of the effects of implant component placement, including femoral antetorsion or combined anteversion, as well as prosthesis-specific factors like head/neck ratio and cup and neck design, on the unrestricted range of motion of the hip joint, free from impingement. Another crucial consideration revolves around the orientation of prosthetic components. Research efforts have focused on determining optimal orientations for both cups and stems, taking into account factors such as anteversion, neck-shaft angles, prosthetic head size, and target ranges of movement [181]. Moreover, the type of implant system used in THA, including short hip stems and hip resurfacing, can impact the range of motion and the likelihood of impingement [182]. Investigating how different implant designs affect impingement-free ROM is therefore crucial. Further insights into THA impingement have emerged from studies examining the interplay between cup and stem anteversions during hip motion. These studies reveal distinct effects of cup and stem anteversions on the position of the femoral head within the acetabular liner during various activities, underscoring the significance of considering both components for an accurate assessment of hip motion [183].

However, these kinematic methodologies primarily focus on studying the relative movement between the femur and pelvis to predict impingement, while neglecting the influence of overall body motion dynamics, particulary spine stiffness. It has been reported in the literature that spine stiffness and spinal fusion are critical factors in obtaining optimal implant positioning for such patients. As discussed in Section 2.3.2, clinical evidence indicates that spinal stiffness affects pelvic tilt

and hip range of motion, thereby increasing the likelihood of impingement. lumbar-pelvic stiffness and sagittal imbalance have been identified as factors contributing to dislocation. To address this concern, new mathematical algorithms have been proposed to determine patient-specific safe zones for THA components. These algorithms integrate standing and sitting sagittal pelvic tilt to optimize implant orientations and prevent impingement [184, 182]. Several studies have explored additional sources of hip dislocation, such as bony coverage [185], bony impingement [186], edge-loading [187], and wear [188], to ascertain the optimal cup orientation. However, there's still a pressing need for a modeling platform capable of accurately predicting the motion of pelvis and femur during a dynamic analysis of the entire body, while also considering the influence of a flexible spine.

2.4.5 Conclusion

In conclusion, musculoskeletal modeling and simulation have revolutionized our understanding of human motion and its biomechanical intricacies. Through computer-generated models, researchers have been able to replicate a wide range of movements, shedding light on muscle activation patterns, joint forces, and joint ROM. These simulations have not only deepened our comprehension of human movement but also paved the way for novel strategies to enhance human health by optimizing surgery procedures like THA. Moreover, advancements in predictive simulations offer a powerful tool for studying various scenarios and optimizing outcomes providing patient-specific recommendation. While challenges persist, such as defining appropriate cost functions and considering subject-specific conditions, the potential for further advancements in this field is vast.

In the context of hip biomechanics and impingement analysis, computational

models such as Finite Element Analysis (FEA) have been instrumental in assessing impingement risks and optimizing implant orientations. However, there remains a need to improve this analysis by considering the dynamics of human motion, accounting for factors like spine stiffness. This approach has the potential to offer a more accurate representation of human motion, with significant implications for Total Hip Arthroplasty (THA) surgical planning. Further insights into predictive simulations and cup implant optimization, considering the effects of spinopelvic measures, spine stiffness, and spinal fusion, will be detailed in Chapter 5.

Chapter 3

Automatic Extraction of Anatomical Landmarks using Deep Learning Approaches and Patient Categorization Based on Spinal Conditions

3.1 Chapter Overview

This chapter presents a physics-informed deep learning method designed to extract spinopelvic measures from X-ray images. Its performance is assessed against manual annotations. For this purpose, two datasets, comprising a total of 1470 images, were collected to evaluate the model's performance in Section 3.3.3. We propose a

novel method in Section 3.3.4 of detecting landmarks as objects, incorporating their geometrical relationships as constraints (***LanDet***). The model performance and accuracy of automated measurements are presented in Section 3.4.1, in comparison with manual annotations (MA) from a PhD student as well as three senior orthopedic surgeons. To assess model reliability and compare it against surgeons, the intraclass correlation coefficient (ICC) metric is used in Section 3.4.2. The model demonstrated better consistency with surgeons, with all values over 0.88, compared to what was previously reported in the literature. The outcomes of this chapter facilitate the extraction of critical spinopelvic measures, crucial for pre- and post-THA procedures. Additionally, the automated approach aids in patient categorization, a pivotal step in assigning patient-specific spine stiffness parameters for the predictive model discussed in Chapter 5.

3.2 Introduction

The chapter explores the assessment and prediction of spinopelvic measures, a topic of much interest in both clinical and research communities [32, 33]. Radiological examination of the spine and pelvis is crucial for treating hip and spinal disorders [35, 30, 36]. Machine learning techniques, particularly deep learning, have significantly improved automated image analysis, finding extensive application in radiology and identification of spinal disorders [37, 32].

Sagittal spinopelvic balance is pivotal for comprehending spinal deformities, THA pre-operative planning, and treatment selection, but manual measurements of spinopelvic factores can be subjective and prone to error [30, 38, 39]. Advanced AI and deep learning techniques offer promise in automating anatomical measure

extraction from spine radiographs, potentially enhancing efficiency and accuracy [45, 41]. Studies have proposed innovative methods utilizing deep learning algorithms for automated spinal alignment measurement, showing accurate predictions despite inherent challenges [31, 28, 37], which have been discussed in Chapter 2. However, it is important to assess their performance, considering variations in image quality and the presence of hip and spinal pathologies, and compare automated measurements to manual assessments [30, 31, 28].

This chapter also introduces a novel approach using bounding boxes for landmark detection, addressing drawbacks of heatmap-based regression. This new deep learning model not only detects each anatomical landmark as a unique object, but also establishes a relationship graph between objects as geometrical constraints, enhancing accuracy in locating landmarks, a challenge of misdetection of adjacent landmarks reported previously in the literature [31, 29, 44]. Employing this approach proves advantageous when dealing with near-identical objects, such as the femoral heads, within a single image. It significantly streamlines the process of locating these landmarks, along with adjacent spinal landmarks of a similar nature, thereby reducing overall complexity of detecting required landmarks to calculate spinopelvic measures.

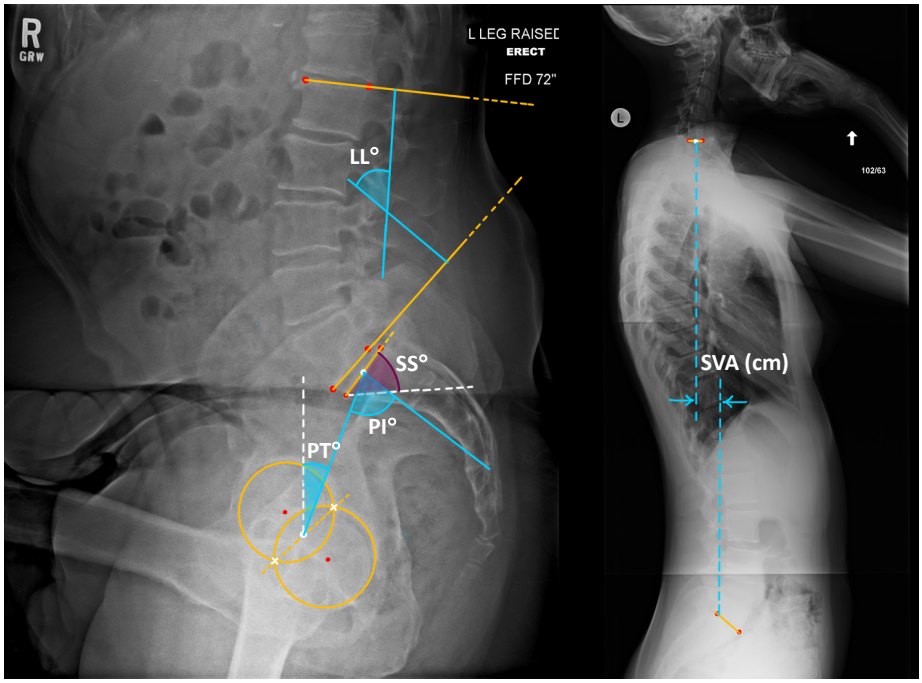
3.3 Materials and Methods

3.3.1 Spinopelvic Geometric Measurements

In this research we targetted five anatomical measures to be extracted automatically, which are Sacrum Slope (SS), Pelvic Tilt (PT), Pelvic Incidence (PI), Lumbar Lordosis (LL), and Sagittal Vertical Axis (SVA). As the Figure 3.1 shows, SS is the angle

between the tangent line to the upper end plate of S1 (connecting line of posterior and anterior corners) and the horizontal reference line. PT is the angle between the vertical reference line and the connecting line between midpoint of sacrum upper end plate and the midpoint of connecting line between the intersection of femoral head circles (hip axis). Pelvic Incidence (PI) is a morphologic measure defined as the angle between the perpendicular line to the mid-point of the upper end plate of last vertebra of the sacrum (S1) and the connecting line of this point to the midpoint of connecting line between the intersection of femoral head circles [3]. This measure is defined as an anatomical measure and strictly related to the shape of the pelvis [5]. This measure mostly remains constant in each pelvic posture and it is equal to the sum of two measures (PT and SS) [6].

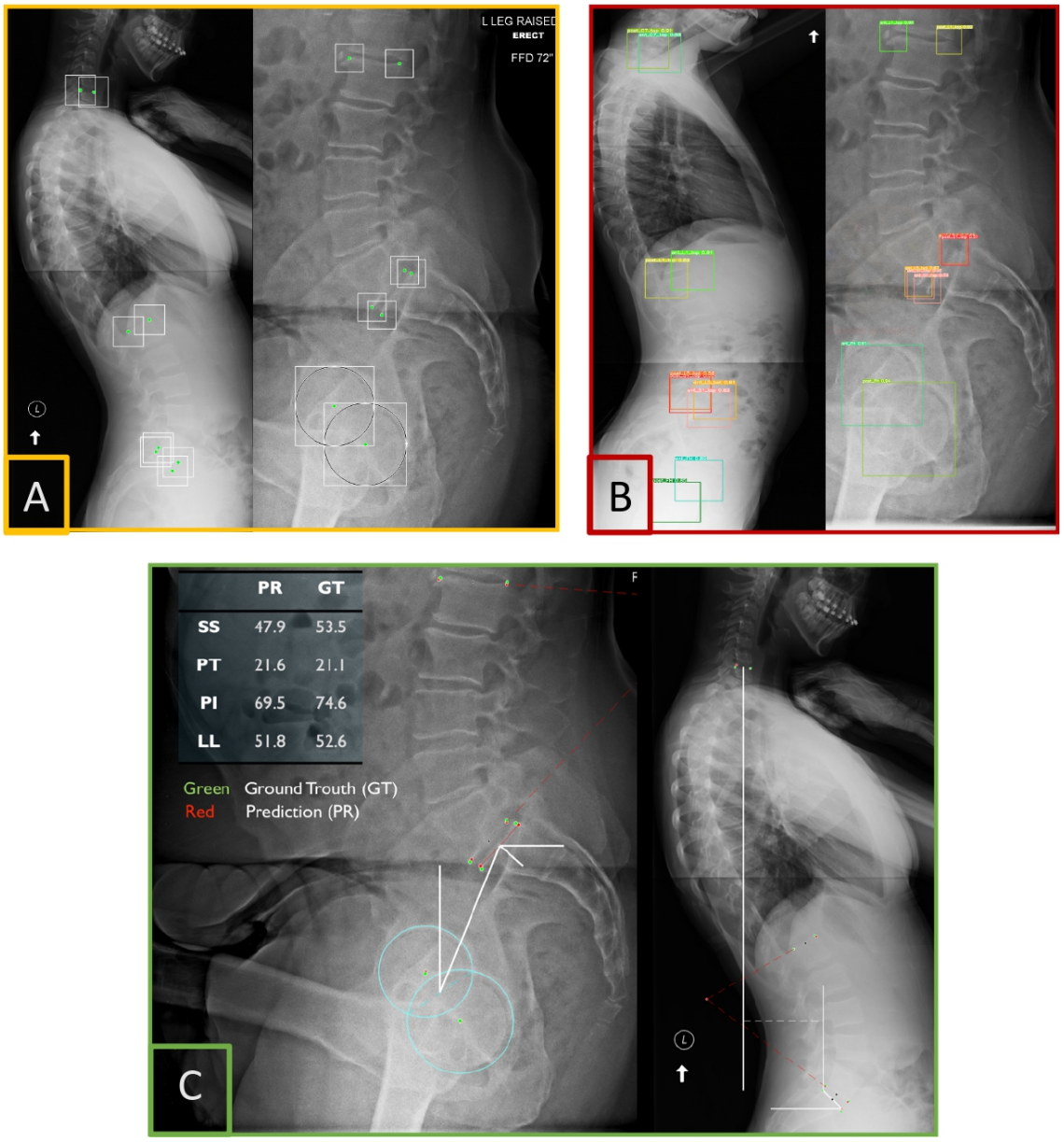
Figure 3.1: Main spinopelvic measures in lateral X-ray images, considering both femoral heads to calculate the center of rotation for the pelvis



3.3.2 Detection Using Landmarks as Constraint Objects

To automatically extract spinopelvic measures of interest (such as SS, PT, PI, LL, and SVA), we adopt a landmark detection approach that treats landmarks as objects. Our method utilizes a deep learning physics-based object detection algorithm, which overcomes limitations of heatmap-based regression methods, including issues with overlapping heatmap signals and post-processing requirements (McNally et al., 2021). In our approach, landmarks are represented as objects with bounding boxes centered at the landmark coordinates (bx, by) and equal width (bw) and height (bh). Our labeled dataset comprises 10 classes of landmark objects (c_i), including the centers of femoral heads and the anterior/posterior points of S1, L1, C7 superior end plates, and L5 inferior end plate. Each label includes the class number and the bounding box features $C_i = (c_i, bx_i, by_i, bw_i, bh_i)$. Our deep learning model predicts objects with varying confidence levels (Fig. 3.2-B), and the object with the highest confidence is used to extract the desired landmarks. To explain the rationale for considering constraints between these anatomical landmarks, we can consider the scenario where a surgeon intends to annotate a lateral X-ray image in order to measure the SS. When the posterior corner of the superior sacrum end plate is identified, the surgeon can leverage the predictable relationship within the sacrum as a solid body to determine the corresponding anterior point. We refer to this relationship as a geometric constraint, and the same concept has been applied for other landmarks. Imposing these constraints helps the model not only understand the features of each object (landmarks) but also enables a holistic understanding of the entire image and the interrelationships (constraints) among these landmarks. The final detected landmarks are subsequently used to calculate the desired measurements (Figure 3.2-C).

Figure 3.2: A: Manual labeling of landmarks and specifying bounding boxes. B: Extracted landmarks as objects with different confidences, trained model output, evaluated with the test set. C: choosing the highest confidence for each landmark as the prediction results and calculation of the spinopelvic measures



3.3.3 Dataset and Data Preparation

We collected a total of 1,150 lateral spine X-ray images (Dataset 1, DS1) from patients referred to Grand River Hospital (GRH) in Kitchener, Canada, between 2016 and 2022. Additionally, we incorporated a dataset (Dataset 2, DS2) of 320 lateral lumbar spine and pelvic images provided by Intellijoint Surgical. Our datasets encompass different range of cases, including patients with hip or spine implants and images from both sitting and standing postures. Unlike some other research [31, 30], we included all images, even those with poor contrast or partial spine visibility. To address these issues, we employed appropriate image processing filters to enhance annotation accuracy for parts with high or low intensity. By including partial spine images, our dataset enables the model to identify anatomical landmarks effectively, even in incomplete images. The utilization of two distinct datasets enabled us to evaluate the model's performance on different data sizes and imaging systems. DS1 consisted of images captured using ordinary X-ray devices, while DS2 utilized the EOS imaging system. To facilitate training, validation, and testing, we divided the datasets into sets comprising 80%, 10%, and 10% of the total data, respectively.

A Matlab graphical user interface (GUI) was developed to facilitate image annotation (Figure 3.2-A). In this process, 10 anatomical landmarks (superior posterior and anterior corners of S1, posterior and anterior femoral heads, inferior posterior and anterior corners of L5, superior posterior and anterior corners of L1, superior posterior and anterior corners of C7) are manually annotated in each image using the GUI. The GUI allows annotators to identify the desired points, which automatically generates corresponding bounding boxes. For accurate femoral head annotations, annotators are required to specify three points on the edge of each femoral head. The GUI then calculates and visualizes the center of the femoral heads based on the

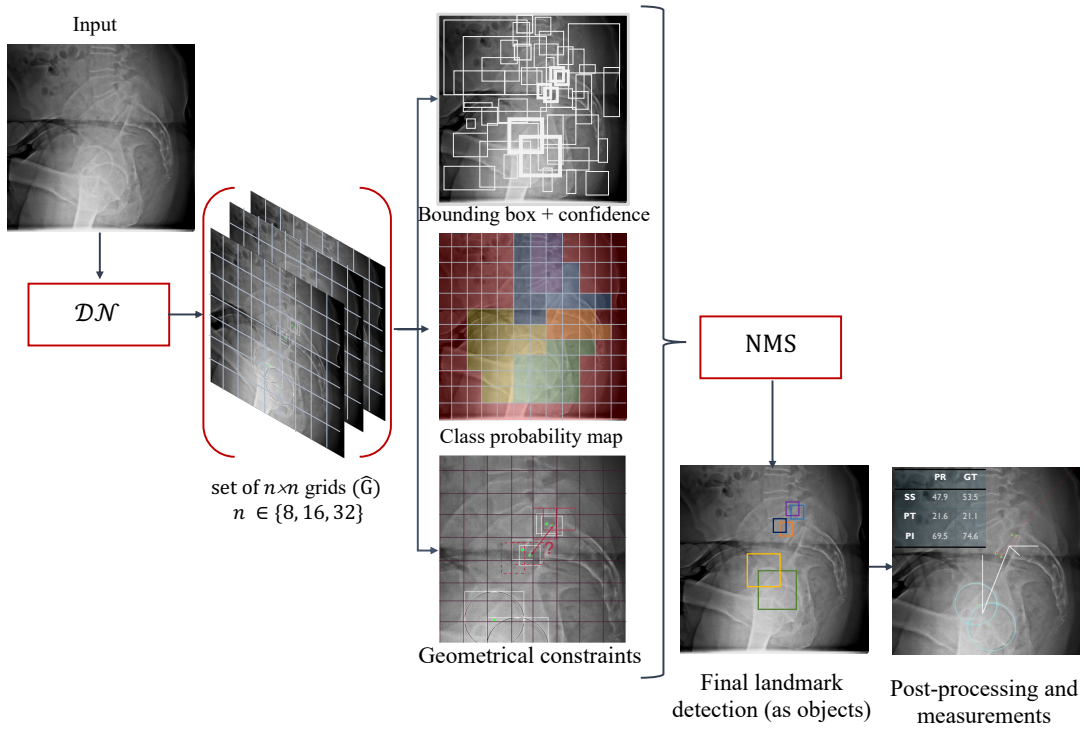
specified points. The sizes of the bounding boxes are optimized for the best mAP (i.e., maximum mean Average Precision) value to consider landmarks as objects, set at 5% of the maximum image size. However, for the femoral heads, the bounding box sizes vary depending on the size of the femoral head circles. To ensure consistency, the coordinates and bounding box sizes are normalized to the maximum dimension of the image, resulting in coordinate values ranging from 0 to 1. The resulting labels are shown in Figure 3.2-A. Three expert orthopedic surgeons annotated the test dataset for benchmarking the model's accuracy. They used the developed GUI mirroring the actual software's functionalities, such as zoom and brightness adjustment. Their task was to mark images as they would pre-surgery, conducting independent validation without further guidance from us.

3.3.4 Model Architecture

Heatmap-based regression has been widely used in tasks like landmark detection [29, 30, 31], despite its drawbacks such as quantization error and high computational requirements [60]. To address these limitations and provide a more efficient alternative, we introduce a novel approach called ***LanDet*** (**Land**mark **Det**ection). Instead of relying on heatmaps, ***LanDet*** models individual landmarks as objects within a dense single-stage anchor-based detection framework. Furthermore, the relations between landmarks are imposed to the detection architecture as geometrical constraints. This innovative method aims to improve the efficiency and accuracy of anatomical landmark detection and clinical measurements without the need for heatmaps.

As can be seen in Figure 3.3, our model works by splitting the image into grid cells; each cell is responsible for predicting bounding boxes, by evaluating whether or not the center of the bounding box lies in the cell. Anchor boxes enable the

Figure 3.3: ***LanDet*** utilizes a dense detection network denoted as DN that is trained with the multi-task loss $LanDet_loss$. The purpose of this network is to transform an input image represented by I into a collection of output grids denoted as $\hat{G}$. These grids contain the predicted landmark objects represented by $\hat{O}_l$. To obtain potential detection, a technique called non-maximum suppression (NMS) [60] is employed for $\hat{O}_l$. The geometrical constraints are applied on these candidate detections to generate the final predictions for $\hat{O}_l$, which are then be used to calculate desired measures.



model to predict more than one object in a single cell. Figure 3.3 displays a diagram illustrating the ***LanDet*** pipeline. This pipeline utilizes a deep convolutional neural network denoted as DN, which takes an input image I with dimensions $h \times w \times 3$ and transforms it into a collection of three output grids denoted as $\hat{G}$. These grids contain the predicted objects denoted as $\hat{O}$. Each individual grid, denoted as $\hat{G}_n$, has dimensions $\frac{h}{n} \times \frac{w}{n} \times N_a \times N_o$, where n takes on values from the set $\{8, 16, 32\}$. The transformation performed by the deep network can be expressed as the following equation:

$$DN(I) = \hat{G} \tag{3.1}$$

N_a represents the count of anchor channels, while N_o corresponds to the number of output channels for each object. The feature extractor DN follows the YOLO-style approach [67] and makes effective use of Cross-Stage-Partial (CSP) bottlenecks [189, 60].

Due to the properties of strided convolutions, the characteristics of an output grid cell $\hat{G}_n^{i,j}$ are influenced by the image patch I_p, defined as $I_{n_i:n(i+1),n_j:n(j+1)}$. Consequently, if the center of a target object (b_x, b_y) lies within I_p, the corresponding output grid cell $\hat{G}_n^{i,j}$ is responsible for detecting that object. The effective range of perception of an output grid expands as n increases, implying that smaller output grids are more effective at detecting larger objects. The boounding box sizes are set to be 5% of the maximum size of the image for the landmarks on the spinal part, and for the femoral heads, the bounding box sizes are equal to the diameter of femoral cup so that it can enclose that part.

The output grid cells $\hat{G}_n^{i,j}$ encompass N_a anchor channels, which are associated with anchor boxes $A_n = \{(A_{w_a}, A_{h_a})\}_{a=1}^{N_a}$. To assign a target object O to an anchor channel, a tolerance-based matching of their respective sizes is employed. This

approach introduces redundancy, allowing the grid cells $\hat{G}_n^{i,j}$ to detect multiple objects and specialize in detecting objects of various sizes and shapes. Moreover, additional redundancy in detection is achieved by enabling the neighboring grid cells $\hat{G}_n^{i\pm1,j}$ and $\hat{G}_n^{i,j\pm1}$ to detect objects within the same image patch I_p [190, 191].

Loss Function

To introduce the relations between each landmark to the model, we modified the main object detection loss function to incorporate the geometric constraints. A set of target grids G is created, and a multi-task loss function $LanDet_{loss}$ is employed to train the model to learn various aspects, including the objectness $\hat{p}_o$ (represented by l_{obj}), the intermediate bounding boxes $\hat{t}$ (l_{box}), the class scores $\hat{c}$ (l_{cls}), and the intermediate constraint satisfaction $\hat{r}$ (l_{cnst}). To compute the loss components for a single image, the following procedure is followed:

$$LanDet_{loss} = l_{box} + l_{obj} + l_{cls} + \sum_{i=1}^{k} w_i.l_{cnst} \tag{3.2}$$

where k is the number of defined constraints and w_i are the weights for each of the constraints. the components of this loss function are defined as followed:

$$l_{\text{obj}} = \sum_{n} \frac{1}{\text{num}(G_n)} \sum_{G_n} \text{BCE}(\hat{p}_o, p_o \cdot \text{IoU}(\hat{t}, t)) \tag{3.3}$$

$$l_{\text{box}} = \sum_{n} \frac{1}{\text{num}(O \in G_n)} \sum_{O \in G_n} (1 - \text{IoU}(\hat{t}, t)) \tag{3.4}$$

$$l_{\text{cls}} = \sum_{n} \frac{1}{\text{num}(O \in G_n)} \sum_{O \in G_n} \text{BCE}(\hat{c}, c) \tag{3.5}$$

$$l_{\text{cnst}} = \sum_{n} \frac{1}{\text{num}(O \in G_n)} \sum_{i \in O_{l_i}} \sum_{j \in O_{l_j}} f_c(\hat{r}_{ij}, r_{i_j}) \tag{3.6}$$

where BCE (binary cross-entropy), and "intersection over union" IoU (measures the overlap between the predicted bounding box and the ground truth bounding box [192]), are crucial elements and defined as follows:

$$\text{BCE}(c, \hat{c}) = -\left(c \cdot \log(\hat{c}) + (1 - c) \cdot \log(1 - \hat{c})\right) \tag{3.7}$$

$$\text{IoU} = \frac{\text{Area of Intersection}}{\text{Area of Union}} \tag{3.8}$$

Furthermore, f_c denotes a regression-based function that characterizes the correlation among landmarks. These constraints pertain to the interrelations between landmarks on the same spinal vertebrae, as well as the Pelvic Incidence (PI) measure. As explained in Chapter 1, PI is a geometric constant unique to each patient, remaining invariant even with changes in posture. For any angular constraint (e.g., PI), f_c represents a cosine similarity function and for the distance constraints (e.g., anterior and posterior corners of each vertebra), f_c represents the absolute distance loss. When $G_n^{i,j,a}$ represents a target object O, the value of the target objectness p_o is

determined by multiplying it with the IoU score to encourage specialization within the anchor channel predictions [67]. Conversely, when $G_n^{i,j,a}$ does not represent a target object, p_o is set to 0. Practical implementation involves applying the losses to a batch of images using batched grids. The total loss $LanDet_{loss}$ is computed as a weighted sum of the loss components, scaled by the batch size n_b:

$$LanDet_{loss} = n_b(\lambda_{\text{obj}} l_{\text{obj}} + \lambda_{\text{box}} l_{\text{box}} + \lambda_{\text{cls}} l_{\text{cls}} + \lambda_{\text{cnst}} \sum_{i=1}^{k} w_i.l_{cnst}).$$

where each λ is the weight for the corresponding loss measurement.

3.3.5 Experiments

The ***LanDet*** model underwent training and testing on three distinct datasets: DS1, DS2, and their combined set. This evaluation was performed both with and without the incorporation of physics-informed constraints. The model's performance was assessed using the metrics outlined in Section 3.3.6, and the results were compared against each other as well as against state-of-the-art methods detailed in Section 3.4.1.

For implementation, PyTorch 2.0 was employed, with most hyperparameters inherited and fine-tuned from [193]. All models were trained for 300 epochs using stochastic gradient descent with Nesterov momentum [194], weight decay, and a learning rate decayed over a single cosine cycle [195], with an initial 3-epoch warm-up period [196]. The input images were resized and padded to 640×640 while preserving the original aspect ratio. Data augmentation techniques during training encompassed mosaic [197], translations, horizontal flipping, and scaling. The models were trained on a Geforce RTX-4070Ti GPU with 32 GB of memory, employing batch sizes of 32.

Validation was conducted after each epoch, preserving the model weights that yielded the highest validation Average Precision (AP).

3.3.6 Model Performance and Evaluation Metrics

To evaluate landmark detection as objects, mean Average Precision (mAP) was used. The calculation of mAP involves several metrics and components, including intersection over union (IOU), precision, recall, precision-recall curve, and average precision (AP). To assess the accuracy of the model predictions, we employ the relative root mean square error (RRMSE) to compare the predicted values (PR) with the manual annotation labels (MA). The RRMSE is computed using the following equation:

$$\text{RRMSE} = \frac{\sqrt{\frac{1}{N}\sum_{i=1}^{N}(y_i - v_i)^2}}{\sqrt{\frac{1}{N}\sum_{i=1}^{N}(y_i - \bar{y})^2}} \tag{3.9}$$

Here, y_i represents the manually-measured quantity we aim to predict, v_i denotes our model's prediction, and $\bar{y}$ is the mean of the manual annotation labels, defined as $\bar{y} = \frac{1}{N}\sum_{i=1}^{N} y_i$. The RRMSE is a dimensionless metric, where a lower value indicates better accuracy (0 being the optimal value and 1 representing the threshold of uselessness). Additionally, we define the detection accuracy as:

$$\text{Accuracy} = (1 - \text{RRMSE}) \times 100 \tag{3.10}$$

To evaluate the consistency among surgeons' annotations and the quality of the manual annotation labeling, we involved three senior surgeons to review and annotate

the test dataset. We calculated the intraclass correlation coefficient (ICC) between each reviewer, as well as between the MA and PR measurements. This analysis helps us assess the level of agreement and inconsistencies in the annotations. We have also evaluated the model reliability by comparing the surgeons' measurements with model prediction using the ICC metric. The ICC is a measure used to assess the reliability or agreement among surgeons, MA, and PR in this study. As suggested in [198], we have used the single-rating consistency model as follows:

$$ICC = \frac{MSBS - MSWS}{MSBS + (m-1)\ MSWS} \tag{3.11}$$

where:

$MSBS$: represents the Mean Square Between Subjects (variance between raters),

$MSWS$: represents the Mean Square Within Subjects (variance within raters),

m : represents the number of raters,

Using this metric, we can evaluate the model's reliability by examining the ICC value for each measure in our comparison.

3.4 Results and Discussion

In this section, we present the results and discuss the performance of the ***LanDet*** model on the test datasets, which consisted of 140 images from both DS1 and DS2. The model successfully detected all landmarks in 137 images, achieving an overall

detection rate of 98%. However, it encountered difficulties in two images where it failed to identify the femoral heads and one image where the sacrum landmarks were missed. Note that during manual annotation, the annotators also faced challenges in identifying femoral heads in six test images due to obstacles or partial image cutoffs in that specific area. However, the model predicted the location of femoral heads in these challenging cases, demonstrating its robustness. Moreover, the model showed excellent performance in detecting landmarks, even in scenarios involving spinal or hip implants and low-quality images, despite the limited data available for these cases in the training and validation datasets. We further discuss the accuracy of the model's landmark detection in the following sections.

3.4.1 Model Performance and Accuracy of Automated Measurements

We assessed the performance of the ***LanDet*** model using two separate datasets and combined them into an extended dataset. The inclusion of these datasets separately allowed us to examine the model's performance on different-sized datasets (DS1: 1150 images and DS2: 320 images) and evaluate its performance on two types of X-ray images from different devices (DS1: ordinary and DS2: EOS). Table 3.1 presents the results of the ***LanDet*** model's performance, including the average error, mean and standard deviation of predicted values, mean and standard deviation of manual annotation data, and the accuracy of the model's predictions. The table reveals that the SVA and PT measures demonstrated highest accuracy in DS1, with the model achieving 92.8% and 91.1% accuracy, respectively. Conversely, in DS2, PT and PI measures exhibited the highest accuracy, with 89.2% and 86.6%, respectively. Notably, the model demonstrated good performance even in the dataset with a limited number

Table 3.1: Statistical comparison of the mean values of reference manual parameter measurements (MA) and those obtained automatically by the prediction model (PR). The mean average error (MAE) are presented along with standard deviations (SD) of each parameter evaluated in the two datasets (DS1 & DS2). The relative accuracy of prediction (Acc) is also calculated and presented in last row of each dataset.The highest measured accuracy is shown with **bold** font in each dataset.

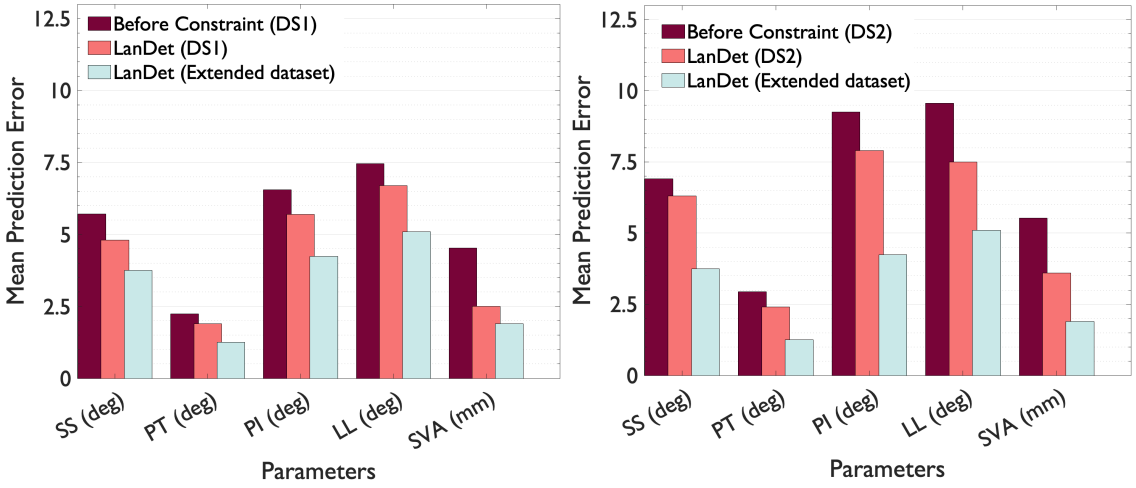
Parameter	**SS°**	**PT°**	**PI°**	**LL°**	**SVA mm**
DS1 MAE	4.8	1.8	5.7	6.7	2.5
DS1 PR (±SD)	42.5 (8.7)	18.1 (10.6)	53.6 (10.2)	48.5 (21.4)	38.2 (3.6)
DS1 MA (±SD)	38.9 (10.3)	19.3 (9.4)	50.8 (12.6)	46.2 (16.2)	34.9 (3.2)
DS1 Acc (%)	*90.2*	*91.1*	*90.1*	*88.6*	***92.8***
DS2 MAE	6.2	2.4	7.9	7.5	3.6
DS2 PR (±SD)	34.9 (11.8)	21.7 (21.4)	62.4 (10.7)	33.9 (17.1)	33.1 (2.5)
DS2 MA (±SD)	30.5 (10.4)	22.1 (19.5)	56.7 (13.7)	37.1 (17.8)	29.8 (2.1)
DS2 Acc (%)	*84.7*	***89.2***	*86.6*	*81.2*	*83.1*

of images (DS2), particularly in the prediction of the PT measure. While increasing the number of images in the dataset led to improved detection performance, the model's performance remained commendable in DS2.

To highlight the impact of the physics-informed constraint approach, we compared the model's predictions before and after applying this technique in a landmark detection as objects model (Figure 3.4). As shown in the figures, the average errors for all measures decreased as a result of the model better understanding the relations between different measures through this approach.

After combining the datasets, we evaluated our model on a larger dataset and assessed its final accuracy. The accuracy results for SS, PT, PI, LL, and SVA were 93.1%, 94.6%, 93.4%, 91.2%, and 94.5% respectively (Table 3.3). Notably, the increased number of images in the training dataset and the higher quality of images in DS2 contributed to improved detection accuracy, with all exceeding 90%. Among

Figure 3.4: Comparison of model performance: ***LanDet*** model with physics-informed constraint versus landmarks as objects model (before constraint) for two datasets. Additionally, the figure presents the performance of the ***LanDet*** model on the combined dataset, allowing for a comparison of its performance on each dataset.



them, PT achieved the highest accuracy of 94.6%.

Table 3.2: Comparison of LanDet Model Estimation Errors with Literature Reports

Measure	**LanDet Model Mean Error and SD**	**Literature (Reported Mean Error and SD)**	
		Upper Range	**Lower Range**
SS	$3.2 \pm 3.1°$ $R = 0.89$	$8.4 \pm 6.3°$ $R = 0.76$	$2.7 \pm 2.9°$ $R = 0.85$
PT	$1.3 \pm 1.1°$ $R = 0.98$	$2.7 \pm 2.5°$ $R = 0.9$	$1.2 \pm 1.7°$ $R = 0.98$
PI	$4.2 \pm 3.1°$ $R = 0.95$	$9.5 \pm 7.1°$ $R = 0.72$	$3.8 \pm 2.0°$ $R = 0.96$
LL (L5-L1)	$5.1 \pm 6.4°$ $R = 0.86$	$11.2 \pm 5.0°$ $R = 0.79$	$4.2 \pm 2.3°$ R = "not reported"
SVA	2.1 ± 1.9 mm $R = 0.98$	3.6 ± 3.5 mm $R = 0.96$	2.0 ± 2.4 mm $R = 0.99$

Table 3.2 illustrates the comparative performance of our model against reported accuracies in the literature across various measures. The table is structured to provide a clear and concise comparison of the metrics, but it should be mentioned that the dataset used in each study is different from each other and from our datasets.

Sacrum Slope (SS): Our model predicts SS with a mean error and standard deviation of $3.2 \pm 3.1°$ and a Pearson correlation coefficient (R) of 0.89. The LanDet model significantly outperforms the lower reported accuracy range of $8.4 \pm 6.3°$, $R = 0.76$ [40], demonstrating enhanced precision. While it shows a slightly higher mean error than the upper range in the literature ($2.7 \pm 2.9°$, $R = 0.85$) [199], the

high correlation coefficient indicates its reliability.

Pelvic Tilt (PT): The model shows a mean error of $1.3 \pm 1.1°$ with an R of 0.98 for PT. This performance is within the highest accuracy range reported in the literature, which spans from $2.7 \pm 2.5°$, $R = 0.9$ [30] to $1.2 \pm 1.7°$, $R = 0.98$ [31]. This indicates that our model is not only consistent with top-performing models but also tends towards a lower error margin, highlighting its precision.

Pelvic Incidence (PI): For PI, our model registers $4.2 \pm 3.1°$, $R = 0.95$, compared to a reported range in the literature of $9.5 \pm 7.1°$, $R = 0.72$ [40] to $3.8 \pm 2.0°$, $R = 0.96$ [199]. Here, our model demonstrates significant accuracy, surpassing the lower range of reported values and closely matching the higher accuracy models in both precision and correlation.

For the Lumbar Lordosis (LL) measure, our model's performance is represented as $5.1 \pm 6.4°$ with a Pearson correlation coefficient (R) of 0.86. When compared with the reported accuracies in the literature, our model demonstrates competitive performance. The lower range of accuracy in the literature is reported as $11.2 \pm 5.0°$, $R = 0.79$ [40], while the upper range is $4.2 \pm 2.3°$ [41], with the correlation coefficient not reported.

Sagittal Vertical Axis (SVA): Our model estimates SVA with a mean error of 2.1 ± 1.9 mm and a correlation coefficient of 0.98. This compares favorably with the literature range of 3.6 ± 3.5 mm, $R = 0.96$ [28] to 2.0 ± 2.4 mm, $R = 0.99$ [31]. Our model's results for SVA are commendable, situating it well within the range of existing models and demonstrating a good balance between accuracy and reliability.

In summary, our model exhibits robust performance across a range of measures, consistently matching or surpassing the literature-reported accuracy. This highlights the model's potential as an effective tool in its respective field, particularly noteworthy

Table 3.3: Statistical comparison of mean values of reference manual parameter measurements (MA) and those obtained automatically by the prediction ***LanDet*** model (PR) for the combined dataset. The mean average error (MAE) are presented along with standard deviations (SD) of each parameter evaluated in the two datasets (DS1 & DS2). The table also include the correlation analysis using R Pearson correlation coefficients, and relative accuracy of prediction (Acc).

	MAE (±SD)	PR (±SD)	MA (±SD)	Correlation		Acc (%)
				R	p	
SS°	3.2 (2.7)	39.8 (9.4)	37.9 (10.3)	0.89		*93.1*
PT°	1.3 (1.1)	19.2 (13.3)	20.2 (12.9)	0.98		***94.6***
PI°	4.2 (3.1)	53.7 (12.4)	52.8 (12.3)	0.96	<0.0001	*93.4*
LL°	5.1 (6.4)	38.3 (19.5)	40.3 (16.7)	0.86		*91.2*
SVA$_{mm}$	2.1 (1.9)	3.5 (3.1)	3.3 (2.9)	0.98		*94.5*

in its precision and reliability. There are some measures that our model accuracy is less than what has been reported in the literature. Noting that the dataset size, image quality, and number of detection classes are different in each study as well as our study, the discrepancies could be because of the mentioned reasons. For instance, [31] had a dataset including 2500 images compared to our dataset of 1400 images. On the other hand, [199] mentioned that cases involving minors whose skeletons have not fully matured and instances of degenerative disk disease, where the vertebra corners are challenging to discern, were omitted from their dataset. Additionally, only high-quality images with appropriate contrast and brightness levels for clear observation were included, while we almost did not exclude any images from our dataset to represent its capability for a real-world application.

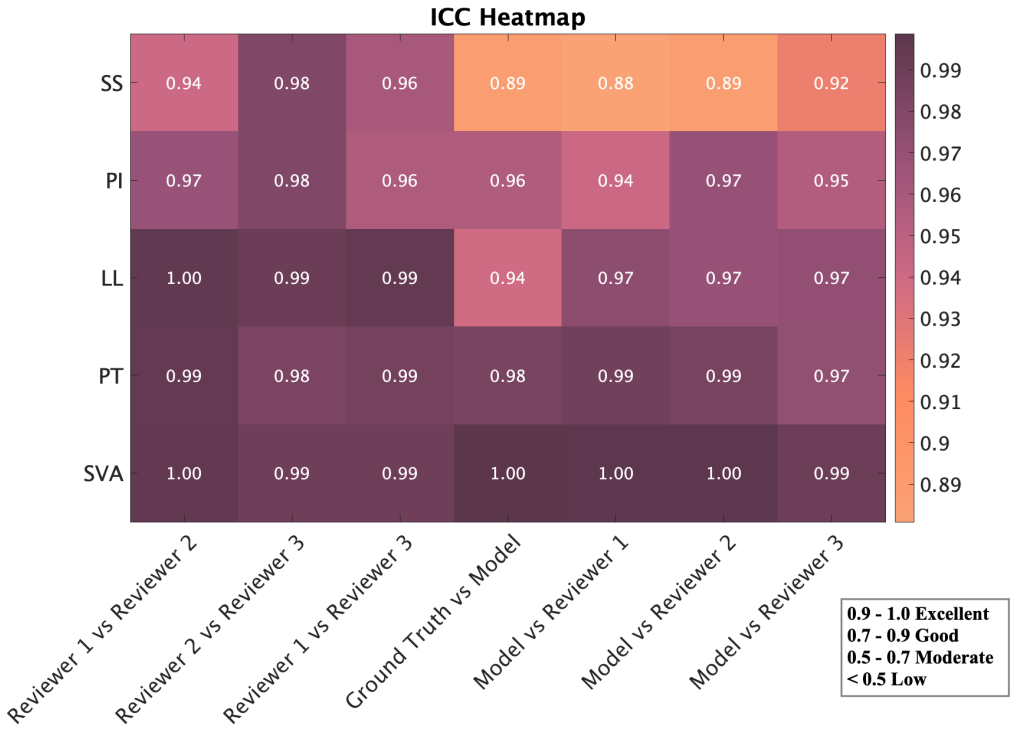
In conclusion, our model demonstrated competitive performance across various measures compared to the literature. These results highlight the effectiveness of utilizing physics-informed constraint method, which we used in our landmark detection

as object algorithm (***LanDet***). The model has shown promising performance in detecting landmarks, and the physics-informed constraint approach is proven to be effective of improving the accuracy across different measures. Also, combining the datasets has enhanced the model's robustness and generalizability to new imaging sources and devices.

3.4.2 Model Reliability and Level of Agreement Between the Model and Surgeons

To evaluate the model reliability and to compare the model performance against surgeons, the automatic extracted measures from the model is compared to measures form three surgeon annotations. For this purpose, ICC metric is used and the results are shown in Figure 3.5. Our model showed a better consistency with surgeons compared to what has been previously reported in the literature [31]. Mean ICC values reported in [31] are as follows: SVA at 0.99, PT at 0.96, LL at 0.90, SS at 0.84, and PI at 0.78. The ICC values for our model and reviewers in Figure 3.5, shows higher values (i.e. better consistency) in all measures.The ***LanDet*** deep learning model was able to meet the reliability of surgeon reviewers in all of the measures, as the ICC values for model versus surgeons closely mirrored those for surgeon versus surgeon, with all but three SS values (0.88, 0.89, 0.89) over the score of 0.9, indicating excellent correlation in each comparison [198]. Our findings align with the conclusions drawn in previous research, which also reported the highest error or variability and less consistency in measuring SS [200, 30, 31].

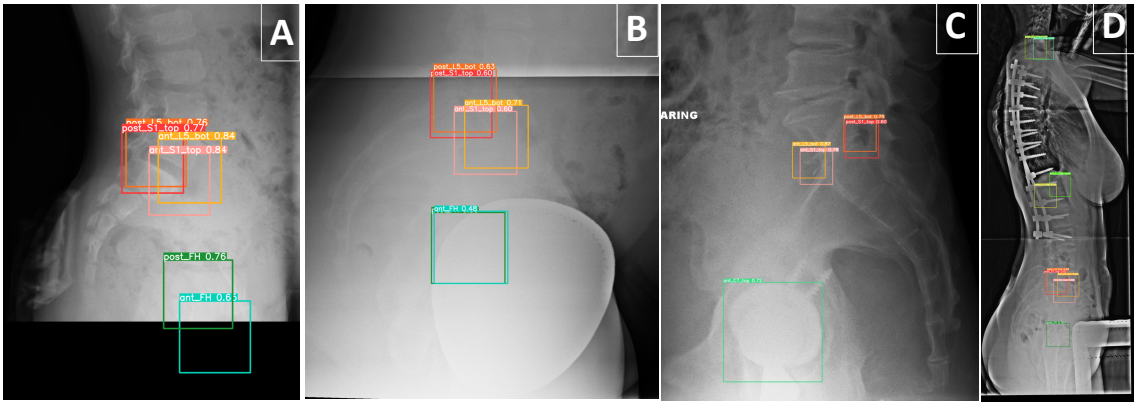
Figure 3.5: ICC metric results for the evaluation of model reliability by comparing the extracted results from the model with manual annotation by three surgeons (Reviewer1: senior spine surgeon, Reviewer2: senior neurosurgeon, and Reviewer3: senior orthopedic surgeon).



3.4.3 Limitations and Advantages

The performance of the model not only aligns well with existing literature and correlates well to surgeons' annotations but also showcases exceptional proficiency in managing unique scenarios and addressing challenges associated with the identification of adjacent landmarks. This is primarily attributed to the incorporation of geometrical constraints in the LanDet physics-informed deep learning model. We evaluated the model on two distinct datasets, demonstrating its adaptability to different scenarios and images from diverse sources. Figure 3.6 showcases four specific instances where the model accurately identified the required landmarks, even with patients having spinal or hip implants or images with partial cutoff or obstructed by protective shields. Despite the scarcity of training images for such special cases, our model proved successful in handling them effectively. It is worth noting that manually annotating landmarks in such cases, particularly those with obstacles or partial image cutoff, can be challenging.

Figure 3.6: Challenging cases successfully addressed by the model in the datasets: A) Partially cut-off images, B) Images with obstacles in the hip region, C) Images from patients with hip implants, D) Images from patients with spinal implants.



Previous studies in the literature [31, 30] have highlighted the challenge of missing

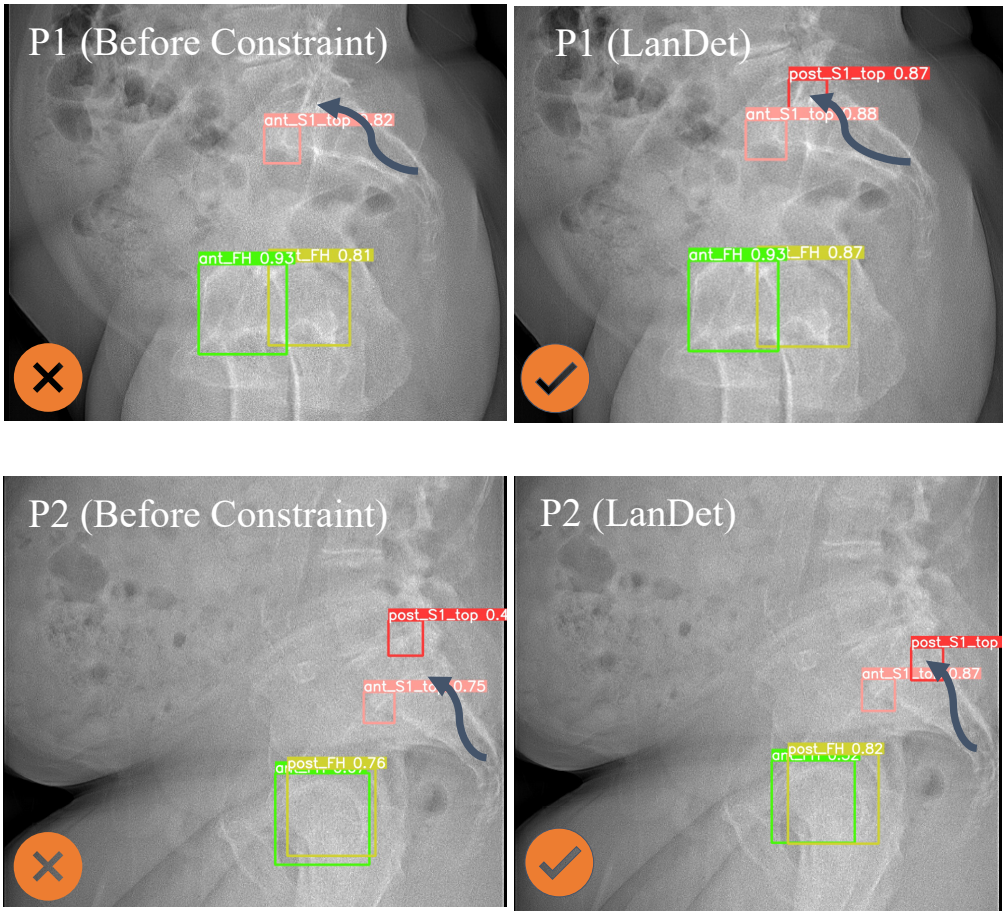
specific landmarks and difficulty in distinguishing between adjacent and similar anatomical landmarks. In our research, we encountered similar issues until we introduced physics-informed constraints into our model. As illustrated in Figure 3.7, the ***LanDet*** model successfully addresses these challenges by incorporating the concept of landmarks as objects with the integration of physics-informed constraints.

The primary limitation of LanDet is the availability of data. As expected, a larger training dataset would likely lead to better model performance. While the model demonstrated robustness in detecting landmarks in challenging cases, improving the accuracy of these detections would be possible by increasing the number of images from patients with abnormalities or spinal implants in the dataset.

3.5 Conclusion

In this chapter, we presented a novel deep learning approach for detecting anatomical landmarks as objects, surpassing the limitations of previous models that heavily relied on heat-map regression. By incorporating physics-informed constraints into our deep learning models, we achieved significant improvements in landmark detection accuracy. Moreover, our approach demonstrated robustness in challenging scenarios, including cases with implants, protected regions, and partially obscured images, even when training data for such scenarios was limited. Furthermore, our model effectively addressed the issue of mis-detection of similar or adjacent landmarks. The landmark detection performance for SS, PT, PI, LL, and SVA measures was evaluated, comparing results between datasets of different sizes and against the existing literature. Our model achieved competitive performance while offering the aforementioned advantages. To assess the reliability of our model, we compared its

Figure 3.7: The advantage of applying physics-informed constraints, which improved the accuracy of localization of some similar and adjacent landmarks. The superior posterior corner of S1 is not detected before applying constraints, P1 (without constraints), which is solved by LanDet that incorporate geometrical constraints (P1 LanDet). Also, a mis-detection of L5 superior posterior (P2 without constraint) instead of S1 superior posterior is resolved by LanDet (P2 LanDet).



predictions against those of three senior surgeons, using the ICC metric. The results revealed a high level of agreement between our model and the expert surgeons.

In conclusion, our proposed deep learning approach presents a significant advancement in the field of anatomical landmark detection. Its success in handling challenging scenarios and achieving comparable performance to expert evaluations makes it a valuable tool for clinical applications and research studies. The integration of physics-informed constraints into the deep learning framework opens new possibilities for accurate and robust landmark detection in medical imaging. In Chapter 4 and Chapter 5, we illustrate the utilization of the advanced ***LanDet*** deep learning model for the efficient extraction of spinopelvic measures and the subsequent patient categorization based on automated measurements. This categorization is instrumental in determining the optimal patient-specific cup implant orientation by assigning the appropriate spinal stiffness parameters.

Chapter 4

Motion Capture Experiment and Radiographic Analysis

4.1 Chapter Overview

In Chapter 2, we reviewed the literature and the findings in Section 2.3.2 were primarily centered on X-ray image analysis of sitting and standing postures. While X-ray analysis is essential for THA surgery, it's critical to explore the dynamic transition between sitting and standing positions further. To address this, we conducted two experiments in Section 4.2: motion capture and radiographic analyses. These experiments allowed us to assess spine stiffness and different spinopelvic motions and to understand the effect of different spinal conditions on lower limb motion. The radiographic analysis demonstrates the current method for evaluating spinopelvic stiffness, highlighting the significance of the automatic extraction of spinopelvic measures introduced in Chapter 3.

However, as our literature review in Chapter 2 highlighted, static X-ray images may not fully capture the dynamics of human motion. Although X-rays are integral to pre-operative planning, the motion capture experiment reveals a crucial moment when impingement can occur. This moment occurs in a transitional phase, not in the typical sitting or standing positions, and varies for each patient-specific condition. Although motion capture is not a routine pre-operative procedure, it underscores the necessity for predictive simulations, a concept elaborated upon in Chapter 5. This predictive simulation is pivotal in addressing these dynamic considerations.

4.2 Case-Study Experiments: Motion Capture and Radiographic Analyses of Human Sit-to-stand Movement

To investigate the importance of a dynamic motion analysis rather than relying on static X-ray images, two case study experiments were performed, and their results compared to those in the literature. In the first experiment, we used sitting and standing X-ray images for 87 patients. Different spinopelvic measures were extracted, and a functional relationship between spine stiffness and these measures has been introduced. In addition, patients with spinal fusion were considered as a separate group, and their spinopelvic measures were compared to those of the first group. The second experiment in this study was a dynamic motion analysis using motion capture data. In this experiment, the importance of dynamic motion analysis for pre-operative planning has been discussed. The results of our dynamic motion analysis matched those of the static X-ray data analysis, and provided more information on the dynamic

transition from sitting to standing posture as well as the most probable moment in a sit-to-stand motion during which an impingement or dislocation can happen. The motion capture method has been used to highlight the power of a dynamic motion analysis over a static X-ray. Other methods that can be used for a dynamic motion analysis are predictive dynamic simulation or video fluoroscopy. We demonstrated that some information is missing in static X-ray studies, which a dynamic motion analysis can provide. For this purpose, motion capture analysis was used, which has less limitation for data collection comparing to video fluoroscopy, and more clinically reliable than a predictive dynamic simulation.

4.2.1 Radiographic Analysis

The effect of spine stiffness and different spinopelvic measures on pelvic movement have been discussed in Section 2.3, and relevant studies have been reviewed. In this section, we evaluate some of the hypotheses proposed in the literature by analyzing X-ray images. In total, the sitting and standing X-rays of 87 patients were selected (174 X-ray images). Spinopelvic measures (i.e., SS, PT, PI, and LL) were extracted for each patient for both postures, as shown in Figures 4.1 and 4.2. Patients were categorized based on their spinopelvic measures and prior spine fusion surgery. As can be seen in Figure 4.3, patients with normal spinopelvic movement (68%), patients with a restriction in pelvic range of motion from sitting to standing ($\Delta PT < 10^{\circ}$) (27%), and patients with prior spine fusion surgery (5%) are all included. Using the automatic extraction of spinopelvic measures from Chapter 3, we extracted the required measures for this study [38].

The changes in sacral slope (ΔSS) and lumbar lordosis (ΔLL) between sitting and standing have been compared for each patient. A stationary pelvis (i.e. $\Delta SS \leq 10^{\circ}$)

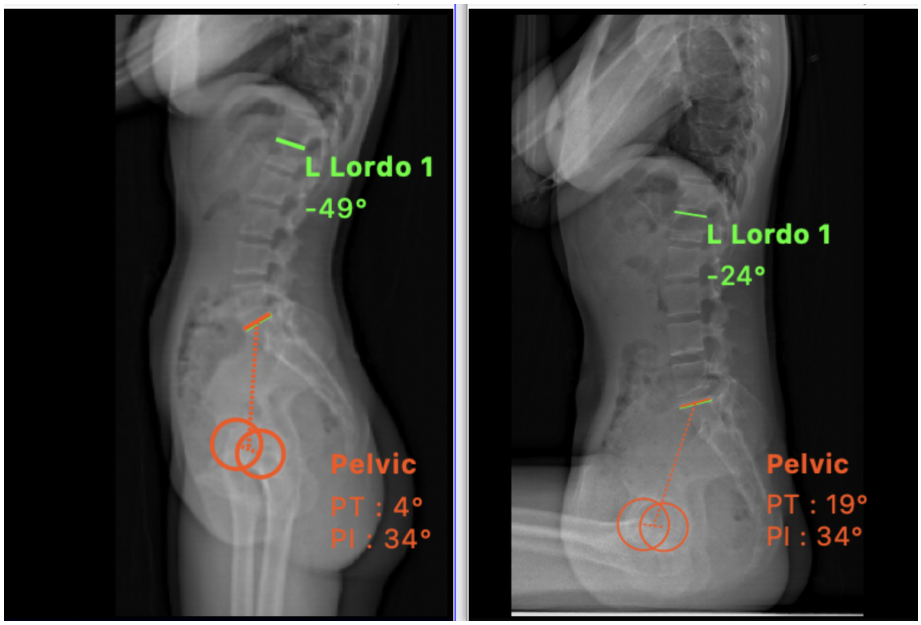


Figure 4.1: Spinopelvic measures changing between standing (left) and sitting (right) postures for patient with no prior fusion surgery. The pelvis is tilted effectively, with a change of 15 ° ($\Delta PT = 15°$), and the spine has contributed to the motion with a change in LL ($\Delta LL = 25°$).

Table 4.1: Spinopelvic measures and their changes from standing to sitting position for patients with prior fusion surgery

Levels of fusion	ΔSS	ΔLL	$PI - LL$ (standing)
L5-L4	10°	9°	−5°
L4-L3	17°	11°	−27°
S1-L5-L4	4°	8°	21°
S1-L5-L4	6°	4°	8°

was considered as the main criterion affecting the outcome of a THA surgery, primarily because spinal stiffness leads to a restriction in the pelvic range of motion. As can be seen in Figure 4.4, all patients with a stationary pelvis (ΔPT or $\Delta SS < 10°$) had restriction in the change of LL ($\Delta LL < 20°$). But this hypothesis is not valid in reverse, which means that some patients with $\Delta LL < 20°$ had a normal pelvic motion. Thus, limited ΔLL can be considered as a risk factor for PT restriction, and increased risk of impingement or dislocation after THA, but pelvis motion analysis is necessary to understand the effect of restricted spinal motion. This hypothesis has been evaluated for the category of patients with prior fusion surgery. As can be seen in Table 4.1, although the fusion surgery caused a restriction in LL change ($\Delta LL < 20°$), the consequence of that on ΔSS ($= \Delta PT$) was different in each level of fusion. Different levels of fusion and other factors like physiological and anatomical features appear to have influenced the resulting ΔSS. Unlike some reports that correlate the pelvic inclination to PI [201, 13], our data shows no meaningful relationship between a change of pelvic inclination (or ΔPT) and PI. The last thing that we evaluated was the alignment criterion ($PI - LL$) for standing position. We cannot find any meaningful relationship between a stiffer spine or stationary pelvis with spinal deformity ($PI - LL > 10°$) defined in [21]; however we did not evaluate the effect of this criterion on increasing rates of dislocation.

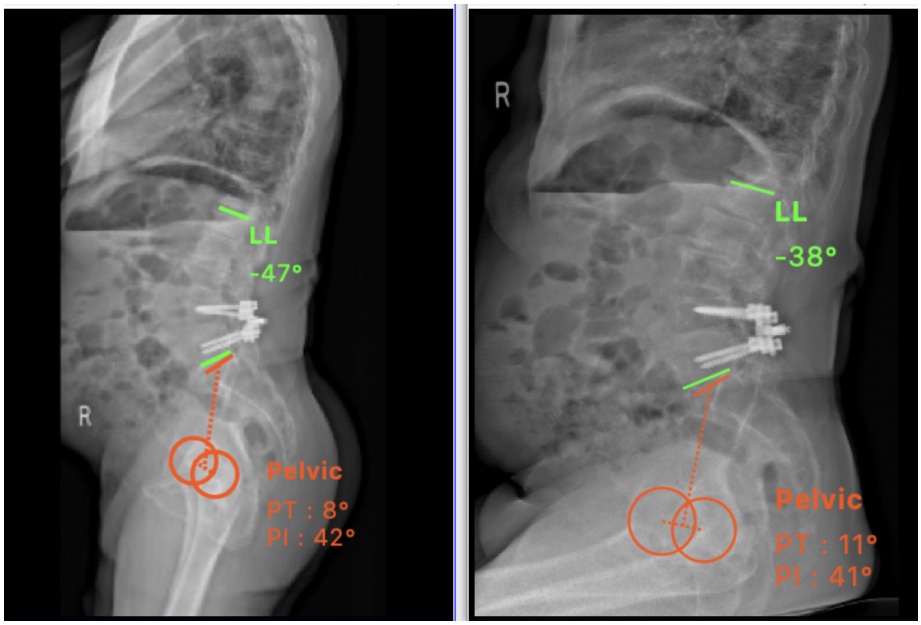


Figure 4.2: Spinopelvic measures changing between standing (left) and sitting (right) postures for a patient with prior fusion surgery. Because of the stiffer spine ($\Delta LL = 9°$), the pelvis has lost the ability to tilt through a large angle ($\Delta PT = 3°$), increasing the patient's risk of dislocation after THA.

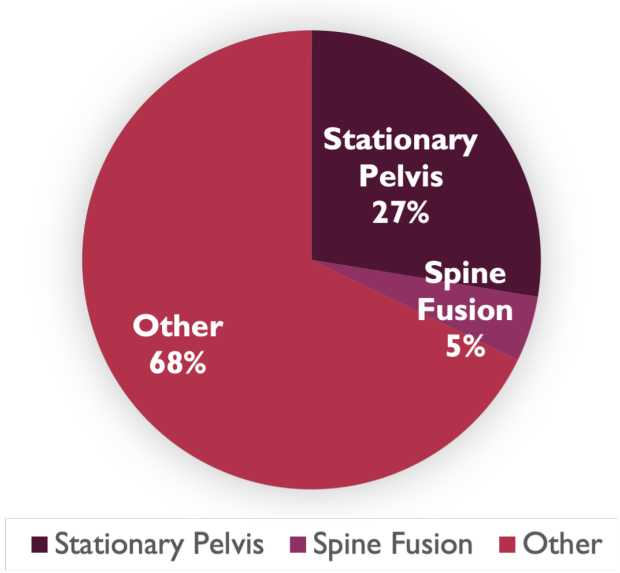


Figure 4.3: Data distribution and patient categorization

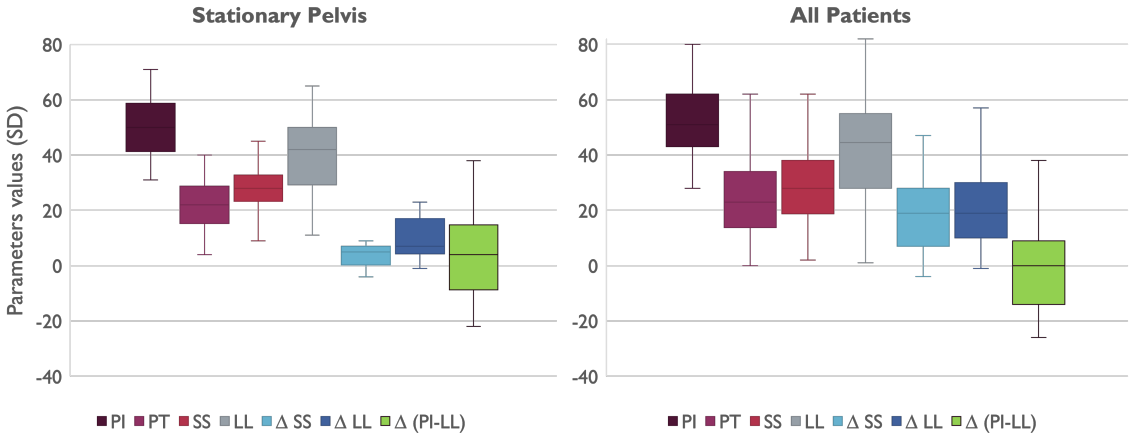


Figure 4.4: A comparison of spinopelvic measures for the category of stationary pelvis and all patients. The box and whisker plots indicate the mean, minimum, maximum, lower quartile, and upper quartile of the data.

4.2.2 Motion Capture Analysis

Static X-ray images provide information only for sitting and standing postures. Tracking the spinopelvic measures and joint angles during the transition between the two would be an advantage of motion capture analysis.

An experimental study was performed to measure the kinematic behavior of the spinopelvic complex during a sit-to-stand movement. For this purpose, a motion capture setup has been used at the University of Waterloo after we got ethics approval from the ethics committee on "multibody biomechanical modelling of activities of daily living. In this process, using six Eagle cameras and passive markers, we extracted the positions and orientations of each body segment (i.e. head, spine, and legs). Six participants were instructed to perform five trials of sit-to-stand and stand-to-sit motions with their hands crossed on their chests. We later chose two of them who had differennt spinopelvic movement and presented the results for these two. The information on these participants is provided in Table 4.2. For each trial, a normal sit-to-stand motion has been performed from a sitting posture on a stool with a height of 60 cm. Anatomical marker placement is shown in Table 4.3 and Figure 4.5, providing the position and orientation of body segments. Using this information, joint angles during the motion have been calculated (Appendices A and B). The results are presented in Figure 4.6.

4.2.3 Different Spinopelvic Motions

The joint angles extracted using experimental motion capture data provide information about spinopelvic behavior during a sit-to-stand motion. Three variables have been extracted from the joint angle results for further analysis. Figure 4.7 shows the

Table 4.2: Volunteer participant information

Participant information	1	2
Gender	Male	Male
Age	28	29
Weight	86.5 Kg	55.6 Kg
Height	177.2 cm	175.6 cm

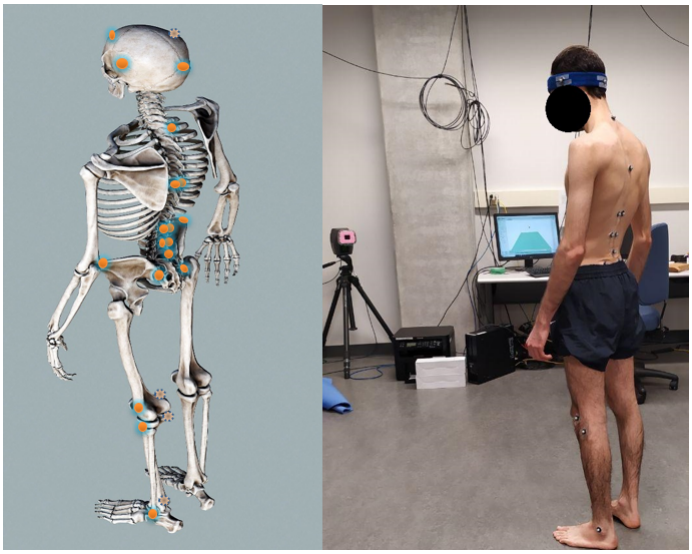


Figure 4.5: Marker placement on the subject

Table 4.3: Anatomical marker placement

Anatomical landmarks	Details
Pelvis	ASIS (Anterior superior iliac spine) PSIS (Posterior superior iliac spine)
Thigh	MFC (Medial femoral condyle) LFC (Lateral femoral condyle)
Shank	MTC (Medial tibial condyle) LTC (Lateral tibial condyle) Medial malleolus on the shank Lateral malleolus on the shank
Spine and Head	Lumbar part: L5, L3, L1 Thoracic part: T6 Cervical part: C7 Head: Front, Back, Right Left

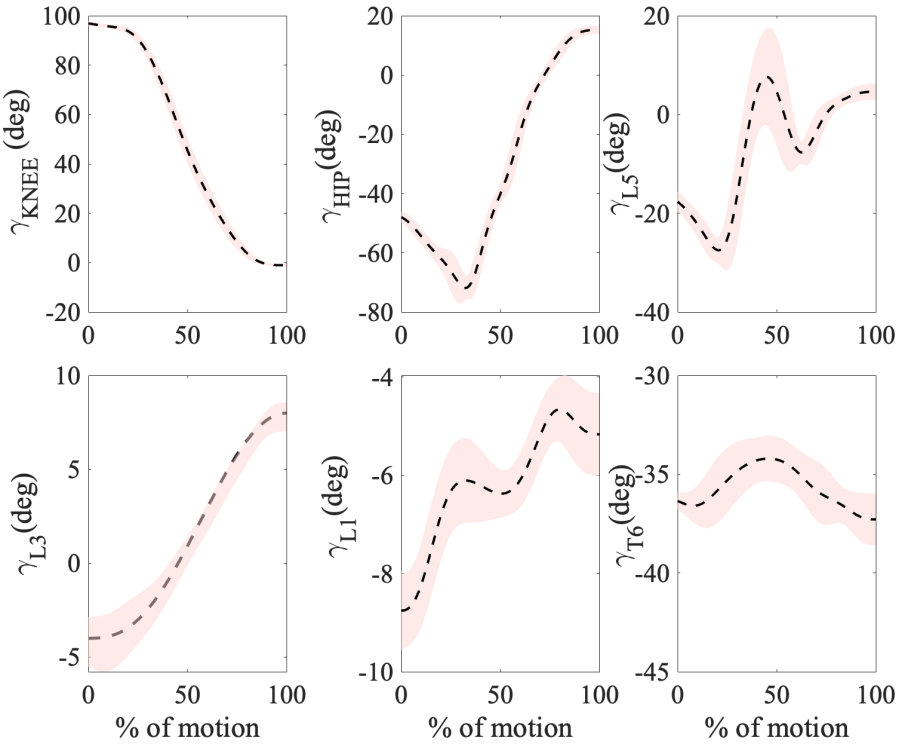


Figure 4.6: Joint angle results from the motion capture experiment, with dashed lines representing mean values and shaded areas denoting standard deviation across trials.

trajectories of pelvic tilt (PT), lumbar lordosis (LL), and hip joint angle during the motion for both subjects from sitting to standing. Comparing these results to the static x-ray images for standing or sitting posture confirms that a dynamic motion analysis is more informative than static x-rays. Comparing lumbar lordosis and pelvic tilt changes during the motion for these two subjects, it can be concluded that subject 1 has a stiffer spinopelvic complex (less LL and PT change during the motion). The results from this method not only provide ΔPT and ΔLL (static comparison of sitting and standing postures), but also allow us to follow the trajectory of changes in PT and LL throughout the whole range of motion. Using static X-ray images may not predict the critical moment when the risk of impingement or dislocation is most acute. Examining the results in Figure 4.7, the higher hip joint angle with less pelvic tilt could be assumed to be the most problematic moment for impingement or dislocation after THA (subject 1). Figure 4.7 shows that the most critical moment for a probable dislocation is neither sitting nor standing. The points with a higher hip joint angle (Point P1: subject1, Point P2: subject 2) coincide with lower pelvic tilt and are the critical moments. As can be seen in Figure 4.7, the potential critical moment for a possible dislocation is a subject-specific moment between sitting and standing posture when the subject is leaned forward and ready for standing up (different time for points P1 and P2).

Considering results from both motion capture analysis and X-rays, a hypothesis can be developed on the effects of spine stiffness on different spinopelvic motions. As can be seen in Figures 4.4 and 4.7, all patients with restricted pelvic tilt ($\Delta PT < 10^\circ$) have restricted spinal motion ($\Delta LL < 20^\circ$). In addition to these restrictions, the dynamic motion analysis showed less variation in LL for the subject with stiffer spine (not just in sitting and standing) during the movement as well. Thus, lower variation

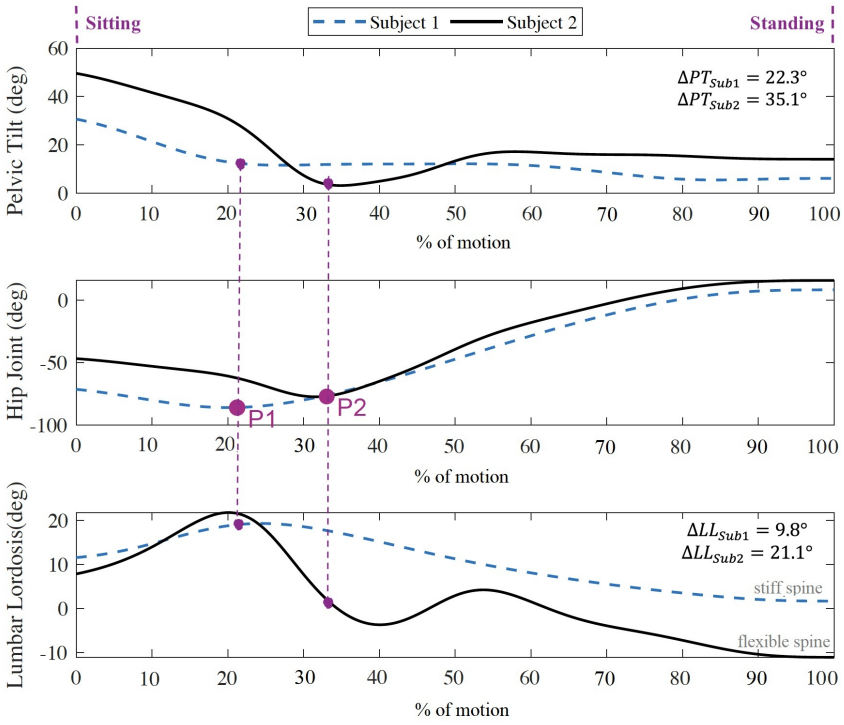


Figure 4.7: Motion capture experiment results: A comparison between hip joint angle, pelvic tilt, and lumbar lordosis changes during motion for two subjects with different spinal stiffnesses.

in LL from standing to sitting should be considered as a risk factor for pre-operation THA surgery planning as recently suggested by Vigdorchik et al. [21]. But PT, LL and hip joint angle should also be considered together to decide whether a spinopelvic complex is stiff or not. The stiffer the spinopelvic complex, the less contribution of the spine and pelvis to postural changes. The less the pelvis contributes to the motion when the hip joint has the same or more range of motion, the greater the risk of impingement due to the more-stationary pelvis in these subjects. Indeed, the pelvis in subjects with a stiffer spinopelvic complex provides less backward tilting in the middle of the motion as well as less forward tilting at the end of a sit-to-stand motion (Figure 4.7). The results from dynamic motion analysis here are consistent

with reports in the literature; for instance, Espasito et al. claim that "Patients who dislocated had significantly less spine flexion, less change in pelvic tilt, and more hip flexion from standing to sitting positions compared to patients with normal spines" [19]. Moreover, as we have shown, using dynamic motion analysis may help to detect the critical moment of a possible dislocation, a valuable advantage in pre-operative THA planning.

4.3 Discussion and Conclusion

This research has reviewed relevant clinical studies on the effects of spinopelvic measures on THA surgery. Regarding the suggestions and conclusions provided in most studies reviewed in this paper, the importance of patient-specific THA surgery planning that considers different spine stiffness and spinopelvic measures becomes clear. Comparing the summary of research in Table 2.1, it can be concluded that recent research is focused on finding a correlation between different spinopelvic measures and the outcome of THA surgery, as well as the effects of spine fusion surgery and spine stiffness. To evaluate some of the recommendations in the literature, two experiments were designed to analyze spinopelvic measures and motion. The results of our experimental motion capture and radiographic (X-ray) analysis were compared, showing the influence of different spine properties and spinopelvic relationships on pelvic tilt (PT) and hip range of motion (ROM). The change of pelvis and lower limb motion resulting from different spine types and/or spinopelvic measures can affect the risk of impingement or dislocation post-surgery. The results from X-ray data analysis showed that patients with restricted spine movement ($\Delta LL < 20°$) experience restriction in pelvic motion ($\Delta PT < 10°$) (all patients with a stationary

pelvis ($\Delta PT < 10°$) had restriction in the change of LL ($\Delta LL < 20°$)).

Although using predictive dynamic simulation or video fluoroscopy can be more practical options for a dynamic motion analysis, using motion capture analysis provides more information compared to X-ray analysis, and with fewer clinical restrictions. We did not want to introduce an alternative to X-rays; instead, our intention of using this dynamic motion analysis was to clarify the fact that some information missing from static X-ray studies can be provided by dynamic motion analysis. Comparing the results (i.e., PT, LL, and hip joint angle) to X-ray analysis showed that the most likely moment for a dislocation is neither sitting nor standing. As shown in Figure 4.7, the critical moment for a possible dislocation is a subject-specific moment between sitting and standing posture when the subject is leaning forward and ready to stand (a different time for each subject: points P1 and P2). Also, the dynamic motion analysis showed that if we only stick to the restricted pelvic tilt ($\Delta PT < 10°$) criterion in the preoperative analysis, we would not be able to identify some candidates with spine stiffness. For instance, in our dynamic motion analysis the subject with a stiffer spine ($\Delta LL < 20°$) did not have pelvic tilt restriction($\Delta PT < 10°$), but experiences less variation in LL and PT (not just in sitting and standing) during the movement. In a standard X-ray analysis utilizing only static sitting and standing positions, a subject with a stiff spine might be overlooked. However, incorporating dynamic motion analysis can help in identifying such cases more effectively. Consequently, the last observation from our dynamic motion analysis is that valuable information is missing if we follow only a static X-ray approach before THA surgeries. In fact, tracking the change of hip joint angle and spinopelvic measures (LL and PT) during motion is as important as X-ray analysis that provides information only from sitting or standing postures. Hip joint changes are correlated to some spinopelvic measures and spine

stiffness. The results from our dynamic motion analysis showed that less variation in LL from standing to sitting should be considered a risk factor in pre-operative planning. A crucial aspect to note is that evaluating PT, LL, and the hip joint angle collectively is essential in determining the stiffness of the spinopelvic complex. Therefore, integrating dynamic motion analysis, which offers additional insights into patient-specific spinopelvic motion, is strongly advised for enhancing the outcomes of THA surgery in future pre-operative planning. In Chapter 5, we explore predictive simulation and the optimization of patient-specific cup implant orientation, a key strategy to prevent impingement.

Chapter 5

Predictive Human Model of Sit-to-Stand Motion Influenced by Spine Stiffness to Optimize Cup Implant Orientation in THA

5.1 Chapter Overview

The traditional Lewinnek safe zone used as a guideline for Total Hip Arthroplasty (THA) surgery has been found to be inadequate, as dissatisfaction rates have risen after this surgery [18]. It is evident that spinopelvic parameters and spine stiffness, factors that have been overlooked previously, must be taken into account for optimal surgical outcomes. In addition, in Chapter 2 and 4, we discussed the necessity of a dynamic analysis of motion to achieve an optimized cup implant orientation for THA.

In this chapter, a novel predictive dynamic modelling approach is proposed to address the aforementioned gaps. This approach involved the development of a multibody model of a human that contained nonlinear spinal elements, which was validated by comparing it to literature in-vitro experiments and conducting a motion capture experiment explained in Chapter 4. To simulate human sit-to-stand motion, this model was employed with an optimal control approach based on trajectory optimization. Human joint angles were extracted from conducted simulations of different scenarios: normal, fused, and stiff spines.This chapter will discuss recommended optimized cup orientations for patients with anterior or posterior pelvic tilt, which influence lower limb movement. It will also cover scenarios combining pelvic tilt with a stiff spine. Different spinal stiffness parameters are used for the stiff spine condition based on spinopelvic measures and patient categorization. This process can be done automatically based on the approach presented in Chapter 3. The optimal acetabular cup orientation was calculated based on implant impingement criteria using predicted motions for different spinal condition scenarios, and the results compared to the clinically recommended orientation values for the same categories of patients in Section 5.4.4. This research is the first of its kind to examine spine flexibility in different scenarios and its impact on lower limb motion. The findings of this chapter could help improve THA surgical planning and reduce the risk of hip impingement or dislocation after THA.

5.2 Introduction

One of the most important parts of a THA surgery is cup positioning and orientation [24] to reduce the risk of later impingement or hip dislocation. The widely-adopted

guideline for the cup orientation is the Lewinnek safe zone [25]. However, this metric was shown to have minimal correlation with the risk of hip dislocation [13, 26, 27], which also depends on factors such as pelvic tilt (PT) and spine flexibility that are ignored by the Lewinnek guidelines.

Considering the spine for lower limb motion analyses might at first glance be seen to require excessive work for only negligible outcome, but a look at the increasing number of patient complaints after THA surgeries [18] highlights the importance of considering other factors like the spine stiffness, pelvic motion, and spinal fusion in lower limb dynamic analysis. Recent clinical evaluations show increased rates of dissatisfaction after THA, indicating that relying on the traditional Lewinnek safe zone [25] is not practical for all patients [21, 13, 20]. It appears that, for optimal cup positioning and orientation during the THA, not only the lower limb dynamics but also the effects of the spine on lower limb motion must be considered [21]. Different spinal conditions and stiffness have a direct effect on THA surgery; if the spine is too stiff or rigid, the prosthetic implant may not be properly aligned or seated, leading to joint instability, pain, and even implant failure [13]. Additionally, a stiff spine can limit the range of motion of the hip joint, resulting in decreased function. Therefore, it is important to assess spine stiffness prior to THA surgery to ensure the best outcome. Thus, surgeons should consider different spine types and their effects on lower limb motion in their preoperative plannings. The more flexible the spine, the more contribution it has in daily activities [13]. As discussed in Chapter 4, currently, surgeons use lateral X-ray images of the spine and pelvis, usually from standing and sitting postures, to plan the THA surgery [22]. Relying only on these two X-ray images might not be sufficient to obtain the spine stiffness, since it cannot be easily evaluated using static X-ray from two stationary positions. Thus, we are motivated

to move from stationary X-ray image analysis to a full dynamic motion analysis before and after THA surgery, which includes spine stiffness evaluation. The following paragraphs explain different reasons for spinal stiffness, the current surgical approach to include the spine, and how using a predictive dynamic model can improve THA surgery outcomes.

Individuals with stiffer spines (restricted spinal joint angles), which may arise from spinopelvic abnormalities, spinal fusion surgery, and aging, will have different spinal dynamic behaviors during daily activities such as sit-to-stand motion. Currently, assessing spine stiffness involves comparing sitting and standing X-ray images and analyzing spinopelvic parameters, such as pelvic tilt in sitting and standing postures [201]. In cases of stiff spines, some surgeons consider modifying the implant position and orientation (categorizing patients and providing qualitative modifications tailored to each category) in order to incorporate the effect of the stiffer spine [21, 202]. However, the exact mechanisms involved and their influence on an operation's outcome have not yet been clarified [6]. Therefore, a quantitative analysis that suggests patient-specific implant orientation becomes necessary.

As discussed in Chapter 2, the main reason reported for changes in spinal stiffness is spinal fusion surgery [10, 97, 98, 99, 100]. However, spine disorders [98], and aging [203] are also reported to have some effect on the spine mobility, which is introduced as "late dislocation". Recent research gave spine fusion surgery as the main reason for spine stiffness, which can affect the outcome of THA surgery [97, 99, 98]. When a spinal fusion results in a fixed spinal alignment [27] or involves the sacrum and some levels of the lumbar spine, the risk of impingement increases as a result of excessive spinal stiffness [105]. In addition, changes in biomechanical properties of the spine elements (i.e., Inter-vertebral Discs (IVDs), ligaments, and muscles), which

can be the result of aging or disc degeneration [204, 205, 206], can result in different spine stiffnesses. Surgeons categorize their patients based on different spine-hip relationships and propose different implant cup positioning and orientation according to these categories [21, 109]. Although these qualitative representations of different spine-hip relations help surgeons to consider different approaches for those who might have stiffer spines, they do not identify the underlying mechanism of how different levels of fusion, aging, or spine deformity can affect lower limb motion.

In this chapter, we present a predictive dynamic model for human motion simulation, aiming to bridge the existing knowledge gap in THA and enhance preoperative surgery planning. Given the prevalence of implant impingement or dislocation after THA during the sit-to-stand motion [207], which is a highly repetitive daily activity, our focus lies on the predictive simulation of this specific motion. We further investigate various scenarios involving the dynamic model of patients with different spinal conditions. This modelling approach has the potential to provide surgeons with numerical insights into the predicted dynamic motion beyond those given by static X-rays. Moreover, the forward dynamics method is used to simulate different scenarios and answer "what if?" questions in terms of spinopelvic and lower limb motion. Note that the US Food and Drug Administration (FDA) has supported the use of computational models to improve medical device performance [107]. By employing this parametric analysis using predictive models, surgeons can modify stiffness factors and directly observe the effects on lower limb dynamic motion, which is an improvement from the general categorization and treatment advice outlined in [98, 21].

5.3 Method

5.3.1 Overview

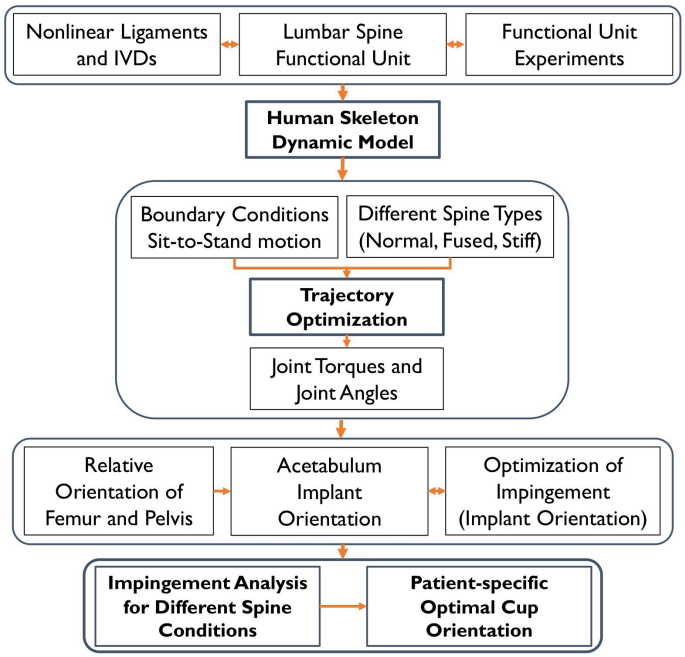


Figure 5.1: The framework of evaluating the effect of different spine conditions on lower limb motion and obtaining optimal cup orientation to avoid implant impingement after THA.

The main components of the proposed methodology are presented in Fig.5.1. To begin, a functional lumbar spine unit is designed and modelled with nonlinear ligaments and intervertebral discs (IVDs). This model is then validated by comparing its range of motion with literature in-vitro experiments. Subsequently, the validated functional unit is used to create a 10 degree of freedom (DOF) full body human skeletal model in MapleSim [Maple, v 2022.2, Canada]. An optimal control method based on trajectory optimization is then applied to this model to simulate human sit-to-stand motion. The joint angles generated by this simulation are validated with a

motion capture experiment. This predictive model is then used to identify the relative orientation of the femur and pelvis for different spinal conditions and spinopelvic stiffness. An optimization algorithm is employed to optimize the acetabulum implant to prevent impingement. Utilizing this framework, a novel patient categorization is used to propose different cup orientation angles.

5.3.2 Biomechanical Modeling of a Functional Spine Unit Considering Non-linear Passive Spine Elements

A five degree of freedom multibody lumbar spine model has been developed using the MapleSim software (Figure 5.2). In this dynamic model, spine vertebrae are assumed to be rigid bodies that are connected with five joints and six groups of ligaments: Anterior longitudinal (ALL), Posterior longitudinal (PLL), Ligamentum flavum (FL), Supraspinous (SSL), Capsular (CL), and Interspinous (ISL) ligaments. The anatomical insertion points for each ligament are provided in Table 5.1 [208].

In-vitro experiments on ligaments in the literature and the resulting stress-strain curves from mechanical tensile experiments [209] reveal that the mechanical behavior of lumbar spine ligaments can be modeled as nonlinear elements [210, 211, 212, 213]. As a result, the ligaments have been defined as nonlinear spring and dampers in the model, with the insertion points for nonlinear spring and damper replicating the same anatomical insertion points. Additionally, to accurately model the behavior of the ligaments, it is important to include the fact that they are only active when they are in tension. To do this, the nonlinear expression is generalized as proposed by Damn et al. [211] and the coefficients are adjusted according to the literature in-vitro experiments and the motion capture experiment that we have performed. The

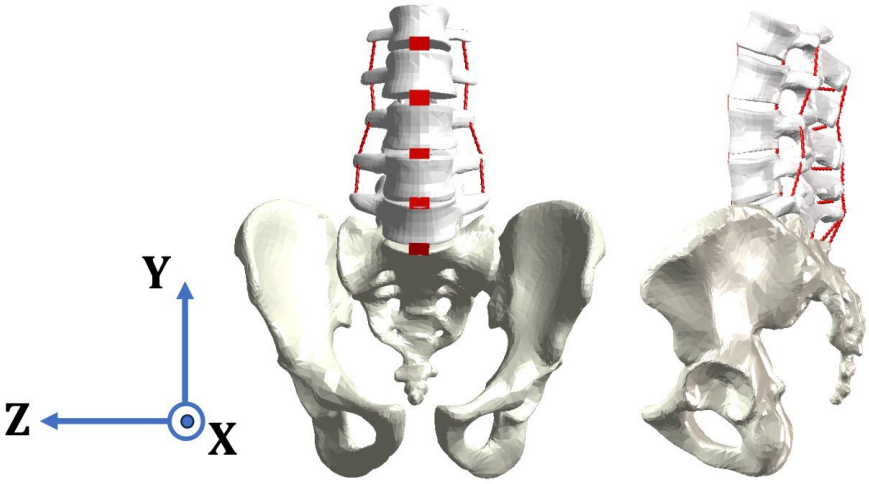


Figure 5.2: Lumbar spine functional unit with the pelvis and connecting nonlinear ligaments and IVDs

Table 5.1: Ligament insertion points

Ligament	Description
ALL	Origin from anterior tubercle of atlas (C1), insert to the sacrum.
PLL	Origin from axis (C2) in dorsal surface of the body, insert to the sacrum.
FL	Origin from axis (C2) in spinal canal, insert to the sacrum
CL	Originates bilaterally on the anteroinferior aspect of the lamina, inserts on the posterosuperior aspect of the lamina
ISL	Attach to the spinous processes respectively, of adjacent vertebrae.
SSL	Originates as the ligamentum nuchae, attaches to the tip of each spinous process.

following equations explain how nonlinear behavior is incorporated into the modeling of the ligaments:

$$F^L = F_k^L + F_d^L \tag{5.1}$$

$$F_k^L = a \ln\left(e^{\frac{\varepsilon+b}{d}} + 1\right) + c \tag{5.2}$$

where F^L is the applied force by the ligaments and is a function of the ligament's relative stretch to their rest length (i.e., strain, ε) and the rate of the relative stretch ($\frac{d\varepsilon}{dt}$). This force includes the resulting force from the nonlinear springs F_k^L and dampers F_d^L. The relation for the nonlinear spring is defined by Equation 5.2, in which the coefficients a, b, c and d are specified for each ligament in Table 5.2.

Table 5.2: Parameter values describing nonlinear behavior of ligaments and IVDs as suggested by [211, 136] and fine-tuned according to the experiments (Eq.5.2 and Eq.5.5).

	$a\ (N)$	$b\ (m)$	$c\ (N)$	$d\ (m)$
ALL	174.500	−9.060	−24.530	5.625
PLL	52.121	−42.971	−2.500	15.002
FL	45.351	4.310	53.833	−10.251
CL	94.334	19.271	−81.254	71.521
ISL	0.442	−3.612	0.000	0.024
SSL	1.213	−21.971	0.000	1.372
SSL_neg	−51.432	−35.000	−0.028	4.718
	$p_1\ (N.m)$	p_2	$p_3\ (N.m)$	-
Flexion	9.512	0.006	−1.523	-
Extension	5.139	0.008	23.622	-

The damping force is assumed to be a function of spring force:

$$F_d^L = f\ F_k^L\ \frac{d\varepsilon}{dt} \tag{5.3}$$

as suggested by [211] and [136], where $f = 10\ (s/m)$.

The literature experiments on intervertebral discs (IVDs) have revealed that these elements exhibit a nonlinear behaviour [214, 211, 215]. Mechanical properties of healthy and degenerated IVDs have been extracted from the the literature [205]. In order to capture this nonlinear behaviour, a multibody model was developed that included nonlinear springs and dampers. This model was able to predict the nonlinear mechanical response of IVDs in the lumbar region from pelvis to vertebra L1. Mathematically, the nonlinear behaviour of IVDs has been modelled using rotational springs and dampers. This has enabled a better understanding of the biomechanics of the lumbar spine and its related elements.

$$T^D = T^D_k + T^D_d \tag{5.4}$$

$$T^D_k = p_1 \tanh\left(\frac{\varphi^3}{p_2}\right) + p_3\ \varphi \tag{5.5}$$

$$T^D_d = \delta^D_d\ \frac{d\varphi}{dt} \tag{5.6}$$

where T^D is the applied torque by IVDs in flexion and extension and is a function of joint angle (φ) and angular speed ($\frac{d\varphi}{dt}$). The resulting torque is from the nonlinear springs T^D_k and dampers T^D_d. Equation 5.5 is a nonlinear expression representing the spring behavior in the IVD model. The coefficients in this equation are specified in Table 5.2 and the damping coefficient δ^D_d is 100 $Nm.s$ as suggested by [211, 216].

5.3.3 Multibody Dynamics Human Skeletal Model

A 10-Degree-of-Freedom (DOF) sagittal human dynamic model has been developed using the MapleSim software, featuring 7 DOF for the spine (revolute joints connecting the S1-L5, L5-L4, L4-L3, L3-L2, L2-L1, L1-T12, and T6-T5 rigid vertebrae) and 1 DoF in each joint in the lower limbs (hip, knee, and ankle joints) (Figure 5.3). The joint coordinate system is based on the standard for joint kinematics recommended by the International Society of Biomechanics (ISB)[217]. This model assumes stationary feet relative to the ground and symmetrical sit-to-stand movement in the sagittal plane. Nonlinear elements such as lumbar spine ligaments and intervertebral discs have been added to the model, resulting in a forward dynamic model of the human skeleton. Symbolic dynamic equations are automatically generated by MapleSim, which can be written in the following form:

$$\mathbf{u} = \mathbf{M}\,\ddot{\mathbf{x}} + \mathbf{C} + \mathbf{G} \tag{5.7}$$

where $\boldsymbol{u}$ are the 10 joint torques, $\mathbf{x}$ are the joint angles, $\dot{\mathbf{x}}$ are the joint velocities, $\ddot{\mathbf{x}}$ are the joint accelerations, $\mathbf{M}(\mathbf{x})$ is the mass matrix, $\mathbf{C}(\mathbf{x}, \dot{\mathbf{x}})$ is the vector of Coriolis and centripetal forces, and $\mathbf{G}(\mathbf{x})$ contains gravitational forces.

Modeling, Geometry, and Anthropometric Data

To have an accurate dynamic model of a specific subject, anthropometric data must be obtained accordingly. The mass properties of the upper body were extracted from [218], while coefficients of the regression equation $y = b0 + b1 \times BM + b2 \times BH$ necessary for estimating the anthropometric data of the lower limb were taken from [219]. This equation relates the segment mass properties (y) to the body mass (BM)

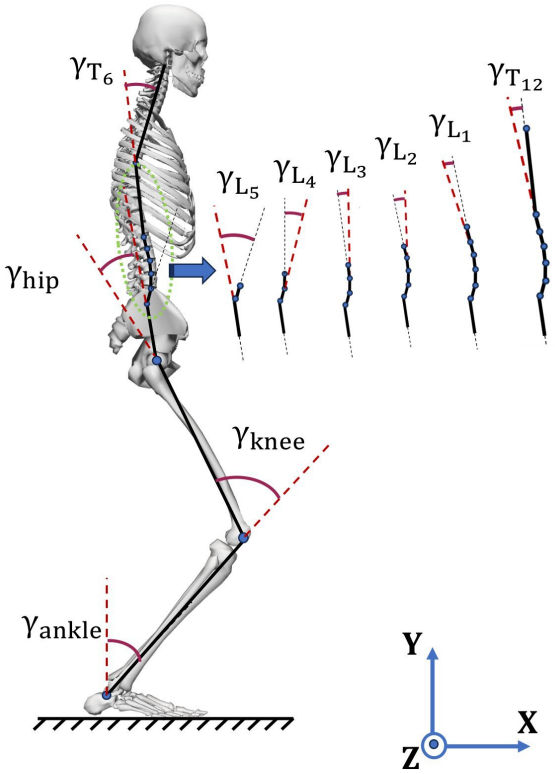


Figure 5.3: Definition of joint angles in the model. Five DoF is considered for the lumbar spine (γ_{L5}, γ_{L4}, γ_{L3},γ_{L2},γ_{L1}), two for the thoracic spine (γ_{T12}, γ_{T6}), and three for lower body (γ_{hip}, γ_{knee}, γ_{ankle}).

and height (BH) of subjects. Furthermore, the mass assignment for different body segments are listed in Table 5.3, and the center of mass (COM) for each segment of the upper limb was the proposed COM from [220]. Lastly, the length of each body segment was extracted from the motion capture experiment measurements for each individual subject.

Table 5.3: Anthropometric data for participant 2.

Body part	Mass (Kg)	$I_z(Kg.m^2)$
Shank	5.22	0.0567
Thigh	6.28	0.0875
Pelvis	7.84	0.0060
L5-L4	2.65	0.0013
L4-L3	1.98	0.0011
L3-L2	2.36	0.0018
L2-L1	2.05	0.0014
L1-T6	8.62	0.0191
T6-Head	7.22	0.0393
Total body Mass (kg)	61.62	-

5.3.4 Optimization and Predictive Simulation

A dynamic predictive simulation can be used to gain insight into how spine stiffness, spine fusion surgery, and aging influence the outcome of a THA surgery. To achieve this, an optimal control approach is employed with a dynamic human model to predict sit-to-stand motion. Symbolic dynamic equations extracted from MapleSim are utilised to compute exact gradients and boost numerical convergence. Trajectory optimization is employed to discretise the continuous movement, and to predict joint angles in each step. OptimTraj, a MATLAB [MathWorks, R2022b, U.S.A] library designed for continuous-time single-phase trajectory optimization problems, was used [221]. Different methods can be used to solve such problems [151, 221], with the direct collocation method being employed in this research. Symbolically-extracted equations of motion from MapleSim were applied to the method as dynamic constraints, forming

a general optimisation problem of the following form:

$$\min_{\mathbf{x}(t),\ \mathbf{u}(t)} J_B\left(t_0,\ t_f,\ \mathbf{x}\left(t_0\right),\ \mathbf{x}\left(t_f\right)\right) + \int_{t_0}^{t_f} J_P\left(\tau, \mathbf{x}\left(\tau\right), \mathbf{u}\left(\tau\right)\right) d\tau \tag{5.8}$$

Subject to the following constraints:

$\dot{\boldsymbol{x}}(t) = f\left(t, \boldsymbol{x}(t), \boldsymbol{u}(t)\right)$	System dynamics
$C_p\left(t, \boldsymbol{x}(t), \boldsymbol{u}(t)\right) \leq 0$	Path constraints
$C_B\left(t_0,\ t_f,\ \boldsymbol{x}(t_0)\, \boldsymbol{x}(t_f)\right) \leq 0$	Boundary constraints
$\boldsymbol{x}^- \leq \boldsymbol{x}(t) \leq \boldsymbol{x}^+$	Bounds on states
$\boldsymbol{u}^- \leq \boldsymbol{u}(t) \leq \boldsymbol{u}^+$	Bounds on controls
$t^- \leq t_0 < t_f \leq t^+$	Bounds on initial and final time
$\boldsymbol{x}_0^- \leq \boldsymbol{x}(t_0) \leq \boldsymbol{x}_0^+$	Bounds on initial state
$\boldsymbol{x}_F^- \leq \boldsymbol{x}(t) \leq \boldsymbol{x}_F^+$	Bounds on final state

where J_B are the boundary conditions, and the integral part (J_P) represents the cost function for this optimization along the motion. The cost function that has been used in our trajectory optimization is:

$$J_P = \sum_{i=1}^{n} \int_{t_0}^{t_f} \left(\frac{u_i}{u_i^{max}}\right)^2 + \sum_{i=1}^{n} \int_{t_0}^{t_f} w_i\, \dddot{x}_i^{\,2}, \tag{5.9}$$

where $n = 10$, u_i are joint torques, $\dddot{x}_i$ are joint jerks (the derivative of joint acceleration), and w_i are weights. The selected cost function, emphasizing normalized joint torques with additional weighted factors of velocity and jerk, yielded the lowest error rates in predicted joint angles when compared to motion capture data. This superior performance was determined through a systematic process of tweaking and evaluating various combinations of joint torques, velocities, and jerks. Initially, a

simple normalized joint torque was used as a baseline, then velocities and jerks were incrementally integrated with adjusted weights. This approach revealed that minimizing energy through normalized joint torques, while also considering excursion via weighted normalized joint jerk, most accurately reflected the experimental results. To define the sit-to-stand motion, initial and final states, which are extracted from motion capture data, were imposed to the problem and the trajectory of motion was predicted.

There are various approaches for solving continuous-time single-phase trajectory optimization problems. In this research, a direct collocation method has been adopted. This method is particularly advantageous due to its discretization of the problem, which translates the trajectory optimization problem into a nonlinear problem [221]. The number of discretization points is a key factor that influences the accuracy and reliability of the solution. Thus, a convergence analysis was conducted to assess the variation in the results after changing the discretization points and ensuring convergence.

5.3.5 Effects of Different Spinal Conditions

Three different spinal conditions were assumed in the model and the sit-to-stand motion was simulated in each condition.

1. **Normal spine**: The first assumption is subjects with normal spine stiffness. For this category, the joint angle results from the predictive simulation were compared to the results from the motion capture experiment (healthy subject with normal spinal condition) to validate the model. After the model is validated, two other spinal conditions are applied in the model to predict the effects of

spine fusion and different spine stiffness on lower limb motion.

2. **Fused spine**: Different levels of spinal fusion were assumed in the model according to a clinical report on the prevalence of fusion at different levels [21]. The fusion is modeled by considering some limitation on the range of motion of spinal joints (i.e., S1-L5, L5-L4, L4-L3, L3-L2). For the fusion at each level, we limited the range of motion for that specific joint to 1-2 degrees to represent the effects of fusion. For example, if the fusion is assumed at L5-L4 and L4-L3 levels, the range of motion for these two joints are limited in the predictive simulation. Some studies reported that sacrum involvement in a spinal fusion would cause more spinal stiffness [27]. Therefore, a comparison is provided by including and excluding the sacrum from the spinal fusion in the simulated motion.

3. **Anatomical or aged stiff spine**: The mechanical properties of ligaments, muscles, and IVDs can be changed due to aging or IVD degeneration. According to some research on how aging [204, 222] and degeneration [205] would change the mechanical properties of these elements, we modified the spine stiffness in our model by applying these changes in the model to see how a stiff spine would affect pelvic tilt and lower limb motion. We have increased the spine stiffness properties of the ligaments and IVDs by 50% [204, 222] to model the spine with higher stiffness. The values of parameters in Eq. 5.2 and Eq. 5.5 (describing the stiff spine) are reported in Table 5.4.

5.3.6 The Effect of Anterior and Posterior Pelvic Tilt

Pelvic tilt is an essential aspect of postural evaluation and musculoskeletal health,

Table 5.4: Parameter values describing nonlinear behavior of ligaments and IVDs (Eq.5.2 and Eq.5.5) for stiff spine

	$a\ (N)$	$b\ (m)$	$c\ (N)$	$d\ (m)$
ALL	261.750	−9.060	−36.795	5.625
PLL	78.182	−42.971	−3.750	15.002
FL	68.026	4.310	80.749	−10.251
CL	141.501	19.271	−121.881	71.521
ISL	0.663	−3.612	0.000	0.024
SSL	1.8195	−21.971	0.000	1.372
SSL_neg	−77.148	−35.000	−0.042	4.718
	$p_1\ (N.m)$	p_2	$p_3\ (N.m)$	-
Flexion	14.268	0.006	−2.284	-
Extension	7.708	0.008	35.433	-

which can be quantitatively assessed by measuring the angle formed by a line drawn between two anatomical landmarks: the Anterior Superior Iliac Spine (ASIS) and the Pubic Symphysis as shown in Figure 5.4.

A neutral pelvic tilt is indicated by an ASIS-to-pubic symphysis angle almost zero, which means that ASIS is co-planar with pubic symphysis to the vertical. This reflects a balanced alignment of the pelvis, which supports optimal load distribution across the musculoskeletal system and is considered ideal for spinopelvic health and functional movement efficiency[223].

Anterior Pelvic Tilt (APT) occurs when the pelvis tilts forward, causing the ASIS to descend relative to the pubic symphysis. This is quantified by an increased ASIS-to-pubic symphysis angle, typically positive degrees. APT is often associated with a hyperlordotic lumbar curve and can be linked to muscle imbalances, such as tight hip flexors and weak abdominals [224].

Posterior Pelvic Tilt (PPT) is characterized by a backward rotation of the pelvis,

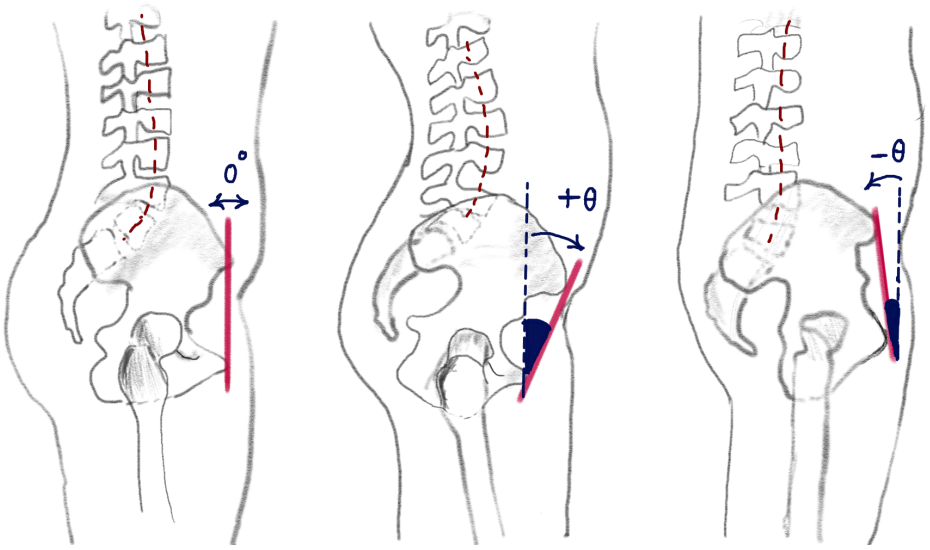


Figure 5.4: Definitions of neutral (left), anterior (center), and posterior (right) pelvic tilt conditions.

elevating the ASIS relative to the pubic symphysis and creating a negative ASIS-to-pubic symphysis angle. This condition is often related to tight hamstrings and weakened hip flexors and lumbar extensors, leading to a flattened lumbar curve [223, 224].

Recent studies have elucidated the impact of the different types of pelvic tilt conditions on spinopelvic and lower-limb dynamics [13, 225]. These findings are particularly relevant in Total Hip Arthroplasty (THA), where pelvic tilt orientation (i.e., posterior or anterior) necessitates tailored cup placement strategies for optimal outcomes. In cases of posterior pelvic tilt, there is an elevated risk of anterior impingement and posterior dislocation. Consequently, clinical guidelines suggest an increased anteversion angle for the cup implant in such scenarios [226]. Conversely,

for patients exhibiting anterior pelvic tilt, there is a heightened risk of posterior impingement and anterior dislocation. In these instances, it is advisable to reduce both the anteversion and inclination angles of the cup implant to mitigate the risk of impingement [227].

To the best of our knowledge, no existing study has evaluated the combined effects of pelvic tilt and spinal stiffness within the context of predictive simulation. This research gap has inspired our investigation, wherein we employ a predictive model to simulate the sit-to-stand motion under various scenarios: distinct pelvic tilt conditions and combined conditions of fused spine and pelvic tilt. We intend to analyze and optimize acetabular cup orientation for each specific spine-pelvis scenario using the impingement analysis method, detailed in Section 5.3.7.

5.3.7 Impingement Analysis and Implant Positioning Optimization

A practical application of the developed predictive model is as a tool to address different patient-specific scenarios by optimizing implant positioning and orientation in THA surgery. One of the main reasons for patient dissatisfaction or artificial hip joint dislocation after THA surgery is implant impingement. To optimize cup positioning and orientation in THA surgery, one of the main criteria is to avoid implant impingement. Following a similar definition proposed by [228], and the criterion introduced by [229], an optimization approach can be used to maximize the angular distance between the stem on the femoral component and the edge of the acetabular cup, in order to avoid any impingement. This angular distance, henceforth referred to as the "Angular Impingement Distance (AID)", can be calculated using

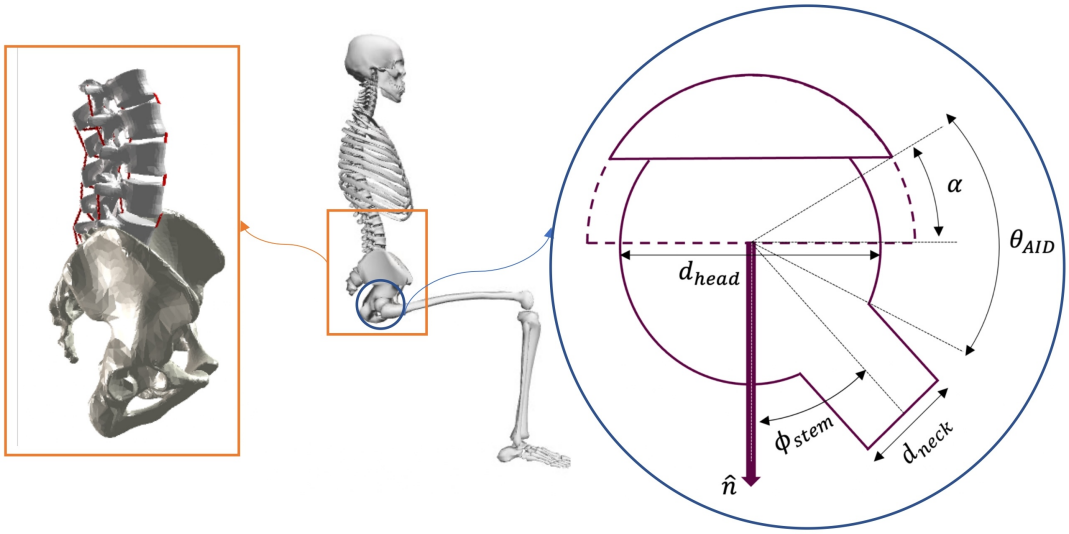


Figure 5.5: The simulation model (center), including detailed spine model (left) and AID impingement definition (right).

the following equation:

$$\theta_{\text{AID}} = \frac{\pi}{2} + \alpha - sin^{-1}\left(\frac{d_{neck}}{d_{head}}\right) - \phi_{stem} \tag{5.10}$$

where α is the constant cup opening angle, d_{neck}, d_{head} are the diameters of the neck and head of the femoral component, and ϕ_{stem} is a varying angle between the stem and the cup's axis of symmetry, marked by unit vector $\hat{n}$ (Fig. 5.5). If the AID is greater than zero, there is no impingement; however, if it's negative, it indicates implant impingement.

To prevent implant impingement, we should maximize the angular distance (θ_{AID}) calculated from Eq.5.10 at every instance of the motion. To achieve this, an optimization technique is employed to maximize the minimum AID during the motion. This approach ensures that the cup component and femoral implant (stem) are kept

at their maximum possible distance throughout the motion.

$$\underset{\beta_{Ant},\beta_{Inc}}{\operatorname{argmax}} \left(\min_{t_0<t<t_f} \theta_{AID}\left(t, \beta_{Ant}, \beta_{Inc}\right) \right) \tag{5.11}$$

subjected to:

$$\beta_{IncMin} \leq \beta_{Inc} \leq \beta_{IncMax}$$

$$\beta_{AntMin} \leq \beta_{Ant} \leq \beta_{AntMax}$$

where β_{Ant}, β_{Inc} are the radiographic cup anteversion and inclination angles, respectively as defined by [4] (Figure 5.6).

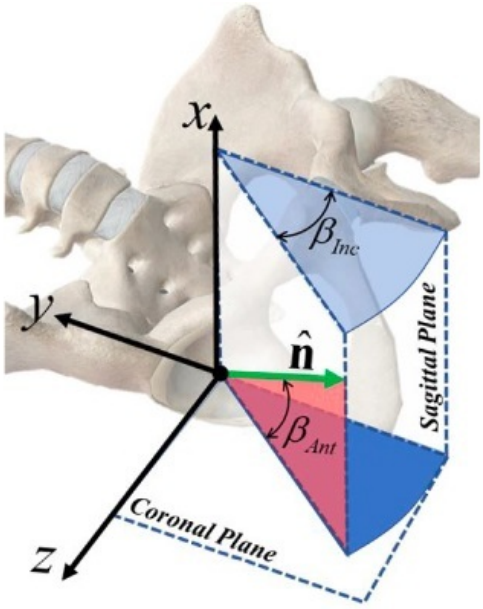


Figure 5.6: Radiographic anteversion (β_{Ant}) and inclination (β_{Inc}) [4]. The International Society of Biomechanics (ISB) standard is used to define the pelvis local coordinate frame, origin at hip joint centre [230]

The predefined values used for $\beta_{IncMin}, \beta_{IncMax}$, β_{AntMin}, and β_{AntMax} are obtained from clinical research [21, 202], and β_{Inc} and β_{Ant} have been optimized for patients with different spinopelvic mobility and stiffness. The reason that we are more focused

on the anteversion cup positioning angle is that in the sagital motion, different spine stiffness would change the relative pelvic tilt. Some studies in the literature showed that every 1° of change in pelvic tilt would resulting the acetabular anteversion (β_{Ant}) to be changed by $0.7° - 0.8°$ and only $0.2° - 0.3°$ change in the acetubular inclination (β_{Inc}) angle [231, 19, 88].

5.4 Results and Discussion

5.4.1 Validation of Lumbar Spine Functional Unit and Predictive Dynamic Model

Two experiments have been used to assess the accuracy of the predictive model's kinematic and dynamic performance. To begin, an in-vitro experiment [232] from the literature was used to validate the detailed spine dynamics model. The inverse dynamic model of the functional spine unit was employed to calculate the mechanical response of the unit to the loading conditions reported in the literature. The range of motion of the unit under bending moments of 5 Nm and 10 Nm for flexion and extension was then evaluated and compared to the model results listed in Table 5.5. Validation of the functional spine dynamic model using an in-vitro experiment to perform different loading conditions, and comparing the resulting range of motion between the model and literature, showed that the model is capable of predicting the spine range of motion.

The second step involved comparing the resulting motion from the predictive simulation to the motion capture experiment explained in Chapter 4. As discussed previously, the detailed spine unit was used to develop a human predictive dynamic

Table 5.5: Validation of the functional spine dynamic model using in-vitro experiment performing different loading condition and comparing resulting range of motion (ROM) between the model and literature [232].

ROM	Flex (Model)	Flex (Exp)	Ext (Model)	Ext (Exp)
Bending moment [5 Nm]	7.3°	5.5 – 11.5°	5.2°	2.5 – 6.5°
Bending moment [10 Nm]	9.7°	7 – 15.5°	6.3°	5 – 12.5°

model. The joint angle results from the human dynamic model were compared to those of the motion capture experiment for the corresponding subject, as shown in Fig 5.7. The difference between experimental and numerical results is mostly due to the fact that the markers were placed on the skin, meaning that the relative motion of the skin on the joints affects the resulting joint movements captured by the motion capture system. Also we could not use more markers on the spine due to very close distances between vertebrae and because the tracking of markers during the experiment can be difficult because of occlusion and overlapping of reflective signals. The prediction error for each joint (compared to the mean value of the motion capture joint angle results for subject 2) was calculated using the Root Mean Square (RMS) error formulation as:

$$RMSE = \frac{1}{n_g} \sum_{i=1}^{n_g} \sqrt{\left(q_i^{(opt)} - q_i^{(exp)}\right)^2} \tag{5.12}$$

where q_{opt} is the predicted joint angle in each grid point, q_{exp} is the experimental result, and $n_g = 80$ is the number of grid points in the optimization (Table 5.6).

Comparing the ROM for each joint and the calculated RMSE in Table 5.6, we can see that the error for spinal joints, particularly the upper ones, is greater than that of lower limb joints. This is mainly attributed to the presence of soft tissue and skin effects that are more pronounced on spinal joints. However, the results for lower

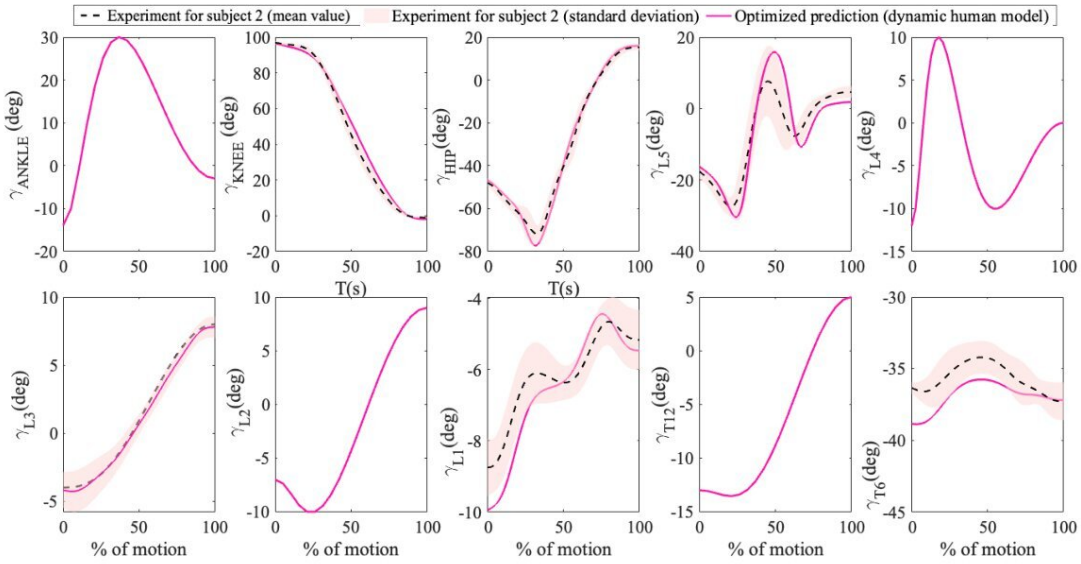


Figure 5.7: Validation of the predictive model using the results from motion capture experiment for subject 2.

Table 5.6: RMS error for each joint angle for subject 2

Joint	Knee	Hip	L5	L3	L1	T6
ROM [degree]	95	98	35	12	9	10
RMSE [degree]	0.24	0.83	1.94	0.31	0.86	1.24

limb joints are encouraging.

5.4.2 Prior Spine Fusion Surgery and the Risk of Hip Dislocation in a THA Surgery

Effect of Spine Fusion Surgery on Spine Stiffness

Spinal fusion is a surgical process in which two or more levels of the spine vertebrae are fused together to reduce or eliminate movement between them. This process makes

the spine stiffer, consequently decreasing the contribution of the spine in motions such as sit-to-stand. Subsequently, the hip joint must compensate for the lack of mobility of the spine, leading to an increased ROM in the hip joint angle and an increased risk of impingement. Employing the predictive human dynamic model, fusion has been integrated into different levels of the spine. Figure 5.8 illustrates the results for the simulation of the sit-to-stand motion for normal and stiff spines. A comparison of hip joint angle, PT, and LL trajectories is depicted in this figure, demonstrating how a stiff spine, with less contribution of the spine in the motion (i.e., less LL variation), affects PT and hip joint angle in different cases. It is evident that for subjects with stiff spines, the pelvis must compensate for the lack of contribution of the lumbar spine in the sit-to-stand motion, causing the pelvis to have a more forward tilting in the middle of the motion (15-30% of motion) as well as less backward tilting at the end of the motion (80-100% of motion). This could lead to an increased risk of anterior impingement and posterior dislocation in the midst of a sit-to-stand motion, as well as an increased risk of posterior impingement and anterior dislocation at the end of the sit-to-stand motion or during a bending forward motion, which is more common in such spinal conditions [203].

Spine Stiffness and Different Levels of Spine Fusion and Predicted Effects on THA Outcome

Vigdorchik et al. [21] evaluated THA outcomes for 3777 patients and found that over 53% of the study population had a stiff spine or malalignment. The research demonstrated the breakdown of patients with a stiffer spine resulting from fusion surgery to different levels of fusion, but did not provide any specific guidelines for each level of fusion in the spine. In response to this, our predictive simulation revealed

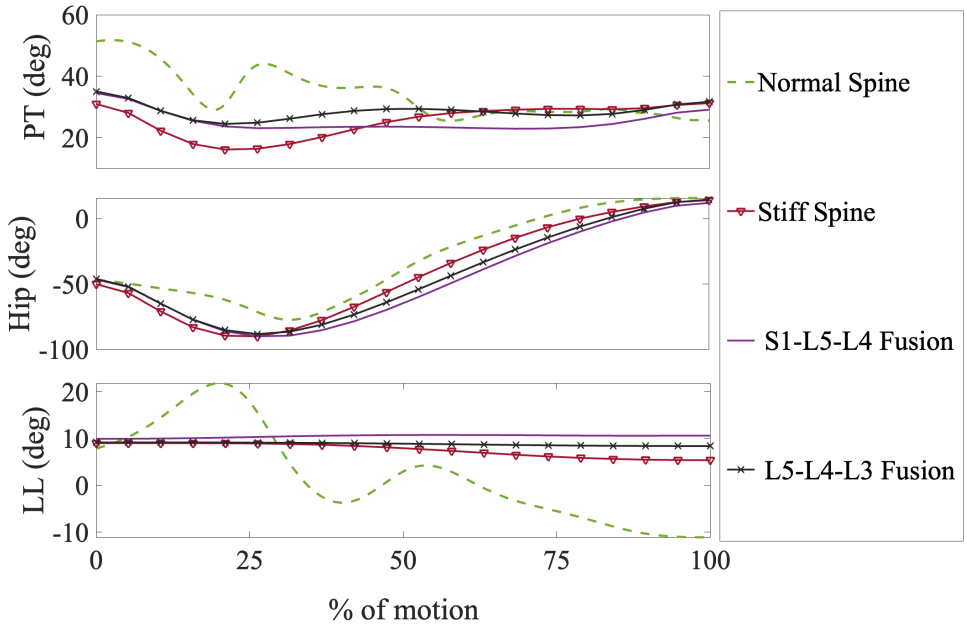
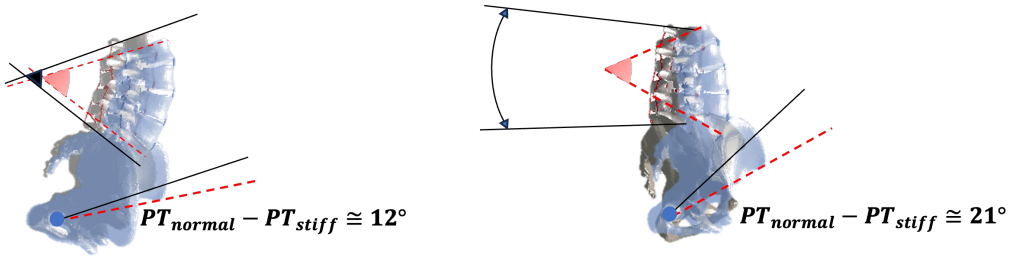


Figure 5.8: A comparison of the predictive model results for the normal, stiff, and fused spine in different levels.

that different levels of fusing can have different effects on lower limb motion and hip ROM, as depicted in Fig. 5.8. Comparing the pelvic tilt (PT) and lumbar lordosis (LL) in the predicted motion of normal and fused spinal conditions revealed distinct spinopelvic motion patterns. There is a condition that patients may have an anatomically stiff spine along with a long fusion, which considered as a worst case scenario. As depicted in Figure 5.9, in the fused-stiff spine condition, while the LL remains constant, the pelvis tilts more forward during the mid-phase of the motion (lift-off phase) to compensate for the reduced spinal contribution, and tilts less backward at the conclusion of the motion (standing phase). This alteration in pelvic tilt increases the risk of implant impingement, a concern we delve into further



A: Spine and pelvis at ~20-30% of motion (lift off phase)

B: Spine and pelvis at ~90-100% of motion (standing phase)

Figure 5.9: Comparison of predictive model motion results for the spine and pelvis in normal (solid shape and lines) and stiff-fused (worst-case scenario, anatomically stiff spine along with a long fusion including S1-L5-L4-L2) (transparent shape and dashed lines) conditions during two phases of sit-to-stand motion: A) Lift-off phase, B) Standing phase.

using the angular impingement distance (AID) metric. This motivated us to further evaluate different levels of fusion, sacrum involvement, anatomically stiff and fused stiff spines, in combination with an impingement analysis, to gain an understanding of the effects on THA outcomes. In the following sections, we present the findings of our impingement analysis considering cup orientation in Lewinnek's safe zone, as well as provide surgical recommendations for various spinal conditions through a dynamic motion analysis and cup orientation optimization.

5.4.3 Impingement Analysis Results: Is The "Lewinnek safe zone" Really Safe?

By utilizing the method for the analysis of implant impingement (Eq.5.10), we tracked the risk of impingement during a sit-to-stand motion for both healthy and fused spine subjects for the β_{Inc} and β_{Ant} values within the Lewinnek safe zone. The AID metric

was calculated considering all possible combinations of proposed cup anteversion and inclination by Lewinnek, which are $5° \leq \beta_{Ant} \leq 25°$, $30° \leq \beta_{Inc} \leq 50°$ [25]. The AID trajectories are shown in Figure 5.10 during the motion.

The most critical inclination and anteversion values (min[AID]) within the Lewinnek safe zone for both subjects was depicted and the AID trajectories and hip joint angle during the motion are shown in Fig. 5.11. Thus, cup positioning with anteversion and inclination proposed as "Lewinnek safe zone" is not necessarily safe for all patients who undergo THA surgery. Consequently, a dynamic motion analysis and cup orientation optimization is required to avoid implant impingement after THA surgery. There are other research in the literature that address this issue using inverse dynamic models. For instance, Widmer et al.[181] introduce an approach that takes into account both cup and stem orientations, recognizing the limitations of the static assessment employed in the traditional Lewinnek safe zone. The results of the study highlight that the combined target zones for impingement-free cup orientation exhibit polygonal boundaries. Notably, the size and position of these zones are found to be contingent on specific parameters, including neck-shaft angles, stem anteversions, and radiographic cup anteversions. These findings underscore the intricate interplay between design and implantation parameters in achieving optimal outcomes in THA.

5.4.4 Cup Implant Orientation Optimization

The predictive human motion model offers the potential to perform preoperative planning for patients with varying spine conditions. Several clinical studies have proposed modifications to the proposed inclination and anteversion angles suggested by Lewinnek [21, 14, 109]. However, using the same treatment approach in THA surgery for patients with varying spinal mobility and stiffness can increase the risk of

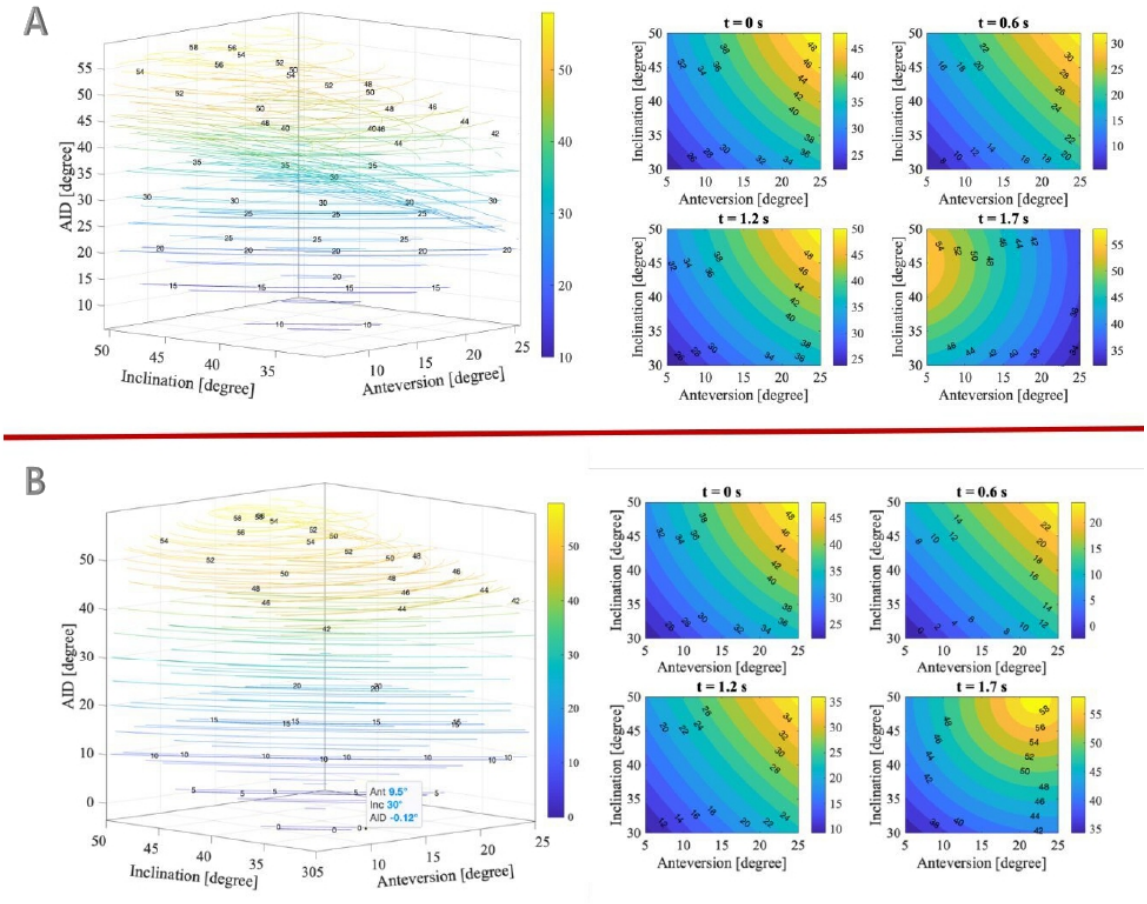


Figure 5.10: Impingement analysis results evaluating Lewinnek safe zone for the predicted motion of healthy (A) and stiff spine (B) subjects. The 3D contour graph (left) shows all possible combinations of anteversion and inclination angles and calculated AID values during the motion. To provide a better insight, some instances of motion are shown as 2D contour graphs (right). The lower the values of AID, the more risk of impingement ($AID = 0$ means the impingement occurred). While healthy spines (graphs above the line) have no close-to-zero AID values, the stiff spine subject (bottom) has some zero or sub-zero values ($t = 0.6s$) indicating a potential moment of impingement.

impingement for those who have had prior surgery or have stiff spines. Our numerical approach (AID calculation throughout the motion) in Fig. 5.12.A illustrates this risk.

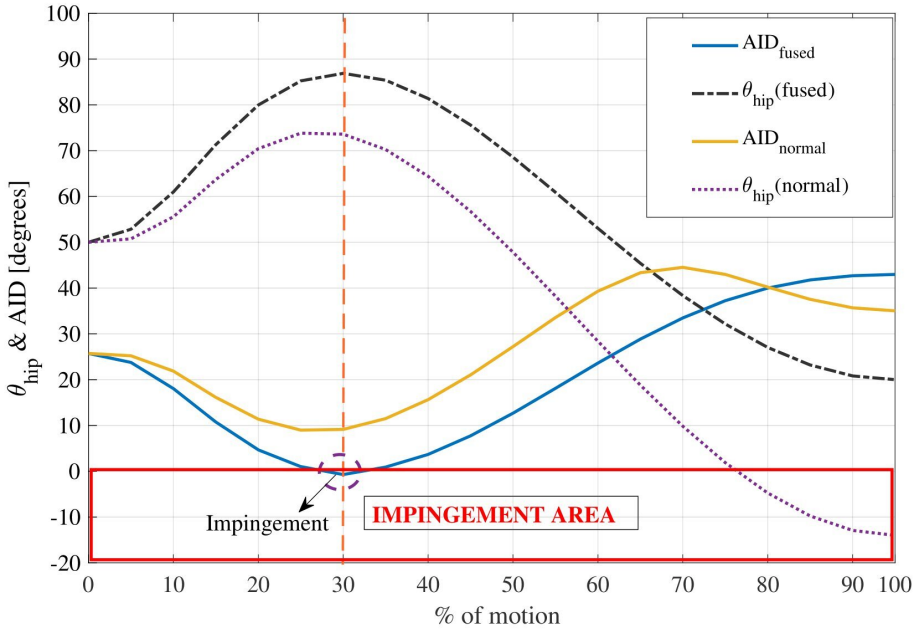


Figure 5.11: Impingement analysis for healthy and fused spine subjects, showing that AID could be less than zero for a fused spine subject (impingement occurred), at critical values for inclination and anteversion that are within the Lewinnek safe zone.

For this impingement analysis, the recommended β_{Inc} and β_{Ant} values for normal mobility by Vigdorchik [21], $\beta_{Inc} = 42°$ and $\beta_{Ant} = 23°$, were adopted for all subjects using implant parameters reported in Table 5.7. As seen in in Fig. 5.12.A, this configuration of β_{Inc} and β_{Ant} angles placed patients with stiffer spine or fused spine at a higher risk of impingement, especially when changing from a sitting to standing position (30-40 % motion). This critical moment for impingement was obtained our experimental results (Fig. 4.7) and predicted motion results (Fig. 5.7).

The higher risk of implant impingement (i.e., the closer the trajectories are to the impingement area) for fused and stiff spine patients without any modification in inclination and anteversion angles, as demonstrated in Fig.5.12.A, motivated us to introduce a new patient categorization (Fig.5.13) and devise an optimization

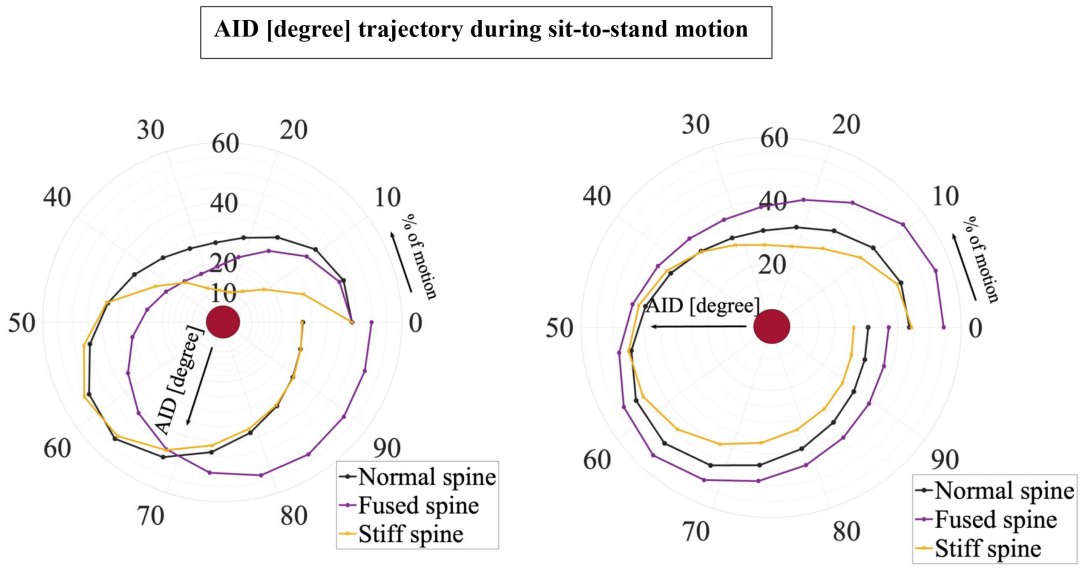
Table 5.7: Implant Parameters Used in Simulation Studies [233]

Parameter	Value
Head diameter (d_{Head})	28 mm
Neck diameter (d_{Neck})	12 mm
Cup opening (α)	180°
Neck-shaft angle	130°
Stem flexion	3°
Stem adduction	5°

approach to determine patient-specific cup positioning angles based on different spine conditions. To that end, we utilized the optimization approach outlined in Eq. 5.8 to calculate optimized values for cup orientation for each spinal condition (Table 5.8).

The impingement analysis for the optimized values of anteversion angle is presented in Fig.5.12.B. As can be observed, the optimized values of anteversion angle ensure that the AID trajectories for different spinal conditions (i.e., normal, anatomically stiff and a L5-L4-L3 fusion) remain far from the impingement area (i.e., $AID \leq 0$), compared to using mean values of anteversion angles that have been recommended in the literature(Fig.5.12.A) [21]. The results for the optimized values in different spinal conditions are shown in Table 5.8 and compared to the clinically recommended values by Vigdorchik et al. [21].

The results of the subject-specific optimized values of cup anteversion angle are presented in Table 5.8. To the best of our knowledge, this is the first prediction of subject-specific cup component anteversion values for different spinal conditions. We compared the results of our predictive model (the optimization of cup orientation) with clinical recommendations for subjects in the same category as we defined. From Table 5.8, the results of our model-based optimization approach have a good correlation to what has been suggested for the same categories of patients. Our subject-specific



A: using clinically recommended values for Inc and Ant **B**: using optimized values for Inc and Ant

Figure 5.12: Implant impingement analysis for A: recommended values of β_{Inc} and β_{Ant} in the literature for normal spine subjects and B: optimized values for each spinal condition to avoid impingement; the more distance the trajectories have from the solid circular impingement area (higher AID values), the safer patients are from implant impingement.

impingement analysis are for different spinal fusion levels. In contrast, the clinical recommendations are based on general patient categorization of normal, deformity, fused, and stiff [21, 202]. Comparing the minimum AID values in the last two columns of Table 5.8 reveals how the new patient categorization presented in this research helps decrease the risk of impingement after THA. Comparing the last two columns of Table 5.8, the more discrepancy between the calculated AIDs for different spinal conditions (optimized values and literature) can be found for the fused spine in different levels, particularly where the sacrum is involved in the fusion. While some simulation values align with the existing literature (e.g., the first row of Table 5.8

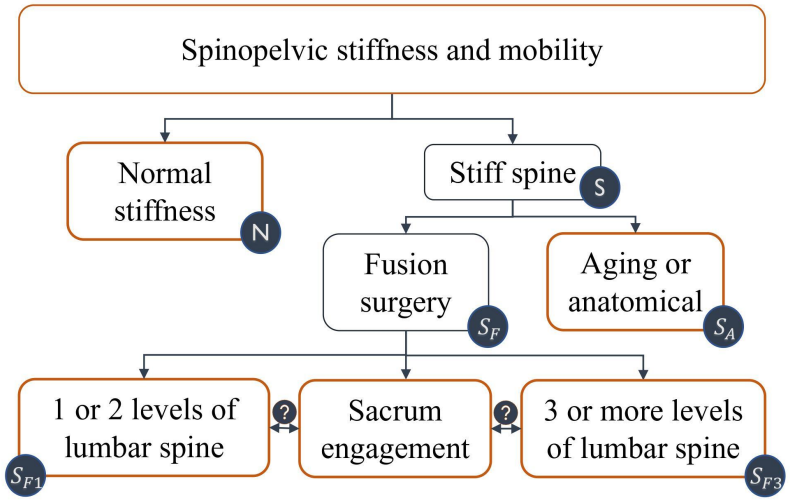


Figure 5.13: A new categorization of patients who are possible candidates to be preoperatively monitored using predictive simulation for an optimal cup anteversion positioning; **N**: normal stiffness and mobility, **S**: stiff spine, which has three subgroups: $\mathbf{S_A}$: spine stiffness due to aging or anatomical parameters (i.e. $\Delta SS < 10$), $\mathbf{S_{F1}}$: one or two levels of lumbar spine fusion, and $\mathbf{S_{F3}}$: three or more levels of lumbar spine fusion. In the spine fusion condition, the sacrum engagement affects the results.

pertaining to normal spines), instances where optimized values diverge from clinical reports suggest a potential reduction in impingement risk. It's worth noting that following clinical recommendations does not lead to an impingement, but it shows a higher risk of impingement according to lower AID values in some cases. Our calculated AID values (based on optimized cup anteversion) indicate a lower risk with higher AID scores than the clinical recommendations. Furthermore, clinical reports do not provide specific recommendations for each fusion level, relying instead on general adjustments for fusion or stiff spine. This may explain the discrepancies between our optimized values and established clinical practices. In fact, we propose a reconsideration of patient-specific cup implant positioning to potentially enhance outcomes in such cases. This indicates that making the patient categorization more

Table 5.8: Comparison of the optimized (model) cup anteversion values for different spinopelvic mobility and stiffness compared to the literature (lit) [21, 202]. The results of fusions with (S1✓) and without (S1×) sacrum involvement are presented. The literature values represent measurements taken one year after surgery, whereas the target values are the benchmarks surgeons aimed for during the implant placement procedure.

Spinal Type	Anteversion			Inclination			AID	
	Model°	Lit° [SD]	Target°	Model°	Lit° [SD]	Target°	Model°	Target°
Normal (N)	23	23 [19 – 25]	20 – 25	38	35 [30 – 40]	30 – 50	26.7	26.4
Anat. Stiff (S_A)	28.8	28 [25 – 33]	25 – 30	40	42 [40 – 45]	30 – 50	20.9	19.8
Short Fusion:								
S1✓, S1-L5 (S_{F1})	32	29 [21 – 34]	20 – 30	43	45 [40 – 50]	30 – 50	26	18.5
S1×, L3-L2 (S_{F1})	27	29 [21 – 34]	20 – 30	40	45 [40 – 50]	30 – 50	23	20.1
Long Fusion:								
S1✓, S1-L5-L4 (S_{F3})	34	29 [21 – 34]	20 – 30	45	45 [40 – 50]	30 – 50	27	19.3
S1×, L5-L4-L3 (S_{F3})	30	29 [21 – 34]	20 – 30	45	45 [40 – 50]	30 – 50	24	19
S1×, L4-L3-L2 (S_{F3})	28	29 [21 – 34]	20 – 30	45	45 [40 – 50]	30 – 50	22.4	18.7
Fused-Stiff (S1✓), S1-L5-L4 (S_{F3}, S_A)	38	32 [22 – 40]	25 – 35	48	47 [45 – 50]	30 – 50	28.5	20.3

subject-specific, as we did in this research, can help to have a better preoperative planning that can lead to a better outcome after THA surgery. We have also compared the results with the modified impingement free combined target zone (safe zone) that is presented by Widmer et al. from their model-based analysis [181]. Our optimized cup anteversion angle shows congruence with the proposed combined target zone, particularly aligning with the 23° to 40° range suggested for the anteversion angle of a fused-stiff spine. Notably, our results also fall within this specified range.

Our findings indicate that a stiffer spine (either anatomically stiff or fused) leads to a noticeable alteration in pelvic tilt during motion (see Fig.4.7 and Fig.5.8). Consequently, it is important to take into account revised orientation values for this specific patient group. When comparing our results with literature on the influence of pelvic tilt on the optimal cup anteversion angle [229], we observe that an increase in

pelvic tilt necessitates higher values ($\geq 25°$) for the cup anteversion angle to prevent impingement, which is concluded in our results (Table 5.8). These values exceed the range suggested by Lewinnek as the "safe zone", underscoring the significance of our patient-specific optimization approach.

5.4.5 Anterior and Posterior Pelvic Tilt and Optimal Implant Placement

In this section, we analyze the impact of various pelvic tilt conditions, both with and without spinal fusion surgery, on sit-to-stand motion using a predictive dynamic model. Initially, the effects of anterior and posterior pelvic tilt were evaluated, excluding cases with a stiff or fused spine. For this purpose we have considered 20° of anterior or posterior pelvic tilt as the patient-specific case scenario.

As Table 5.9 and Figure 5.14 illustrate, neglecting pelvic tilt conditions in Total Hip Arthroplasty (THA) and treating patients as if they were healthy individuals using standard implant orientation values heightens the risk of impingement. Figure 5.14 demonstrates that disregarding specific pelvic tilt conditions and failing to optimize anteversion and inclination angles accordingly increases impingement risk (i.e., the closer the trajectories are to the impingement area). This figure also indicates that optimizing these angles can significantly reduce impingement risk, as evidenced by trajectories moving away from the impingement area.

The findings in Table 5.9 align with clinical recommendations to adjust the anteversion and inclination angles in response to pelvic tilt variations—increasing them for posterior pelvic tilt and decreasing them for anterior pelvic tilt to prevent impingement, as suggested in [226, 227]. Our approach, however, provides specific

Table 5.9: Comparison of clinically recommended implant placement orientation values with optimal values from our predictive model. Upward ↑ (increase) and downward ↓ (decrease) arrows indicate the necessary adjustments in implant orientation compared to a healthy condition without anterior or posterior pelvic tilt.

Pelvic Tilt		**Neutral**	**Anterior**	**Posterior**
Clinical	Inclination (°)	40	40	40
	Anteversion (°)	23	23	23
Optimal	Inclination (°)	40	38 ↓	43 ↑
	Anteversion (°)	23	17 ↓	33 ↑

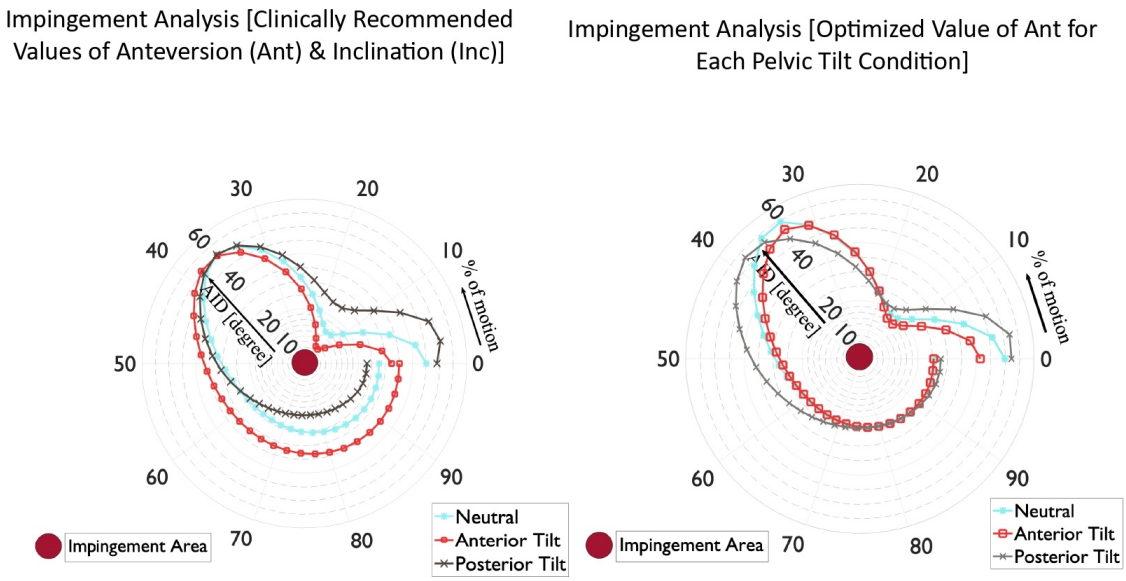


Figure 5.14: AID trajectories for a normal spine (not stiff or fused) with anterior or posterior pelvic tilt conditions. The left polar figure illustrates scenarios where identical orientation values are applied, treating each case as a healthy subject. The right graph displays AID trajectories using the optimized cup implant orientation.

optimal values for each pelvic tilt condition, rather than a general directive to increase or decrease angles.

As highlighted in Section 5.4.4, spinal fusion impacts lower limb dynamics, ne-

cessitating tailored optimization of cup implant orientation for each fusion level. This prompted our evaluation of cases with concurrent spinal and pelvic disorders, specifically spinal fusion accompanied by anterior or posterior pelvic tilt. Although our model can simulate various fusion levels as detailed in Table 5.8, this section focuses on long fusion involving the sacrum (S1-L5-L4) — a worst-case scenario. we aim to understand how hip motion is altered and how to adjust hip implant orientations optimally under these conditions.

Table 5.10: Clinically recommended values versus optimal values from predictive model for cases with spinal fusion (S1-L5-L4) and anterior/posterior pelvic tilt. Upward ↑ (increase) and downward ↓ (decrease) arrows indicate the necessary adjustments in implant orientation compared to a healthy condition without anterior or posterior pelvic tilt.

Pelvic Tilt		**Neutral**	**Anterior**	**Posterior**
Clinical	Inclination (°)	40	40	40
	Anteversion (°)	23	23	23
Optimal	Inclination (°)	45 ↑	48 ↑	41 ↑
	Anteversion (°)	34 ↑	40 ↑	27 ↑

Table 5.10 presents the optimized inclination and anteversion values for specific spinopelvic conditions. Unlike the findings in Table 5.9, which recommend lower anteversion and inclination angles for anterior pelvic tilt in normal spinopelvic conditions, our model suggests an increase in these orientation values for cases with anterior pelvic tilt in a fused spine. In stiff spine scenarios, particularly with long fusion and either anterior or posterior pelvic tilt, an increase in orientation angles is essential. However, in these stiff spine cases, the required increase in orientation angles is smaller for anterior pelvic tilt than for posterior pelvic tilt. Figure 5.15 illustrates that utilizing these optimized orientations effectively shifts the trajectories away from the impingement area, thus lowering the risk of impingement and potential

dislocation.

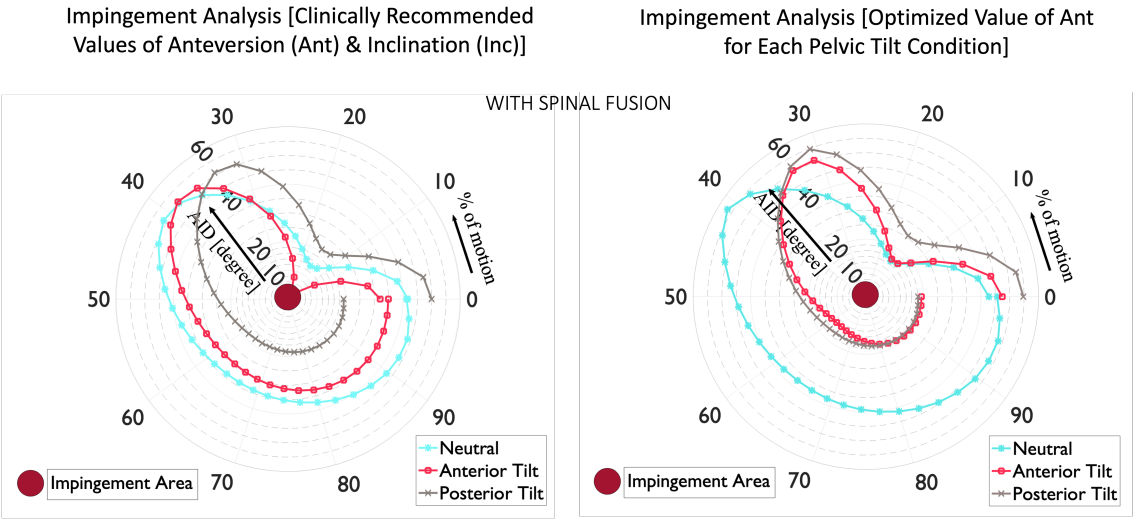


Figure 5.15: AID trajectories for a fused spine (S1-L5-L4) with anterior or posterior pelvic tilt conditions. The left polar figure illustrates scenarios where identical orientation values are applied, treating each case as a healthy subject. The right graph displays AID trajectories using the optimized cup implant orientation.

5.5 Conclusion

In this chapter, a predictive dynamic human model was proposed for preoperative THA surgery planning. By offering predictive simulations that considered different spinal conditions, the model was able to answer"what if" scenarios and evaluate the impact of spine stiffness on lower limb dynamics. The preliminary results from the simulations were encouraging, prompting us to conduct further studies, including impingement analysis, to provide patient-specific suggestions for optimal acetabular cup orientations. By utilizing optimization, this model represents a computationally-efficient way to determine the best patient-specific cup orientation, while taking into

account different spinal conditions and their effect on lower limb motion. This could address a knowledge gap in the current clinical research and methodology on THA surgery, especially considering the effect of flexible/stiff spine on lower limb motion and different pelvic tilt conditions. The present method has several advantages compared to the existing literature, as outlined below:

- **Predictive model (no need for motion capture data):** Predictive modeling offers advantages over inverse dynamic models [229], as it eliminates the need for importing certain motions into the model before it can analyze the dynamics. Instead, our approach utilizes forward dynamics, optimization, and predictive simulations to circumvent this limitation.

- **Spine flexibility:** To the best of our knowledge, this is the first time spine flexibility (e.g. spine stiffness, spinal fusion and aged or anatomically stiff spines) has been examined in a predictive dynamic simulation with an aim to assess its impact on lower limb motion and the success of THA surgeries.

- **Hip-pelvis-spine relationship consideration:** The predictive model allows us to simulate different scenarios of spinal or pelvis disorders (e.g., cases with both a stiff spine and abnormal pelvic tilt).

- **Computationally efficient:** Finite element analysis (FEA) simulations [188, 234] are known to be time-consuming and complicated. In contrast, the method presented in this research is much faster as it is based on symbolic dynamic equations. This makes it a practical choice for pre-operative applications as well as for intra-operative ones.

In conclusion, we have presented a predictive dynamic model, using an optimal control approach, to produce preoperative plans tailored to various spinopelvic conditions. Our findings suggest that a patient's spine stiffness can be taken into account when creating preoperative plans, as it is affected by age, anatomy, or fusion. Our model underscores the need to evaluate different levels of spinal fusion to offer patient-specific recommendations for cup orientation. It also emphasizes the critical importance of considering hip-pelvis-spine relationships in pre-operative planning. The findings in this chapter suggest that overlooking the effects of pelvic tilt or spinal fusion in surgical planning may lead to sub-optimal cup implant orientation, increasing the risk of impingement and subsequent dislocation.However, there are some limitations of this model to be addressed in future studies, such as other factors that should be considered for an optimal cup orientation, including soft tissues, implant design, body impingement, edge loading, and muscle contribution. Other limitations of this study will be discussed in Chapter 6.

Chapter 6

Conclusion

This thesis research addresses two critical objectives aimed at enhancing Total Hip Arthroplasty (THA). The first objective centers on the introduction of an efficient anatomical landmark detection algorithm, known as the "LanDet" deep learning model, detailed in Chapter 3. This innovation not only streamlines the extraction of spinopelvic metrics, thus saving valuable time for surgeons, but also ensures a consistent level of accuracy across practitioners. Additionally, it lays the groundwork for a more efficient patient categorization system, which plays a crucial rule in choosing the surgery procedure accordingly.

The second objective focuses on the optimization of cup implant orientation, taking into account factors such as spine stiffness, pelvic tilt, and spinopelvic metrics. This optimization aims to enhance the outcomes of THA surgery and mitigate the risks of post-operative implant impingement or dislocation. To achieve this, we conducted two case-study experiments, detailed in Chapter 4, employing both motion capture and pre-operative radiographic analysis. These experiments provided insights into how varying spinopelvic conditions impact lower limb motion during a sit-to-stand

motion.

Building on the findings from our experiments, Chapter 5 introduces a multibody dynamic human model with detailed spine elements. This model takes into account the categorization that can be derived from the landmark detection method described in Chapter 3, as well as the different spinopelvic conditions discussed in Chapter 2 and observed in our experiments in Chapter 4. The resulting motion data is then leveraged to optimize cup implant orientation, employing the Angular Impingement Distance (AID) metric and tailoring the positioning to each patient-specific spinopelvic condition.

This end-to-end approach, starting from X-ray images and employing predictive simulation to refine cup implant orientation, not only alleviates the burden of annotating pre-operative X-ray images for surgeons, but also can enhance the precision of THA surgery, particularly in cases involving a stiff spine or spinal fusion. Ultimately, the outcomes of this study contribute to increase a patient satisfaction following THA, while concurrently delivering notable time and cost savings to healthcare systems.

The following paragraphs provide a summary of the results and contributions made in each chapter:

- **Chapter 3** introduced a novel approach called "LanDet" for detecting landmarks as objects, emphasizing their relational geometrical constraints in a physics-informed approach. Using this method, we trained a deep learning model to extract five important spine and pelvis measures: Sacrum Slope (SS), Pelvic Tilt (PT), Pelvic Incidence (PI), Lumbar Lordosis (LL), and Sagittal Vertical Axis (SVA). The model's performance was assessed by comparing its results against a manually-labeled test dataset and the same measures

annotated independently by three surgeons. Evaluation metrics, including Mean Absolute Error (MAE), Standard Deviation (SD), and R Pearson correlation coefficient, yielded results of high accuracy: $[SS^{\circ} : 3.2(2.7), R = 0.89], [PT^{\circ} : 1.3(1.1), R = 0.98], [PI^{\circ} : 4.2(3.1), R = 0.93], [LL^{\circ} : 5.1(6.4), R = 0.86], [SVA(mm) : 2.1(1.9), R = 0.98]$. We used the intraclass correlation coefficient (ICC) to assess the model's reliability, demonstrating consistent performance with surgeons, surpassing what was previously reported in the literature, highlighting the effectiveness of the physics-informed constraint method employed in our landmark detection as an object algorithm. Additionally, we addressed the limitations of heatmap-based methods for anatomical landmark detection, as well as resolving issues related to mis-identification of similar or adjacent landmarks.

- **Chapter 4** presented the results of our experimental motion capture and X-ray analysis, shedding light on the influence of various spine properties and spinopelvic relationships on pelvic tilt (PT) and hip range of motion (ROM). We found that changes in pelvis and lower limb motion resulting from different spine types and spinopelvic parameters could impact the risk of impingement or dislocation post-surgery. Notably, our X-ray data analysis revealed that patients with restricted spine movement ($\Delta LL < 20^{\circ}$) experienced limited pelvic motion ($\Delta PT < 10^{\circ}$), and all patients with a stationary pelvis ($\Delta PT < 10^{\circ}$) showed restrictions in the change of LL ($\Delta LL < 20^{\circ}$). Motion capture analysis offered dynamics insights compared to static X-ray analysis. Our aim was not to replace X-rays but to underscore the added value of dynamic motion analysis, especially in identifying subjects with spine stiffness that might be missed in static X-ray studies. Consequently, our dynamic motion analysis highlighted the

importance of tracking changes in hip joint angle and spinopelvic measures (LL and PT) during motion, offering crucial information for pre-operative planning and improving total hip arthroplasty (THA) surgery outcomes.

- **Chapter 5** introduced a novel predictive dynamic modeling approach, featuring a multibody human model with nonlinear spinal elements, validated through in-vitro experiments and motion capture. This model, integrated with optimal control techniques, simulated human sit-to-stand motion across various scenarios, including normal, fused, and stiff spines. We demonstrated that spine stiffness significantly influenced lower-limb motion and the risk of implant impingement. By examining different scenarios of spine stiffness, such as spinal fusion in different vertebrae levels or anatomical stiffness, We calculated the optimal acetabular cup orientation based on implant impingement criteria. Our preliminary optimization results suggest adjustments in the anteversion cup angle, from 23° (normal spine) to 29° for an anatomically stiff spine, and within the range of $27 - 38°$ for fused spines, depending on the level of fusion. This pioneering research provides valuable insights into spine flexibility in diverse scenarios and its impact on lower limb motion, with potential applications in enhancing THA surgical planning and reducing the risk of hip impingement or dislocation post-surgery.

6.1 Summary of Contributions

The thesis research has made significant contributions, which can be summarized as follows:

1. **Identifying The Importance of Dynamic Motion Analysis**: This study

pioneers a comparative analysis between the traditional pre-operative method using X-ray images, motion capture analysis, and predictive simulation. This analysis revealed the necessity of dynamic motion analysis in studying hip biomechanics, laying the foundation for understanding distinct motion patterns in individuals with varying spinal conditions.

2. **The Effect of Spine Stiffness on THA**: We have thoroughly investigated the impact of spine stiffness on lower limb dynamics and hip biomechanics. Our findings shed light on the relationship between spinal conditions and the performance of total hip arthroplasty (THA), offering valuable insights for orthopedic surgeons and researchers alike.

3. **Innovative Landmark Detection and Anatomical Constraints**: We have introduced a novel single-stage object detection method for landmark detection, representing landmarks as objects. Additionally, our physics-informed anatomical constraint approach addresses critical challenges in the field.

4. **Addressing Mis-Detection of Adjacent Landmarks**: Our research successfully tackles the issue of mis-detection of adjacent landmarks, a problem previously documented in the literature. This advancement contributes to more accurate anatomical landmark detection and surgical planning.

5. **Development of Clinical Guidelines**: We have developed a set of clinical guidelines that can aid healthcare practitioners in making informed decisions about the THA surgical approach for patients with specific spinal conditions. These guidelines have the potential to enhance the quality of care and treatment outcomes, according to more quantified recommendation for hip implant positioning in contrast to more generalized guidelines provided by previous

clinical investigations.

6. **Optimized Cup Implant Orientation for Different Spinal Conditions**: We have introduced a fully predictive simulation approach to optimize cup implant orientation based on different spinal conditions. This approach has the potential to advance surgical planning, particularly in cases of spinal fusion or stiff spines.

7. **Patient Categorization through Predictive Simulation**: We have developed a method to categorize patients using predictive simulation and cup implant orientation optimization, providing a more robust and quantifiable approach compared to traditional clinical methods.

8. **Sacrum Involvement in Fusion and Lower Limb Motion**: Our research highlights the importance of sacrum involvement in fusion and its significant effects on lower limb motion. This insight has implications for surgical decision-making and post-operative rehabilitation.

9. **Short Versus Long Spinal Fusion and Cup Orientation**: We have identified and quantified the differences in optimal cup orientation between short and long spinal fusions. This knowledge can guide surgical strategies for patients with varying extents of spinal fusion.

10. **End-to-End Patient-Specific Cup Implant Orientation**: We propose an end-to-end approach for suggesting patient-specific optimized cup implant orientation, starting from X-ray images and ending with an optimized cup implant orientation, offering a personalized solution for enhanced surgical outcomes.

6.2 Limitations of Current Study and Future Work Recommendations

In this section, we outline the key limitations of our research. These include challenges encountered in the development of the deep learning model for extracting spinopelvic measures, as discussed in Chapter 3. Additionally, we address difficulties faced during the development and validation of the human predictive simulation model, which were presented in Chapters 4 and 5. To offer insights for future research endeavors, we also propose some guidelines on how to effectively tackle these challenges.

- The foremost limitation requiring consideration is the data availability for ***LanDet***. It is anticipated that a more extensive training dataset would result in enhanced model performance. Although the model exhibited robustness in identifying landmarks even in challenging cases, refining the precision of these identifications could be achieved by augmenting the dataset with more images from patients presenting abnormalities or spinal implants.

- The effectiveness of the introduced physics-informed constraint approach has been confirmed through its successful implementation in our object detection approach (***LanDet***). Given the notable enhancement in detection accuracy demonstrated by the results, it is advisable to extend the application of this method to other keypoint detection algorithms for improved performance.

- The motion capture study was limited to a homogeneous participant pool of young, healthy males, omitting the evaluation of varied anthropometric , sex, age ranges, and spinopelvic conditions. Future research should broaden participant diversity to address these gaps.

- The dynamic models here have been validated for healthy subjects only. The validated model then is used to study different spinal condition in a predictive simulation approach. For future experimental validation, including patients with different spinal conditions undergoing THA surgery is recommended.

- We cross-validated the optimized cup orientation and stiffness parameters derived from predictive simulation and patient categorization using our deep learning model. However, it's important to note that we did not validate the modified stiffness parameters applied to patients with a stiff spine. This is because we lacked X-ray images for specific patients to assess both stiffness and spinal fusion, as well as to compare the optimized cup orientation for those particular cases.

- Motion capture has been used to obtain dimensions and kinematic validation, but it has its own inherent drawbacks, as soft tissue (skin motion) artifacts may affect the accuracy of joint angles calculated from motion capture experiments. For future studies, we suggest using videofluoroscopy images that can provide more accurate motion and segment geometry.

- We have limited the motion in a sagittal plane, as we only studied sit-to-stand motion, in our predictive simulation. This causes limitations for activities other than sit-to-stand to be included in this study. For future studies, three dimensional movement can be included by adding more DoF to the dynamic model.

- Although we introduce the predictive optimization approach as a tool to evaluate a wide rage of scenarios, we did not investigated model sensitivity to human subject size and gender. Research on how body mass index or posture-related

disorders affects results are suggested for future studies.

- The ligament insertion points were sourced from the existing literature. Conducting an in-vitro experiment or using MRI images could enhance the accuracy of these insertion points.

- In this study, we did not incorporate subject-specific muscle model parameters, geometry, inertia, and stiffness. For a more accurate subject-specific analysis in future studies, inclusion of these data is essential.

- The study employed a single implant design, which may limit the generalizability of the findings to other designs.

References

[1] Jean Legaye, G Duval-Beaupere, J Hecquet, and C Marty. Pelvic incidence: a fundamental pelvic parameter for three-dimensional regulation of spinal sagittal curves. *European Spine Journal*, 7(2):99–103, 1998.

[2] Tomaž Vrtovec, Michiel MA Janssen, Boštjan Likar, René M Castelein, Max A Viergever, and Franjo Pernuš. A review of methods for evaluating the quantitative parameters of sagittal pelvic alignment. *The Spine Journal*, 12(5):433–446, 2012.

[3] G Duval-Beaupere, C Schmidt, and PH Cosson. A barycentremetric study of the sagittal shape of spine and pelvis: the conditions required for an economic standing position. *Annals of Biomedical engineering*, 20(4):451–462, 1992.

[4] DW Murray. The definition and measurement of acetabular orientation. *The Journal of Bone and Joint Surgery*, 75(2):228–232, 1993.

[5] Diego Garbossa, Matteo Pejrona, Marco Damilano, Valerio Sansone, Alessandro Ducati, and Pedro Berjano. Pelvic parameters and global spine balance for spine degenerative disease: the importance of containing for the well being of content. *European Spine Journal*, 23(6):616–627, 2014.

[6] Sang Hong Lee, Chae Won Lim, Kwi Youn Choi, and Suenghwan Jo. Effect of spine-pelvis relationship in total hip arthroplasty. *Hip & Pelvis*, 31(1):4–10, 2019.

[7] Roger P Jackson and Anne C McManus. Radiographic analysis of sagittal plane alignment and balance in standing volunteers and patients with low back pain matched for age, sex, and size. a prospective controlled clinical study. *Spine*, 19(14):1611–1618, 1994.

[8] Péter Rajnics, Alexandre Templier, Wafa Skalli, Francois Lavaste, and Tamás Illés. The association of sagittal spinal and pelvic parameters in asymptomatic persons and patients with isthmic spondylolisthesis. *Clinical Spine Surgery*, 15(1):24–30, 2002.

[9] Hiroyuki Ike, Lawrence D Dorr, Nicholas Trasolini, Michael Stefl, Braden McKnight, and Nathanael Heckmann. Spine-pelvis-hip relationship in the functioning of a total hip replacement. *Journal of Bone and Joint Surgery*, 100(18):1606–1615, 2018.

[10] Assem A Sultan, Anton Khlopas, Nicolas S Piuzzi, Morad Chughtai, Nipun Sodhi, and Michael A Mont. The impact of spino-pelvic alignment on total hip arthroplasty outcomes: a critical analysis of current evidence. *The Journal of Arthroplasty*, 33(5):1606–1616, 2018.

[11] D Phan, SS Bederman, and R Schwarzkopf. The influence of sagittal spinal deformity on anteversion of the acetabular component in total hip arthroplasty. *The Bone & Joint Journal*, 97(8):1017–1023, 2015.

[12] M Stefl, W Lundergan, N Heckmann, B McKnight, H Ike, R Murgai, and LD Dorr. Spinopelvic mobility and acetabular component position for total hip arthroplasty. *The Bone & Joint Journal*, 99(1_Supple_A):37–45, 2017.

[13] C Rivière, J-Y Lazennec, Catherine Van Der Straeten, E Auvinet, J Cobb, and S Muirhead-Allwood. The influence of spine-hip relations on total hip replacement: A systematic review. *Orthopaedics & Traumatology: Surgery & Research*, 103(4):559–568, 2017.

[14] Zachary C Lum, John G Coury, Jonathan L Cohen, and Lawrence D Dorr. The current knowledge on spinopelvic mobility. *The Journal of Arthroplasty*, 33(1):291–296, 2018.

[15] Pierre Roussouly, Sohrab Gollogly, Olivier Noseda, Eric Berthonnaud, and Johanes Dimnet. The vertical projection of the sum of the ground reactive forces of a standing patient is not the same as the c7 plumb line: a radiographic study of the sagittal alignment of 153 asymptomatic volunteers. *Spine*, 31(11):E320–E325, 2006.

[16] Fraser Birrell, Olof Johnell, and Alan Silman. Projecting the need for hip replacement over the next three decades: influence of changing demography and threshold for surgery. *Annals of the Rheumatic Diseases*, 58(9):569–572, 1999.

[17] Canadian Institute for Health Information. Hip and knee replacements in canada, 2016–2017: Canadian joint replacement registry annual report, 2018.

[18] Canadian Institute for Health Information. Hip and knee replacements in canada, 2017–2018: Canadian joint replacement registry annual report, 2019.

[19] Christina I Esposito, Kaitlin M Carroll, Peter K Sculco, Douglas E Padgett, Seth A Jerabek, and David J Mayman. Total hip arthroplasty patients with fixed spinopelvic alignment are at higher risk of hip dislocation. *The Journal of Arthroplasty*, 33(5):1449–1454, 2018.

[20] Arthur L Malkani, Andrew T Garber, Kevin L Ong, John R Dimar, Doruk Baykal, Steven D Glassman, Adam R Cochran, and Daniel J Berry. Total hip arthroplasty in patients with previous lumbar fusion surgery: are there more dislocations and revisions? *The Journal of Arthroplasty*, 33(4):1189–1193, 2018.

[21] Jonathan M Vigdorchik, Abhinav K Sharma, Aaron J Buckland, Ameer M Elbuluk, Nima Eftekhary, David J Mayman, Kaitlin M Carroll, and Seth A Jerabek. 2021 otto aufranc award: A simple hip-spine classification for total hip arthroplasty: validation and a large multicentre series. *The Bone & Joint Journal*, 103(7 Supple B):17–24, 2021.

[22] J Vigdorchik, N Eftekhary, A Elbuluk, MP Abdel, AJ Buckland, Ran S Schwarzkopf, SA Jerabek, and DJ Mayman. Evaluation of the spine is critical in the workup of recurrent instability after total hip arthroplasty. *The Bone & Joint Journal*, 101(7):817–823, 2019.

[23] Jens Dargel, Johannes Oppermann, Gert-Peter Brüggemann, and Peer Eysel. Dislocation following total hip replacement. *Deutsches Ärzteblatt International*, 111(51-52):884, 2014.

[24] R Biedermann, A Tonin, M Krismer, F Rachbauer, G Eibl, and B Stöckl. Reducing the risk of dislocation after total hip arthroplasty: the effect of orientation of the acetabular component. *The Journal of Bone and Joint Surgery*, 87(6):762–769, 2005.

[25] George E Lewinnek, JL Lewis, RICHARD Tarr, CL Compere, and JR Zimmerman. Dislocations after total hip-replacement arthroplasties. *Journal of Bone and Joint Surgery*, 60(2):217–220, 1978.

[26] Matthew P Abdel, Philipp von Roth, Matthew T Jennings, Arlen D Hanssen, and Mark W Pagnano. What safe zone? the vast majority of dislocated thas are within the lewinnek safe zone for acetabular component position. *Clinical Orthopaedics and Related Research*, 474(2):386–391, 2016.

[27] Christina I Esposito, Brian P Gladnick, Yuo-yu Lee, Stephen Lyman, Timothy M Wright, David J Mayman, and Douglas E Padgett. Cup position alone does not predict risk of dislocation after hip arthroplasty. *The Journal of Arthroplasty*, 30(1):109–113, 2015.

[28] Claudia Iriondo, Sarah Mehany, Rutwik Shah, Upasana Bharadwaj, Emma Bahroos, Cynthia Chin, Mohammad Diab, Valentina Pedoia, and Sharmila Majumdar. Institution-wide shape analysis of 3d spinal curvature and global alignment parameters. *Journal of Orthopaedic Research®*, 40(8):1896–1908, 2022.

[29] Chi-Hung Weng, Chih-Li Wang, Yu-Jui Huang, Yu-Cheng Yeh, Chen-Ju Fu, Chao-Yuan Yeh, and Tsung-Ting Tsai. Artificial intelligence for automatic measurement of sagittal vertical axis using resunet framework. *Journal of clinical medicine*, 8(11):1826, 2019.

[30] Robert Korez, Michael Putzier, and Tomaž Vrtovec. A deep learning tool for fully automated measurements of sagittal spinopelvic balance from x-ray images: performance evaluation. *European Spine Journal*, 29(9):2295–2305, 2020.

[31] Yu-Cheng Yeh, Chi-Hung Weng, Yu-Jui Huang, Chen-Ju Fu, Tsung-Ting Tsai, and Chao-Yuan Yeh. Deep learning approach for automatic landmark detection and alignment analysis in whole-spine lateral radiographs. *Scientific reports*, 11(1):1–15, 2021.

[32] Tomaž Vrtovec and Bulat Ibragimov. Spinopelvic measurements of sagittal balance with deep learning: systematic review and critical evaluation. *European Spine Journal*, 31(8):2031–2045, 2022.

[33] Tomaž Vrtovec, Franjo Pernuš, and Boštjan Likar. A review of methods for quantitative evaluation of spinal curvature. *European spine journal*, 18:593–607, 2009.

[34] Golchehr Amirkhani, Farzam Farahmand, Seied Muhammad Yazdian, and Alireza Mirbagheri. An extended algorithm for autonomous grasping of soft tissues during robotic surgery. *The International Journal of Medical Robotics and Computer Assisted Surgery*, 16(5):1–15, 2020.

[35] Tom PC Schlösser, Michiel MA Janssen, Tom Hogervorst, Tomaž Vrtovec, John de Vos, F Cumhur Öner, and René M Castelein. The odyssey of sagittal pelvic morphology during human evolution: a perspective on different hominoidae. *The Spine Journal*, 17(8):1202–1206, 2017.

[36] Katsutaka Yamada, Yoichi Aota, Takayuki Higashi, Ko Ishida, Takanori Nimura, and Tomoyuki Saito. Accuracies in measuring spinopelvic parameters in full-spine lateral standing radiograph. *Spine*, 40(11):E640–E646, 2015.

[37] Fabio Galbusera, Gloria Casaroli, and Tito Bassani. Artificial intelligence and machine learning in spine research. *JOR spine*, 2(1):e1044, 2019.

[38] AliAsghar MohammadiNasrabadi, William McNally, Gemah Moammer, and John McPhee. Automatic extraction of spinopelvic parameters using deep learning to detect landmarks as objects. In *Medical Imaging with Deep Learning*, 2022.

[39] Hongbo Wu, Chris Bailey, Parham Rasoulinejad, and Shuo Li. Automated comprehensive adolescent idiopathic scoliosis assessment using mvc-net. *Medical image analysis*, 48:1–11, 2018.

[40] Fabio Galbusera, Frank Niemeyer, Hans-Joachim Wilke, Tito Bassani, Gloria Casaroli, Carla Anania, Francesco Costa, Marco Brayda-Bruno, and Luca Maria Sconfienza. Fully automated radiological analysis of spinal disorders and deformities: a deep learning approach. *European Spine Journal*, 28:951–960, 2019.

[41] Teng Zhang, Chuang Zhu, Qiaoyun Lu, Jun Liu, Ashish Diwan, and Jason Pui Yin Cheung. A novel tool to provide predictable alignment data irrespective of source and image quality acquired on mobile phones: what engineers can offer clinicians. *European Spine Journal*, 29:387–395, 2020.

[42] Bahare Samadi, Maxime Raison, Philippe Mahaudens, Christine Detrembleur, and Sofiane Achiche. A preliminary study in classification of the severity of spine deformation in adolescents with lumbar/thoracolumbar idiopathic scoliosis using machine learning algorithms based on lumbosacral joint efforts during gait. *Computer Methods in Biomechanics and Biomedical Engineering*, 26(11):1341–1352, 2023.

[43] Bahare Samadi, Maxime Raison, Philippe Mahaudens, Christine Detrembleur, and Sofiane Achiche. Development of machine learning algorithms to identify

the cobb angle in adolescents with idiopathic scoliosis based on lumbosacral joint efforts during gait (case study). *arXiv preprint arXiv:2301.12588*, 2023.

[44] Sheng Zhou, Hongyan Yao, Chunyu Ma, Xiaofei Chen, Wenqi Wang, Hongli Ji, Linyang He, Mengyan Luo, and Youmin Guo. Artificial intelligence x-ray measurement technology of anatomical parameters related to lumbosacral stability. *European Journal of Radiology*, 146:110071, 2022.

[45] Fabio Galbusera, Tito Bassani, Francesco Costa, Marco Brayda-Bruno, Alberto Zerbi, and Hans-Joachim Wilke. Artificial neural networks for the recognition of vertebral landmarks in the lumbar spine. *Computer Methods in Biomechanics and Biomedical Engineering: Imaging & Visualization*, 6(4):447–452, 2018.

[46] Liansheng Wang, Qiuhao Xu, Stephanie Leung, Jonathan Chung, Bo Chen, and Shuo Li. Accurate automated cobb angles estimation using multi-view extrapolation net. *Medical Image Analysis*, 58:101542, 2019.

[47] Benjamin Aubert, Carlos Vazquez, Thierry Cresson, Stefan Parent, and Jacques A de Guise. Toward automated 3d spine reconstruction from biplanar radiographs using cnn for statistical spine model fitting. *IEEE transactions on medical imaging*, 38(12):2796–2806, 2019.

[48] Kailai Zhang, Nanfang Xu, Chenyi Guo, and Ji Wu. Mpf-net: An effective framework for automated cobb angle estimation. *Medical Image Analysis*, 75:102277, 2022.

[49] Brian H Cho, Deepak Kaji, Zoe B Cheung, Ivan B Ye, Ray Tang, Amy Ahn, Oscar Carrillo, John T Schwartz, Aly A Valliani, Eric K Oermann, et al.

Automated measurement of lumbar lordosis on radiographs using machine learning and computer vision. *Global spine journal*, 10(5):611–618, 2020.

[50] John T Schwartz, Brian H Cho, Peter Tang, Javin Schefflein, Varun Arvind, Jun S Kim, Amish H Doshi, and Samuel K Cho. Deep learning automates measurement of spinopelvic parameters on lateral lumbar radiographs. *Spine*, 46(12):E671–E678, 2021.

[51] Van Luan Tran, Huei-Yung Lin, and Hsiao-Wei Liu. Mbnet: A multi-task deep neural network for semantic segmentation and lumbar vertebra inspection on x-ray images. *Proceedings of the Asian Conference on Computer Vision*, 2020.

[52] Rao Farhat Masood, Imtiaz Ahmad Taj, Muhammad Babar Khan, Muhammad Asad Qureshi, and Taimur Hassan. Deep learning based vertebral body segmentation with extraction of spinal measurements and disorder disease classification. *Biomedical Signal Processing and Control*, 71:103230, 2022.

[53] Shumao Pang, Zhihai Su, Stephanie Leung, Ilanit Ben Nachum, Bo Chen, Qianjin Feng, and Shuo Li. Direct automated quantitative measurement of spine by cascade amplifier regression network with manifold regularization. *Medical image analysis*, 55:103–115, 2019.

[54] Phillip M Cheng, Emmanuel Montagnon, Rikiya Yamashita, Ian Pan, Alexandre Cadrin-Chênevert, Francisco Perdigón Romero, Gabriel Chartrand, Samuel Kadoury, and An Tang. Deep learning: an update for radiologists. *Radiographics*, 41(5):1427–1445, 2021.

[55] Guosheng Yang, Xiangling Fu, Nanfang Xu, Kailai Zhang, and Ji Wu. A landmark estimation and correction network for automated measurement of sagittal

spinal parameters. *Neural Information Processing: 27th International Conference, ICONIP 2020, Bangkok, Thailand, November 18–22, 2020, Proceedings, Part IV 27*, pages 213–221, 2020.

[56] Andrea Cina, Tito Bassani, Matteo Panico, Andrea Luca, Youssef Masharawi, Marco Brayda-Bruno, and Fabio Galbusera. 2-step deep learning model for landmarks localization in spine radiographs. *Scientific Reports*, 11(1):9482, 2021.

[57] Jiawei Huang, Haotian Shen, Jialong Wu, Xiaojian Hu, Zhiwei Zhu, Xiaoqiang Lv, Yong Liu, and Yue Wang. Spine explorer: a deep learning based fully automated program for efficient and reliable quantifications of the vertebrae and discs on sagittal lumbar spine mr images. *The Spine Journal*, 20(4):590–599, 2020.

[58] YiRang Shin, Kyunghwa Han, and Young Han Lee. Temporal trends in cervical spine curvature of south korean adults assessed by deep learning system segmentation, 2006-2018. *JAMA network open*, 3(10):e2020961–e2020961, 2020.

[59] Dong Hyun Kim, Jin Gyo Jeong, Young Jae Kim, Kwang Gi Kim, and Ji Young Jeon. Automated vertebral segmentation and measurement of vertebral compression ratio based on deep learning in x-ray images. *Journal of Digital Imaging*, 34:853–861, 2021.

[60] William McNally, Kanav Vats, Alexander Wong, and John McPhee. Rethinking keypoint representations: Modeling keypoints and poses as objects for multi-person human pose estimation. *arXiv preprint arXiv:2111.08557*, 2021.

[61] Navneet Dalal and Bill Triggs. Histograms of oriented gradients for human detection. *2005 IEEE computer society conference on computer vision and pattern recognition (CVPR'05)*, 1:886–893, 2005.

[62] David G Lowe. Object recognition from local scale-invariant features. *Proceedings of the seventh IEEE international conference on computer vision*, 2:1150–1157, 1999.

[63] Rainer Lienhart and Jochen Maydt. An extended set of haar-like features for rapid object detection. *Proceedings. international conference on image processing*, 1:I–I, 2002.

[64] Paul Viola and Michael Jones. Rapid object detection using a boosted cascade of simple features. *Proceedings of the 2001 IEEE computer society conference on computer vision and pattern recognition. CVPR 2001*, 1:I–I, 2001.

[65] Corinna Cortes and Vladimir Vapnik. Support-vector networks. *Machine learning*, 20:273–297, 1995.

[66] Yoav Freund and Robert E Schapire. A decision-theoretic generalization of on-line learning and an application to boosting. *Journal of computer and system sciences*, 55(1):119–139, 1997.

[67] Joseph Redmon, Santosh Divvala, Ross Girshick, and Ali Farhadi. You only look once: Unified, real-time object detection. *Proceedings of the IEEE conference on computer vision and pattern recognition*, pages 779–788, 2016.

[68] Wei Liu, Dragomir Anguelov, Dumitru Erhan, Christian Szegedy, Scott Reed, Cheng-Yang Fu, and Alexander C Berg. Ssd: Single shot multibox detector.

Computer Vision–ECCV 2016: 14th European Conference, Amsterdam, The Netherlands, October 11–14, 2016, Proceedings, Part I 14, pages 21–37, 2016.

[69] Tsung-Yi Lin, Priya Goyal, Ross Girshick, Kaiming He, and Piotr Dollár. Focal loss for dense object detection. *Proceedings of the IEEE international conference on computer vision*, pages 2980–2988, 2017.

[70] Ross Girshick, Jeff Donahue, Trevor Darrell, and Jitendra Malik. Rich feature hierarchies for accurate object detection and semantic segmentation. *Proceedings of the IEEE conference on computer vision and pattern recognition*, pages 580–587, 2014.

[71] Ross Girshick. Fast r-cnn. *Proceedings of the IEEE international conference on computer vision*, pages 1440–1448, 2015.

[72] Shaoqing Ren, Kaiming He, Ross Girshick, and Jian Sun. Faster r-cnn: Towards real-time object detection with region proposal networks. *Advances in neural information processing systems*, 28, 2015.

[73] Karen Simonyan and Andrew Zisserman. Very deep convolutional networks for large-scale image recognition. *arXiv preprint arXiv:1409.1556*, 2014.

[74] Kaiming He, Xiangyu Zhang, Shaoqing Ren, and Jian Sun. Deep residual learning for image recognition. *Proceedings of the IEEE conference on computer vision and pattern recognition*, pages 770–778, 2016.

[75] Mark Sandler, Andrew Howard, Menglong Zhu, Andrey Zhmoginov, and Liang-Chieh Chen. Mobilenetv2: Inverted residuals and linear bottlenecks. *Proceedings of the IEEE conference on computer vision and pattern recognition*, pages 4510–4520, 2018.

[76] Junhyung Kang, Shahroz Tariq, Han Oh, and Simon S Woo. A survey of deep learning-based object detection methods and datasets for overhead imagery. *IEEE Access*, 10:20118–20134, 2022.

[77] Alex Krizhevsky, Ilya Sutskever, and Geoffrey E Hinton. Imagenet classification with deep convolutional neural networks. *Advances in neural information processing systems*, 25, 2012.

[78] Hongkai Zhang, Hong Chang, Bingpeng Ma, Naiyan Wang, and Xilin Chen. Dynamic r-cnn: Towards high quality object detection via dynamic training. *Computer Vision–ECCV 2020: 16th European Conference, Glasgow, UK, August 23–28, 2020, Proceedings, Part XV 16*, pages 260–275, 2020.

[79] Tsung-Yi Lin, Piotr Dollár, Ross Girshick, Kaiming He, Bharath Hariharan, and Serge Belongie. Feature pyramid networks for object detection. *Proceedings of the IEEE conference on computer vision and pattern recognition*, pages 2117–2125, 2017.

[80] Zhaowei Cai and Nuno Vasconcelos. Cascade r-cnn: Delving into high quality object detection. *Proceedings of the IEEE conference on computer vision and pattern recognition*, pages 6154–6162, 2018.

[81] Jiangmiao Pang, Kai Chen, Jianping Shi, Huajun Feng, Wanli Ouyang, and Dahua Lin. Libra r-cnn: Towards balanced learning for object detection. *Proceedings of the IEEE/CVF conference on computer vision and pattern recognition*, pages 821–830, 2019.

[82] Zhengxiong Luo, Zhicheng Wang, Yan Huang, Liang Wang, Tieniu Tan, and Erjin Zhou. Rethinking the heatmap regression for bottom-up human pose

estimation. *Proceedings of the IEEE/CVF conference on computer vision and pattern recognition*, pages 13264–13273, 2021.

[83] JY Lazennec, A Riwan, F Gravez, MA Rousseau, N Mora, M Gorin, A Lasne, Y Catonne, and G Saillant. Hip spine relationships: application to total hip arthroplasty. *Hip International*, 17(5_suppl):91–104, 2007.

[84] J-Y Lazennec, N Charlot, M Gorin, B Roger, N Arafati, A Bissery, and G Saillant. Hip-spine relationship: a radio-anatomical study for optimization in acetabular cup positioning. *Surgical and Radiologic Anatomy*, 26(2):136–144, 2004.

[85] GQ Zheng, YG Zhang, JY Chen, and Y Wang. Decision making regarding spinal osteotomy and total hip replacement for ankylosing spondylitis: experience with 28 patients. *The Bone & Joint Journal*, 96(3):360–365, 2014.

[86] Jean Legaye. Influence of the sagittal balance of the spine on the anterior pelvic plane and on the acetabular orientation. *International orthopaedics*, 33(6):1695–1700, 2009.

[87] WM Tang, KY Chiu, MFY Kwan, and TP Ng. Sagittal pelvic mal-rotation and positioning of the acetabular component in total hip arthroplasty: three-dimensional computer model analysis. *Journal of orthopaedic research*, 25(6):766–771, 2007.

[88] Zhinian Wan, Aamer Malik, Branislav Jaramaz, Lisa Chao, and Lawrence D Dorr. Imaging and navigation measurement of acetabular component position in tha. *Clinical Orthopaedics and Related Research*, 467(1):32–42, 2009.

[89] Vaibhav Kanawade, Lawrence D Dorr, and Zhinian Wan. Predictability of acetabular component angular change with postural shift from standing to sitting position. *Journal of Bone and Joint Surgery*, 96(12):978–986, 2014.

[90] Jean-Yves Lazennec, Patrick Boyer, Michel Gorin, Yves Catonné, and Marc Antoine Rousseau. Acetabular anteversion with ct in supine, simulated standing, and sitting positions in a tha patient population. *Clinical Orthopaedics and Related Research*, 469(4):1103–1109, 2011.

[91] Hironori Ochi, Tomonori Baba, Yasuhiro Homma, Mikio Matsumoto, Hidetoshi Nojiri, and Kazuo Kaneko. Importance of the spinopelvic factors on the pelvic inclination from standing to sitting before total hip arthroplasty. *European Spine Journal*, 25(11):3699–3706, 2016.

[92] Nancy E Lane. Osteoarthritis of the hip. *New England Journal of Medicine*, 357(14):1413–1421, 2007.

[93] Assem A Sultan, Anton Khlopas, Inyang Udo-Inyang, Morad Chughtai, Nipun Sodhi, Suela Lamaj, Roland Starr, Nicolas S Piuzzi, Anil Bhave, and Michael A Mont. Hip osteoarthritis patients demonstrated marked dynamic changes and variability in pelvic tilt, obliquity, and rotation: A comparative, gait-analysis study. *Surgical technology international*, 32:285–292, 2018.

[94] Youngwoo Kim, Claudio Vergari, Yu Shimizu, Hiroyuki Tokuyasu, and Mitsuru Takemoto. The impact of hip mobility on lumbar and pelvic mobility before and after total hip arthroplasty. *Journal of Clinical Medicine*, 12(1):331, 2022.

[95] Charles Rivière, Stefan Lazic, Louis Dagneaux, Catherine Van Der Straeten, Justin Cobb, and Sarah Muirhead-Allwood. Spine–hip relations in patients with hip osteoarthritis. *EFORT open reviews*, 3(2):39–44, 2018.

[96] Abhinav K Sharma and Jonathan M Vigdorchik. The hip-spine relationship in total hip arthroplasty: how to execute the plan. *The Journal of Arthroplasty*, 36(7):S111–S120, 2021.

[97] AJ Buckland, V Puvanesarajah, J Vigdorchik, Ran Schwarzkopf, Amit Jain, Eric Otto Klineberg, Robert A Hart, JJ Callaghan, and H Hassanzadeh. Dislocation of a primary total hip arthroplasty is more common in patients with a lumbar spinal fusion. *The Bone & Joint Journal*, 99(5):585–591, 2017.

[98] Jonathan M Vigdorchik, Abhinav K Sharma, Douglas A Dennis, Leonard R Walter, Jim W Pierrepont, and Andrew J Shimmin. The majority of total hip arthroplasty patients with a stiff spine do not have an instrumented fusion. *The Journal of Arthroplasty*, 35(6):S252–S254, 2020.

[99] Jeffrey J Barry, David C Sing, Thomas P Vail, and Erik N Hansen. Early outcomes of primary total hip arthroplasty after prior lumbar spinal fusion. *The Journal of Arthroplasty*, 32(2):470–474, 2017.

[100] Jean Y Lazennec, Ian C Clark, Dominique Folinais, Imen N Tahar, and Aidin E Pour. What is the impact of a spinal fusion on acetabular implant orientation in functional standing and sitting positions? *The Journal of Arthroplasty*, 32(10):3184–3190, 2017.

[101] Nicholas A Bedard, Christopher T Martin, Sean E Slaven, Andrew J Pugely, Sergio A Mendoza-Lattes, and John J Callaghan. Abnormally high dislocation

rates of total hip arthroplasty after spinal deformity surgery. *The Journal of Arthroplasty*, 31(12):2884–2885, 2016.

[102] T Eneqvist, S Nemes, H Brisby, P Fritzell, G Garellick, and O Rolfson. Lumbar surgery prior to total hip arthroplasty is associated with worse patient-reported outcomes. *Bone & Joint Journal*, 99(6):759–765, 2017.

[103] Connor A King, David C Landy, John M Martell, Hue H Luu, Lewis L Shi, and Michael J Lee. Time to dislocation analysis of lumbar spine fusion following total hip arthroplasty: breaking up a happy home. *The Journal of Arthroplasty*, 33(12):3768–3772, 2018.

[104] Arthur L Malkani, Kevin J Himschoot, Kevin L Ong, Edmund C Lau, Doruk Baykal, John R Dimar, Steven D Glassman, and Daniel J Berry. Does timing of primary total hip arthroplasty prior to or after lumbar spine fusion have an effect on dislocation and revision rates? *The Journal of Arthroplasty*, 34(5):907–911, 2019.

[105] CG Salib, N Reina, KI Perry, MJ Taunton, DJ Berry, and MP Abdel. Lumbar fusion involving the sacrum increases dislocation risk in primary total hip arthroplasty. *The Bone & Joint Journal*, 101(2):198–206, 2019.

[106] Edward M DelSole, Jonathan M Vigdorchik, Ran Schwarzkopf, Thomas J Errico, and Aaron J Buckland. Total hip arthroplasty in the spinal deformity population: does degree of sagittal deformity affect rates of safe zone placement, instability, or revision? *The Journal of Arthroplasty*, 32(6):1910–1917, 2017.

[107] Tina M Morrison, Pras Pathmanathan, Mariam Adwan, and Edward Margerrison. Advancing regulatory science with computational modeling for medical

devices at the fda's office of science and engineering laboratories. *Frontiers in Medicine*, 5:241, 2018.

[108] Daniel J Blizzard, Brian T Nickel, Thorsten M Seyler, and Michael P Bolognesi. The impact of lumbar spine disease and deformity on total hip arthroplasty outcomes. *Orthopedic Clinics*, 47(1):19–28, 2016.

[109] N Eftekhary, A Shimmin, JY Lazennec, A Buckland, R Schwarzkopf, LD Dorr, D Mayman, D Padgett, and J Vigdorchik. A systematic approach to the hip-spine relationship and its applications to total hip arthroplasty. *The Bone & Joint Journal*, 101(7):808–816, 2019.

[110] Christian Klemt, Sakkadech Limmahakhun, Georges Bounajem, Liang Xiong, Ingwon Yeo, and Young-Min Kwon. Effect of postural changes on in vivo pelvic tilt and functional component anteversion in total hip arthroplasty patients with lumbar disc degenerations. *The Bone & Joint Journal*, 102(11):1505–1510, 2020.

[111] Daniel H Wiznia, Daniel B Buchalter, David J Kirby, Aaron J Buckland, William J Long, and Ran Schwarzkopf. Applying the hip-spine relationship in total hip arthroplasty. *HIP International*, 31(2):144–153, 2021.

[112] Yolanda M Gu, Woosung Kim, Jim W Pierrepont, Qing Li, and Andrew J Shimmin. The effect of a degenerative spine and adverse pelvic mobility on prosthetic impingement in patients undergoing total hip arthroplasty. *The Journal of Arthroplasty*, 36(7):2523–2529, 2021.

[113] Bassel G Diebo, George A Beyer, Preston W Grieco, Shian Liu, Louis M Day, Roby Abraham, Qais Naziri, Peter G Passias, Aditya V Maheshwari, and Carl B

Paulino. Complications in patients undergoing spinal fusion after tha. *Clinical Orthopaedics and Related Research*, 476(2):412, 2018.

[114] Vincent VG An, Kevin Phan, Brahman S Sivakumar, Ralph J Mobbs, and Warwick J Bruce. Prior lumbar spinal fusion is associated with an increased risk of dislocation and revision in total hip arthroplasty: a meta-analysis. *The Journal of Arthroplasty*, 33(1):297–300, 2018.

[115] Jing Loong Moses Loh, Lei Jiang, Hwei Chi Chong, Seng Jin Yeo, and Ngai Nung Lo. Effect of spinal fusion surgery on total hip arthroplasty outcomes: a matched comparison study. *The Journal of Arthroplasty*, 32(8):2457–2461, 2017.

[116] Aliakbar Alamdari and Venkat N Krovi. A review of computational musculoskeletal analysis of human lower extremities. *Human modelling for bio-inspired robotics*, pages 37–73, 2017.

[117] Mahdokht Ezati, Borna Ghannadi, and John McPhee. A review of simulation methods for human movement dynamics with emphasis on gait. *Multibody System Dynamics*, 47:265–292, 2019.

[118] Míriam Febrer-Nafría, Ali Nasr, Mahdokht Ezati, Peter Brown, Josep M Font-Llagunes, and John McPhee. Predictive multibody dynamic simulation of human neuromusculoskeletal systems: a review. *Multibody System Dynamics*, pages 1–41, 2022.

[119] Manish Sreenivasa, Matthew Millard, Idsart Kingma, Jaap H Van Dieen, and Katja Mombaur. Predicting the influence of hip and lumbar flexibility on lifting motions using optimal control. *Journal of biomechanics*, 78:118–125, 2018.

[120] Athena Jalalian, Ian Gibson, and Eng Hock Tay. Computational biomechanical modeling of scoliotic spine: challenges and opportunities. *Spine Deformity*, 1(6):401–411, 2013.

[121] Pamela K Levangie and Cynthia C Norkin. Joint structure and function; a comprehensive analysis. 3rd. *Philadelphia: FA. Davis Company*, 2000.

[122] Alireza Abouhossein, Bernhard Weisse, and Stephen J Ferguson. A multibody modelling approach to determine load sharing between passive elements of the lumbar spine. *Computer methods in biomechanics and biomedical engineering*, 14(06):527–537, 2011.

[123] Albert B Schultz and CARL HIRSCH. Mechanical analysis of harrington rod correction of idiopathic scoliosis. *Journal of Bone and Joint Surgery*, 55(5):983–992, 1973.

[124] Li-Xin Guo, Ee-Chon Teo, and Tian-Xia Qiu. Prediction of biomechanical characteristics of intact and injured lower thoracic spine segment under different loads. *Journal of Musculoskeletal Research*, 8(02n03):87–99, 2004.

[125] Tito Bassani and Fabio Galbusera. Musculoskeletal modeling. In *Biomechanics of the Spine*, pages 257–277. Elsevier, 2018.

[126] Miguel Christophy, Nur Adila Faruk Senan, Jeffrey C Lotz, and Oliver M O'Reilly. A musculoskeletal model for the lumbar spine. *Biomechanics and Modeling in mMchanobiology*, 11(1-2):19–34, 2012.

[127] Dominika Ignasiak, Stephen J Ferguson, and Navid Arjmand. A rigid thorax assumption affects model loading predictions at the upper but not lower lumbar levels. *Journal of Biomechanics*, 49(13):3074–3078, 2016.

[128] Taysa Bervian Bassani, Jéssica M Bonato, Meira MF Machado, Valentín Cóppola-Segovia, Eric LR Moura, Silvio M Zanata, Rúbia MMW Oliveira, and Maria ABF Vital. Decrease in adult neurogenesis and neuroinflammation are involved in spatial memory impairment in the streptozotocin-induced model of sporadic alzheimer's disease in rats. *Molecular neurobiology*, 55(5):4280–4296, 2018.

[129] Archibald Vivian Hill. The heat of shortening and the dynamic constants of muscle. *Proceedings of the royal society of London. series b-biological sciences*, 126(843):136–195, 1938.

[130] Rui Zhu, Wen-xin Niu, Zhi-li Zeng, Jian-hua Tong, Zhi-wei Zhen, Shuang Zhou, Yan Yu, and Li-ming Cheng. The effects of muscle weakness on degenerative spondylolisthesis: A finite element study. *Clinical Biomechanics*, 41:34–38, 2017.

[131] Wei Fan and Li-Xin Guo. Influence of different frequencies of axial cyclic loading on time-domain vibration response of the lumbar spine: a finite element study. *Computers in biology and medicine*, 86:75–81, 2017.

[132] Ming Xu, James Yang, Isador H Lieberman, and Ram Haddas. Lumbar spine finite element model for healthy subjects: development and validation. *Computer methods in biomechanics and biomedical engineering*, 20(1):1–15, 2017.

[133] Iman Shojaei, Brad D Hendershot, Julian C Acasio, Christopher L Dearth, Matthew Ballard, and Babak Bazrgari. Trunk muscle forces and spinal loads in persons with unilateral transfemoral amputation during sit-to-stand and stand-to-sit activities. *Clinical Biomechanics*, 63:95–103, 2019.

[134] Thomas Zander, Antonius Rohlmann, and Georg Bergmann. Influence of different artificial disc kinematics on spine biomechanics. *Clinical biomechanics*, 24(2):135–142, 2009.

[135] Zhitao Xiao, Liya Wang, He Gong, and Dong Zhu. Biomechanical evaluation of three surgical scenarios of posterior lumbar interbody fusion by finite element analysis. *Biomedical engineering online*, 11(1):31, 2012.

[136] TK Rupp, W Ehlers, N Karajan, M Günther, and S Schmitt. A forward dynamics simulation of human lumbar spine flexion predicting the load sharing of intervertebral discs, ligaments, and muscles. *Biomechanics and Modeling in Mechanobiology*, 14(5):1081–1105, 2015.

[137] E Otten. Inverse and forward dynamics: models of multi–body systems. *Philosophical transactions of the royal society of London. Series B: biological sciences*, 358(1437):1493–1500, 2003.

[138] Kap-Soo Han, Thomas Zander, William R Taylor, and Antonius Rohlmann. An enhanced and validated generic thoraco-lumbar spine model for prediction of muscle forces. *Medical Engineering & Physics*, 34(6):709–716, 2012.

[139] Mark De Zee, Lone Hansen, Christian Wong, John Rasmussen, and Erik B Simonsen. A generic detailed rigid-body lumbar spine model. *Journal of Biomechanics*, 40(6):1219–1227, 2007.

[140] Tito Bassani, Elena Stucovitz, Zhihui Qian, Matteo Briguglio, and Fabio Galbusera. Validation of the anybody full body musculoskeletal model in computing lumbar spine loads at l4l5 level. *Journal of Biomechanics*, 58:89–96, 2017.

[141] Alexander G Bruno, Mary L Bouxsein, and Dennis E Anderson. Development and validation of a musculoskeletal model of the fully articulated thoracolumbar spine and rib cage. *Journal of biomechanical engineering*, 137(8), 2015.

[142] Erica Beaucage-Gauvreau, William SP Robertson, Scott CE Brandon, Robert Fraser, Brian JC Freeman, Ryan B Graham, Dominic Thewlis, and Claire F Jones. Validation of an opensim full-body model with detailed lumbar spine for estimating lower lumbar spine loads during symmetric and asymmetric lifting tasks. *Computer methods in biomechanics and biomedical engineering*, 22(5):451–464, 2019.

[143] Riza Bayoglu, Pavel E Galibarov, Nico Verdonschot, Bart Koopman, and Jasper Homminga. Twente spine model: A thorough investigation of the spinal loads in a complete and coherent musculoskeletal model of the human spine. *Medical Engineering & Physics*, 68:35–45, 2019.

[144] Gabriel Abedrabbo Ode, Paul Fisette, Maryline Mousny, Philippe Mahaudens, Christine Detrembleur, Carl-Eric Aubin, and Maxime Raison. Dynamic analysis of intervertebral efforts in scoliosis: a multibody modeling approach. In *Multibody Dynamics 2011-ECCOMAS Thematic Conference*, 2011.

[145] Xiangjie Meng, Alexander G Bruno, Bo Cheng, Wenjun Wang, Mary L Bouxsein, and Dennis E Anderson. Incorporating six degree-of-freedom intervertebral joint stiffness in a lumbar spine musculoskeletal model—method and performance in flexed postures. *Journal of biomechanical engineering*, 137(10), 2015.

[146] Marco Senteler, Ameet Aiyangar, Bernhard Weisse, Mazda Farshad, and Jess G Snedeker. Sensitivity of intervertebral joint forces to center of rotation location

and trends along its migration path. *Journal of Biomechanics*, 70:140–148, 2018.

[147] F Ghezelbash, AH Eskandari, A Shirazi-Adl, N Arjmand, Z El-Ouaaid, and A Plamondon. Effects of motion segment simulation and joint positioning on spinal loads in trunk musculoskeletal models. *Journal of Biomechanics*, 70:149–156, 2018.

[148] A Shirazi-Adl. Analysis of large compression loads on lumbar spine in flexion and in torsion using a novel wrapping element. *Journal of Biomechanics*, 39(2):267–275, 2006.

[149] A Shirazi-Adl. Biomechanics of the lumbar spine in sagittal/lateral moments. *Spine*, 19(21):2407–2414, 1994.

[150] Hans-Joachim Wilke, Peter Neef, Barbara Hinz, Helmut Seidel, and Lutz Claes. Intradiscal pressure together with anthropometric data–a data set for the validation of models. *Clinical Biomechanics*, 16:S111–S126, 2001.

[151] Valerie Norman-Gerum and John McPhee. Constrained dynamic optimization of sit-to-stand motion driven by bézier curves. *Journal of biomechanical engineering*, 140(12), 2018.

[152] Khai-Long Ho Hoang and Katja D Mombaur. Optimal design of a physical assistive device to support sit-to-stand motions. *2015 IEEE International Conference on Robotics and Automation (ICRA)*, pages 5891–5897, 2015.

[153] Conor Jansen and John McPhee. Predictive dynamic simulation of olympic track cycling standing start using direct collocation optimal control. *Multibody System Dynamics*, 49:53–70, 2020.

[154] Colin Brown and John McPhee. Predictive forward dynamic simulation of manual wheelchair propulsion on a rolling dynamometer. *Journal of biomechanical engineering*, 142(7):071008, 2020.

[155] Christopher L Dembia, Nicholas A Bianco, Antoine Falisse, Jennifer L Hicks, and Scott L Delp. Opensim moco: Musculoskeletal optimal control. *PLOS Computational Biology*, 16(12):e1008493, 2020.

[156] Mohsen Sadeghi, Mehran Emadi Andani, Fariba Bahrami, and Mohamad Parnianpour. Trajectory of human movement during sit to stand: a new modeling approach based on movement decomposition and multi-phase cost function. *Experimental brain research*, 229:221–234, 2013.

[157] Katja Mombaur and Khai-Long Ho Hoang. How to best support sit to stand transfers of geriatric patients: Motion optimization under external forces for the design of physical assistive devices. *Journal of biomechanics*, 58:131–138, 2017.

[158] Oscar Chuy, Yasuhisa Hirata, Zhidong Wang, and Kazuhiro Kosuge. Approach in assisting a sit-to-stand movement using robotic walking support system. In *2006 IEEE/RSJ International Conference on Intelligent Robots and Systems*, pages 4343–4348. IEEE, 2006.

[159] Sergey Jatsun, Sergei Savin, Andrey Yatsun, and Ruslan Turlapov. Adaptive control system for exoskeleton performing sit-to-stand motion. *2015 10th International Symposium on Mechatronics and Its Applications (ISMA)*, pages 1–6, 2015.

[160] Katherine A Strausser and H Kazerooni. The development and testing of a human machine interface for a mobile medical exoskeleton. *2011 IEEE/RSJ International Conference on Intelligent Robots and Systems*, pages 4911–4916, 2011.

[161] AliAsghar MohammadiNasrabadi, Farshid Absalan, and Seyed AliAkbar Moosavian. Design kinematics and dynamics modeling of a lower limb walking assistant robot. *Proceedings of the 4th International Conference on Robotics and Mechatron-ics*, 8(2):26–28, 2016.

[162] AliAsghar MohammadiNasrabadi, Farshid Absalan, and Seyed Ali Akbar Moosavian. Design, modeling and simulation of weight compensation walking assistant robot. *Modares Mechanical Engineering*, 17(5):41–51, 2017.

[163] Richard W Bohannon, Susan R Barreca, Megan E Shove, Cynthia Lambert, Lisa M Masters, and Christopher S Sigouin. Documentation of daily sit-to-stands performed by community-dwelling adults. *Physiotherapy theory and practice*, 24(6):437–442, 2008.

[164] Daniel N Huff, Casey A Myers, and Paul J Rullkoetter. Impact of alignment and kinematic variation on resistive moment and dislocation propensity for tha with lipped and neutral liners. *Biomechanics and Modeling in Mechanobiology*, 19:1297–1307, 2020.

[165] Maarten F Bobbert, Dinant A Kistemaker, Marco Aurélio Vaz, and Marko Ackermann. Searching for strategies to reduce the mechanical demands of the sit-to-stand task with a muscle-actuated optimal control model. *Clinical Biomechanics*, 37:83–90, 2016.

[166] Matthew Millard and Katja Mombaur. Sit-to-stand models of older adults should include muscle nonlinearities and arms. *Converging Clinical and Engineering Research on Neurorehabilitation IV: Proceedings of the 5th International Conference on Neurorehabilitation (ICNR2020), October 13–16, 2020*, pages 333–338, 2022.

[167] Milad Geravand, Peter Zeno Korondi, Christian Werner, Klaus Hauer, and Angelika Peer. Human sit-to-stand transfer modeling towards intuitive and biologically-inspired robot assistance. *Autonomous Robots*, 41:575–592, 2017.

[168] Jernej Kuželički, Miloš Žefran, Helena Burger, and Tadej Bajd. Synthesis of standing-up trajectories using dynamic optimization. *Gait & posture*, 21(1):1–11, 2005.

[169] Mariska Wesseling, Loes C Derikx, Friedl De Groote, Ward Bartels, Christophe Meyer, Nico Verdonschot, and Ilse Jonkers. Muscle optimization techniques impact the magnitude of calculated hip joint contact forces. *Journal of orthopaedic research*, 33(3):430–438, 2015.

[170] BW Stansfield, AC Nicol, JP Paul, IG Kelly, F Graichen, and G Bergmann. Direct comparison of calculated hip joint contact forces with those measured using instrumented implants. an evaluation of a three-dimensional mathematical model of the lower limb. *Journal of biomechanics*, 36(7):929–936, 2003.

[171] João Costa, Joaquim Peixoto, Pedro Moreira, António Pedro Souto, Paulo Flores, and Hamid M Lankarani. Influence of the hip joint modeling approaches on the kinematics of human gait. *Journal of Tribology*, 138(3):031201, 2016.

[172] Gerlinde Lenaerts, Friedl De Groote, Bram Demeulenaere, Michiel Mulier, Georges Van der Perre, Arthur Spaepen, and Ilse Jonkers. Subject-specific hip geometry affects predicted hip joint contact forces during gait. *Journal of biomechanics*, 41(6):1243–1252, 2008.

[173] Mahsa Ghaffari, Reza Nickmanesh, Neda Tamannaee, and Farzam Farahmand. The impingement-dislocation risk of total hip replacement: effects of cup orientation and patient maneuvers. *2012 Annual international conference of the IEEE engineering in medicine and biology society*, pages 6801–6804, 2012.

[174] Elhadi Sariali, Todd Stewart, Zhongmin Jin, and John Fisher. Effect of cup abduction angle and head lateral microseparation on contact stresses in ceramic-on-ceramic total hip arthroplasty. *Journal of biomechanics*, 45(2):390–393, 2012.

[175] Qingen Meng, Jing Wang, Peiran Yang, Zhongmin Jin, and John Fisher. The lubrication performance of the ceramic-on-ceramic hip implant under starved conditions. *journal of the mechanical behavior of biomedical materials*, 50:70–76, 2015.

[176] Michael M Morlock, Nick Bishop, Jozef Zustin, Michael Hahn, Wolfgang Rüther, and Michael Amling. Modes of implant failure after hip resurfacing: morphological and wear analysis of 267 retrieval specimens. *JBJS*, 90(Supplement_3):89–95, 2008.

[177] Laura Ezquerra, María Paz Quilez, María Ángeles Pérez, Jorge Albareda, and Belén Seral. Range of movement for impingement and dislocation avoidance in total hip replacement predicted by finite element model. *Journal of Medical and Biological Engineering*, 37:26–34, 2017.

[178] Juliana Hsu, Matias de La Fuente, and Klaus Radermacher. Multi-dimensional range-of-motion-based safe zone for patient-specific total hip arthroplasty. *Computer Assisted Orthopedic Surgery*, 1:175–180, 2017.

[179] Anthony M DiGioia III, Mahmoud A Hafez, Branislav Jaramaz, Timothy J Levison, and James E Moody. Functional pelvic orientation measured from lateral standing and sitting radiographs. *Clinical Orthopaedics and Related Research®*, 453:272–276, 2006.

[180] Robert L Barrack, Carlos Lavernia, Michael Ries, Robert Thornberry, and Evangelos Tozakoglou. Virtual reality computer animation of the effect of component position and design on stability after total hip arthroplasty. *Orthopedic Clinics*, 32(4):569–577, 2001.

[181] Karl-Heinz Widmer. The impingement-free, prosthesis-specific, and anatomy-adjusted combined target zone for component positioning in tha depends on design and implantation parameters of both components. *Clinical orthopaedics and related research*, 478(8):1904, 2020.

[182] Maeruan Kebbach, Christian Schulze, Christian Meyenburg, Daniel Kluess, Mevluet Sungu, Albrecht Hartmann, Klaus-Peter Günther, and Rainer Bader. Do hip resurfacing and short hip stem arthroplasties differ from conventional hip stem arthroplasties regarding impingement-free range of motion? *Journal of Orthopaedic Research®*, 2023.

[183] Aidin Eslam Pour, Ran Schwarzkopf, Kunj Pareshkumar Patel, Manan Anjaria, Jean Yves Lazennec, and Lawrence D Dorr. Is combined anteversion equally affected by acetabular cup and femoral stem anteversion? *The Journal of arthroplasty*, 36(7):2393–2401, 2021.

[184] Hao Tang, Ya Li, Yixin Zhou, Siyuang Wang, Yongqiang Zhao, and Zhuyi Ma. A modeling study of a patient-specific safe zone for tha: calculation, validation, and key factors based on standing and sitting sagittal pelvic tilt. *Clinical Orthopaedics and Related Research®*, 480(1):191–205, 2022.

[185] K-H Widmer. Containment versus impingement: finding a compromise for cup placement in total hip arthroplasty. *International orthopaedics*, 31:29–33, 2007.

[186] Oliver Kessler, Shantanu Patil, Wirth Stefan, Eckart Mayr, Clifford W Colwell Jr, and Darryl D D'Lima. Bony impingement affects range of motion after total hip arthroplasty: A subject-specific approach. *Journal of orthopaedic research*, 26(4):443–452, 2008.

[187] Stephen J Mellon, George Grammatopoulos, Michael S Andersen, Hemant G Pandit, Harinderjit S Gill, and David W Murray. Optimal acetabular component orientation estimated using edge-loading and impingement risk in patients with metal-on-metal hip resurfacing arthroplasty. *Journal of Biomechanics*, 48(2):318–323, 2015.

[188] Jacob M Elkins, John J Callaghan, and Thomas D Brown. The 2014 frank stinchfield award: The 'landing zone'for wear and stability in total hip arthroplasty is smaller than we thought: a computational analysis. *Clinical Orthopaedics and Related Research®*, 473(2):441–452, 2015.

[189] Chien-Yao Wang, Hong-Yuan Mark Liao, Yueh-Hua Wu, Ping-Yang Chen, Jun-Wei Hsieh, and I-Hau Yeh. Cspnet: A new backbone that can enhance learning capability of cnn. *Proceedings of the IEEE/CVF conference on computer vision and pattern recognition workshops*, pages 390–391, 2020.

[190] Glenn Jocher, Alex Stoken, Jirka Borovec, Ayush Chaurasia, Liu Changyu, Adam Hogan, Jan Hajek, Laurentiu Diaconu, Yonghye Kwon, Yann Defretin, et al. ultralytics/yolov5: v5. 0-yolov5-p6 1280 models, aws, supervise. ly and youtube integrations. *Zenodo*, 2021.

[191] Chien-Yao Wang, Alexey Bochkovskiy, and Hong-Yuan Mark Liao. Scaled-yolov4: Scaling cross stage partial network. *Proceedings of the IEEE/cvf conference on computer vision and pattern recognition*, pages 13029–13038, 2021.

[192] Zhaohui Zheng, Ping Wang, Wei Liu, Jinze Li, Rongguang Ye, and Dongwei Ren. Distance-iou loss: Faster and better learning for bounding box regression. *Proceedings of the AAAI conference on artificial intelligence*, 34(07):12993–13000, 2020.

[193] Glenn Jocher. ultralytics/yolov5: v5.0. *GitHub*, 2021.

[194] Yu E Nesterov. A method for solving the convex programming problem with convergence rate. In *Dokl. akad. nauk Sssr*, volume 269, pages 543–547, 1983.

[195] Ilya Loshchilov and Frank Hutter. Sgdr: Stochastic gradient descent with warm restarts. *arXiv preprint arXiv:1608.03983*, 2016.

[196] Priya Goyal, Piotr Dollár, Ross Girshick, Pieter Noordhuis, Lukasz Wesolowski, Aapo Kyrola, Andrew Tulloch, Yangqing Jia, and Kaiming He. Accurate, large minibatch sgd: Training imagenet in 1 hour. *arXiv preprint arXiv:1706.02677*, 2017.

[197] Alexey Bochkovskiy, Chien-Yao Wang, and Hong-Yuan Mark Liao. Yolov4: Optimal speed and accuracy of object detection. *arXiv preprint arXiv:2004.10934*, 2020.

[198] David Liljequist, Britt Elfving, and Kirsti Skavberg Roaldsen. Intraclass correlation–a discussion and demonstration of basic features. *PloS One*, 14(7):e0219854, 2019.

[199] Thong Phi Nguyen, Ji Won Jung, Yong Jin Yoo, Sung Hoon Choi, and Jonghun Yoon. Intelligent evaluation of global spinal alignment by a decentralized convolutional neural network. *Journal of Digital Imaging*, 35(2):213–225, 2022.

[200] Alba Vila-Casademunt, Ferran Pellisé, Emre Acaroglu, Francisco Javier Sánchez Pérez-Grueso, Mar Pérez Martín-Buitrago, Tunay Sanli, Sule Yakici, Ana García de Frutos, Antonia Matamalas, José Miguel Sánchez-Márquez, et al. The reliability of sagittal pelvic parameters: the effect of lumbosacral instrumentation and measurement experience. *Spine*, 40(4):E253–E258, 2015.

[201] Cédric Barrey, Jéroˆme Jund, Olivier Noseda, and Pierre Roussouly. Sagittal balance of the pelvis-spine complex and lumbar degenerative diseases. a comparative study about 85 cases. *European Spine Journal*, 16(9):1459–1467, 2007.

[202] Fabio Mancino, Giorgio Cacciola, Vincenzo Di Matteo, Andrea Perna, Luca Proietti, Alexander Greenberg, Michael-Alexander Malahias, Peter K Sculco, Giulio Maccauro, and Ivan De Martino. Surgical implications of the hip-spine relationship in total hip arthroplasty. *Orthopedic Reviews*, 12(Suppl 1), 2020.

[203] Nathanael Heckmann, Braden McKnight, Michael Stefl, Nicholas A Trasolini, Hiroyuki Ike, and Lawrence D Dorr. Late dislocation following total hip arthroplasty: spinopelvic imbalance as a causative factor. *Journal of Bone and Joint Surgery*, 100(21):1845–1853, 2018.

[204] Frédéric Cornaz, Jonas Widmer, Nadja A Farshad-Amacker, José Miguel Spirig, Jess G Snedeker, and Mazda Farshad. Intervertebral disc degeneration relates to biomechanical changes of spinal ligaments. *The Spine Journal*, 21(8):1399–1407, 2021.

[205] Ron Alkalay. The material and mechanical properties of the healthy and degenerated intervertebral disc. *Integrated biomaterials science*, pages 403–424, 2002.

[206] Matilde Tomasi, Alessio Artoni, Lorenza Mattei, and Francesca Di Puccio. On the estimation of hip joint loads through musculoskeletal modeling. *Biomechanics and Modeling in Mechanobiology*, pages 1–22, 2022.

[207] Miranda C Boonstra, B Wim Schreurs, and Nico Verdonschot. The sit-to-stand movement: differences in performance between patients after primary total hip arthroplasty and revision total hip arthroplasty with acetabular bone impaction grafting. *Physical Therapy*, 91(4):547–554, 2011.

[208] Erfanul Saker and R Shane Tubbs. Anatomy of the lumbar intervertebral discs. *Anatomy of the Lumbar Intervertebral Discs*, pages Chapter 1, Section 1, 10–13, Wheeless, 1992.

[209] Frank A Pintar, Narayan Yoganandan, Thomas Myers, Ali Elhagediab, and Anthony Sances Jr. Biomechanical properties of human lumbar spine ligaments. *Journal of Biomechanics*, 25(11):1351–1356, 1992.

[210] AAASS Shirazi-Adl, Abdul M Ahmed, and Suresh C Shrivastava. Mechanical response of a lumbar motion segment in axial torque alone and combined with compression. *Spine*, 11(9):914–927, 1986.

[211] Nicolas Damm, Robert Rockenfeller, and Karin Gruber. Lumbar spinal ligament characteristics extracted from stepwise reduction experiments allow for preciser modeling than literature data. *Biomechanics and Modeling in Mechanobiology*, 19(3):893–910, 2020.

[212] Falk Mörl, Michael Günther, Julia M Riede, Maria Hammer, and Syn Schmitt. Loads distributed in vivo among vertebrae, muscles, spinal ligaments, and intervertebral discs in a passively flexed lumbar spine. *Biomechanics and Modeling in Mechanobiology*, 19:2015–2047, 2020.

[213] Athena Jalalian, Francis EH Tay, Soheil Arastehfar, and Gabriel Liu. A patient-specific multibody kinematic model for representation of the scoliotic spine movement in frontal plane of the human body. *Multibody System Dynamics*, 39:197–220, 2017.

[214] Frank Heuer, Hendrik Schmidt, Zdenek Klezl, Lutz Claes, and Hans-Joachim Wilke. Stepwise reduction of functional spinal structures increase range of motion and change lordosis angle. *Journal of Biomechanics*, 40(2):271–280, 2007.

[215] Pier Paolo Valentini and Ettore Pennestrì. An improved three-dimensional multibody model of the human spine for vibrational investigations. *Multibody System Dynamics*, 36:363–375, 2016.

[216] Miguel Christophy, Maurice Curtin, Nur Adila Faruk Senan, Jeffrey C Lotz, and Oliver M O'Reilly. On the modeling of the intervertebral joint in multibody models for the spine. *Multibody System Dynamics*, 30:413–432, 2013.

[217] Ge Wu, Sorin Siegler, Paul Allard, Chris Kirtley, Alberto Leardini, Dieter Rosenbaum, Mike Whittle, Darryl D'Lima, Luca Cristofolini, Hartmut Witte, et al. Isb recommendation on definitions of joint coordinate system of various joints for the reporting of human joint motion—part i: ankle, hip, and spine. *Journal of Biomechanics*, 35(4):543–548, 2002.

[218] David J Pearsall, J Gavin Reid, and Lori A Livingston. Segmental inertial parameters of the human trunk as determined from computed tomography. *Annals of Biomedical Engineering*, 24(2):198–210, 1996.

[219] Gongbing Shan and Christiane Bohn. Anthropometrical data and coefficients of regression related to gender and race. *Applied Ergonomics*, 34(4):327–337, 2003.

[220] Albert H Vette, Takashi Yoshida, T Adam Thrasher, Kei Masani, and Milos R Popovic. A complete, non-lumped, and verifiable set of upper body segment parameters for three-dimensional dynamic modeling. *Medical Engineering & Physics*, 33(1):70–79, 2011.

[221] Matthew Kelly. An introduction to trajectory optimization: How to do your own direct collocation. *SIAM Review*, 59(4):849–904, 2017.

[222] Henryk Tkaczuk. Tensile properties of human lumbar longitudinal ligaments. *Acta Orthopaedica Scandinavica*, 39(sup115):1–69, 1968.

[223] James W Day, Gary L Smidt, and Thomas Lehmann. Effect of pelvic tilt on standing posture. *Physical Therapy*, 64(4):510–516, 1984.

[224] Richard Gajdosik, Ralph Simpson, Richard Smith, and Richard L DonTigny. Pelvic tilt: intratester reliability of measuring the standing position and range of motion. *Physical therapy*, 65(2):169–174, 1985.

[225] Thom E Snijders, Tom PC Schlösser, Nathanael D Heckmann, Taro Tezuka, Rene M Castelein, Rob P Stevenson, Harry Weinans, Arthur de Gast, and Lawrence D Dorr. The effect of functional pelvic tilt on the three-dimensional acetabular cup orientation in total hip arthroplasty dislocations. *The Journal of Arthroplasty*, 36(6):2184–2188, 2021.

[226] Manabu Tsukamoto, Makoto Kawasaki, Hitoshi Suzuki, Teruaki Fujitani, and Akinori Sakai. Proposal of accurate cup placement procedure during total hip arthroplasty based on pelvic tilt discrepancies in the lateral position. *Scientific Reports*, 11(1):13870, 2021.

[227] Guoyue Yang, Yayue Li, and Hong Zhang. The influence of pelvic tilt on the anteversion angle of the acetabular prosthesis. *Orthopaedic surgery*, 11(5):762–769, 2019.

[228] Juliana Hsu, Matias de la Fuente, and Klaus Radermacher. Calculation of impingement-free combined cup and stem alignments based on the patient-specific pelvic tilt. *Journal of Biomechanics*, 82:193–203, 2019.

[229] Behzad Danaei and John McPhee. Model-based acetabular cup orientation optimization based on minimizing the risk of edge-loading and implant impingement following total hip arthroplasty. *Journal of Biomechanical Engineering*, 144(11):111008, 2022.

[230] Darryl D D'Lima et al. Standard for hip joint coordinate system recommendations from the isb standardization committee. *Jul*, 17:1–8, 2000.

[231] Lawrence D Dorr, Aamer Malik, Zhinian Wan, William T Long, and Michael Harris. Precision and bias of imageless computer navigation and surgeon estimates for acetabular component position. *Clinical Orthopaedics and Related Research®*, 465:92–99, 2007.

[232] Hans-Joachim Wilke, Hendrik Schmidt, Karin Werner, Werner Schmölz, and Jörg Drumm. Biomechanical evaluation of a new total posterior-element replacement system. *Spine*, 31(24):2790–2796, 2006.

[233] K-H Widmer and B Zurfluh. Compliant positioning of total hip components for optimal range of motion. *Journal of orthopaedic research*, 22(4):815–821, 2004.

[234] Nuno Miguel Barroso Monteiro, Miguel Pedro Tavares da Silva, João Orlando Marques Gameiro Folgado, and João Pedro Levy Melancia. Structural analysis of the intervertebral discs adjacent to an interbody fusion using multibody dynamics and finite element cosimulation. *Multibody System Dynamics*, 25:245–270, 2011.

[235] Donald D Harrison, Tad J Janik, Stephan J Troyanovich, Deed E Harrison, and Christopher J Colloca. Evaluation of the assumptions used to derive an

ideal normal cervical spine model. *Journal of manipulative and physiological therapeutics*, 20(4):246–256, 1997.

[236] Paul W Hodges, AE Martin Eriksson, Debra Shirley, and Simon C Gandevia. Intra-abdominal pressure increases stiffness of the lumbar spine. *Journal of Biomechanics*, 38(9):1873–1880, 2005.

[237] Masoud Malakoutian, John Street, Hans-Joachim Wilke, Ian Stavness, Sidney Fels, and Thomas Oxland. A musculoskeletal model of the lumbar spine using artisynth–development and validation. *Computer Methods in Biomechanics and Biomedical Engineering: Imaging & Visualization*, 6(5):483–490, 2018.

[238] Jeannie F Bailey, Robert P Matthew, Sarah Seko, Patrick Curran, Leslie Chu, Sigurd H Berven, Vedat Deviren, Shane Burch, and Jeffrey C Lotz. Issls prize in bioengineering science 2019: biomechanical changes in dynamic sagittal balance and lower limb compensatory strategies following realignment surgery in adult spinal deformity patients. *European Spine Journal*, 28(5):905–913, 2019.

[239] Robert Peter Matthew, Sarah Seko, Jeannie Bailey, Ruzena Bajcsy, and Jeffrey Lotz. Estimating sit-to-stand dynamics using a single depth camera. *IEEE journal of biomedical and health informatics*, 23(6):2592–2602, 2019.

[240] James Marshall Morris, Donald Brooks Lucas, and Boris Bresler. Role of the trunk in stability of the spine. *Journal of Bone and Joint Surgery*, 43(3):327–351, 1961.

[241] Karl Daggfeldt and Alf Thorstensson. The mechanics of back-extensor torque production about the lumbar spine. *Journal of Biomechanics*, 36(6):815–825, 2003.

[242] Alexander L Bell, Douglas R Pedersen, and Richard A Brand. A comparison of the accuracy of several hip center location prediction methods. *Journal of Biomechanics*, 23(6):617–621, 1990.

[243] Marco Senteler, Bernhard Weisse, Dominique A Rothenfluh, and Jess G Snedeker. Intervertebral reaction force prediction using an enhanced assembly of opensim models. *Computer methods in biomechanics and biomedical engineering*, 19(5):538–548, 2016.

[244] Marco A Marra, Valentine Vanheule, René Fluit, Bart HFJM Koopman, John Rasmussen, Nico Verdonschot, and Michael S Andersen. A subject-specific musculoskeletal modeling framework to predict in vivo mechanics of total knee arthroplasty. *Journal of biomechanical engineering*, 137(2), 2015.

[245] Mariska Wesseling, Friedl De Groote, Christophe Meyer, Kristoff Corten, Jean-Pierre Simon, Kaat Desloovere, and Ilse Jonkers. Subject-specific musculoskeletal modelling in patients before and after total hip arthroplasty. *Computer methods in biomechanics and biomedical engineering*, 19(15):1683–1691, 2016.

[246] James Pierrepont, G Hawdon, BP Miles, B O' Connor, J Baré, LR Walter, E Marel, M Solomon, S McMahon, and AJ Shimmin. Variation in functional pelvic tilt in patients undergoing total hip arthroplasty. *The Bone & Joint Journal*, 99(2):184–191, 2017.

[247] Andrew Stephens, Selin Munir, Siddarth Shah, and William Lindsay Walter. The kinematic relationship between sitting and standing posture and pelvic inclination and its significance to cup positioning in total hip arthroplasty. *International orthopaedics*, 39(3):383–388, 2015.

[248] Cheng Chen, Weiguo Xie, Jochen Franke, PA Grutzner, L-P Nolte, and Guoyan Zheng. Automatic x-ray landmark detection and shape segmentation via data-driven joint estimation of image displacements. *Medical image analysis*, 18(3):487–499, 2014.

[249] Christian Payer, Darko Štern, Horst Bischof, and Martin Urschler. Regressing heatmaps for multiple landmark localization using cnns. In *International Conference on Medical Image Computing and Computer-Assisted Intervention*, pages 230–238. Springer, 2016.

[250] John Rasmussen. The anybody modeling system. In *DHM and Posturography*, pages 85–96. Elsevier, 2019.

[251] James William Pierrepont, Catherine Zoe Stambouzou, Brad Peter Miles, Peter Bede O'Connor, Leonard Walter, Andrew Ellis, Rob Molnar, Jonathan Victor Baré, Michael Solomon, Stephen McMahon, et al. Patient specific component alignment in total hip arthroplasty. *Reconstructive Review*, 6(4), 2016.

[252] Anson Maitland. Nonlinear model predictive control reduction strategies for real-time optimal control. *University of Waterloo*, 2019.

[253] Matthew Millard, Anna Lena Emonds, Monika Harant, and Katja Mombaur. A reduced muscle model and planar musculoskeletal model fit for the simulation of whole-body movements. *Journal of Biomechanics*, 89:11–20, 2019.

[254] Matthew J Weinstein and Anil V Rao. Algorithm 984: Adigator, a toolbox for the algorithmic differentiation of mathematical functions in matlab using source transformation via operator overloading. *ACM Transactions on Mathematical Software (TOMS)*, 44(2):1–25, 2017.

[255] Matthew Millard, Thomas Uchida, Ajay Seth, and Scott L Delp. Flexing computational muscle: modeling and simulation of musculotendon dynamics. *Journal of biomechanical engineering*, 135(2), 2013.

[256] Antonie J Van den Bogert, Thomas Geijtenbeek, Oshri Even-Zohar, Frans Steenbrink, and Elizabeth C Hardin. A real-time system for biomechanical analysis of human movement and muscle function. *Medical & biological engineering & computing*, 51(10):1069–1077, 2013.

[257] Michael Damsgaard, John Rasmussen, Søren Tørholm Christensen, Egidijus Surma, and Mark De Zee. Analysis of musculoskeletal systems in the anybody modeling system. *Simulation Modelling Practice and Theory*, 14(8):1100–1111, 2006.

[258] Yoshihiko Nakamura, Katsu Yamane, Yusuke Fujita, and Ichiro Suzuki. Somatosensory computation for man-machine interface from motion-capture data and musculoskeletal human model. *IEEE Transactions on Robotics*, 21(1):58–66, 2005.

[259] Jason P Halloran, Marko Ackermann, Ahmet Erdemir, and Antonie J Van den Bogert. Concurrent musculoskeletal dynamics and finite element analysis predicts altered gait patterns to reduce foot tissue loading. *Journal of Biomechanics*, 43(14):2810–2815, 2010.

[260] Anil V Rao. A survey of numerical methods for optimal control. *Advances in the Astronautical Sciences*, 135(1):497–528, 2009.

[261] Mohammad Sharif Shourijeh and John McPhee. Forward dynamic optimization of human gait simulations: a global parameterization approach. *Journal of Computational and Nonlinear Dynamics*, 9(3), 2014.

[262] Reza Sharif Razavian, Naser Mehrabi, and John McPhee. A model-based approach to predict muscle synergies using optimization: application to feedback control. *Frontiers in computational neuroscience*, 9:121, 2015.

[263] Thomas Zander, Marcel Dreischarf, Anne-Katrin Timm, Wolfgang W Baumann, and Hendrik Schmidt. Impact of material and morphological parameters on the mechanical response of the lumbar spine–a finite element sensitivity study. *Journal of Biomechanics*, 53:185–190, 2017.

[264] B Garner. A dynamic musculoskeletal computer model for rising from a squatting or sitting position. *MScEng. thesis, The University of Texas at Austin, Austin, TX*, 1992.

[265] Kristin Elizabeth Daigle. *The effect of muscle strength on the coordination of rising from a chair in minimum time: predictions of an optimal control model.* PhD thesis, University of Texas at Austin, 1994.

[266] Dong Chen, Chun-Hui Chen, Li Tang, Kai Wang, Yu-Zhe Li, Kevin Phan, and Ai-Min Wu. Three-dimensional reconstructions in spine and screw trajectory simulation on 3d digital images: a step by step approach by using mimics software. *Journal of Spine Surgery*, 3(4):650, 2017.

[267] Andrea d'Avella and Francesco Lacquaniti. Control of reaching movements by muscle synergy combinations. *Frontiers in computational neuroscience*, 7:42, 2013.

[268] Ivan Zammit-Maempel, Claire-Louise Chapple, and Paula Leslie. Radiation dose in videofluoroscopic swallow studies. *Dysphagia*, 22(1):13–15, 2007.

[269] AAPM White. Clinical biomechanics of the spine. *Clinical Biomechanics of the Spine*, 1990.

[270] M. Broy. Software engineering—from auxiliary to key technologies. In M. Broy and E. Denert, editors, *Software Pioneers*, pages 10–13. Springer, New York, 1992.

[271] Christina I Esposito, Theodore T Miller, Joseph D Lipman, Kaitlin M Carroll, Douglas E Padgett, David J Mayman, and Seth A Jerabek. Biplanar low-dose radiography is accurate for measuring combined anteversion after total hip arthroplasty. *The Musculoskeletal Journal of Hospital for Special Surgery®*, 16(1):23–29, 2020.

[272] Li Cao, Farshid Guilak, and Lori A Setton. Three-dimensional finite element modeling of pericellular matrix and cell mechanics in the nucleus pulposus of the intervertebral disk based on in situ morphology. *Biomechanics and Modeling in Mechanobiology*, 10:1–10, 2011.

[273] Nan Meng, Jason PY Cheung, Kwan-Yee K Wong, Socrates Dokos, Sofia Li, Richard W Choy, Samuel To, Ricardo J Li, and Teng Zhang. An artificial intelligence powered platform for auto-analyses of spine alignment irrespective of image quality with prospective validation. *EClinicalMedicine*, 43, 2022.

[274] Eskil Jörgensen, Christopher Zach, and Fredrik Kahl. Monocular 3d object detection and box fitting trained end-to-end using intersection-over-union loss. *ArXiv*, abs/1906.08070, 2019.

[275] Zengyi Qin, Jinglu Wang, and Yan Lu. Monogrnet: A general framework for monocular 3d object detection. *IEEE Transactions on Pattern Analysis and Machine Intelligence*, 44, 2022.

[276] Patrick D Roberts and Gin McCollum. Dynamics of the sit-to-stand movement. *Biological cybernetics*, 74(2):147–157, 1996.

[277] Kyle D Huffman, Brooke A Sanford, Audrey R Zucker-Levin, John L Williams, and William M Mihalko. Increased hip abduction in high body mass index subjects during sit-to-stand. *Gait & posture*, 41(2):640–645, 2015.

[278] Hooshang Hemami and Vijay C Jaswa. On a three-link model of the dynamics of standing up and sitting down. *IEEE Transactions on Systems, Man, and Cybernetics*, 8(2):115–120, 1978.

[279] Asif Mughal and Kamran Iqbal. 3d bipedal model with holonomic constraints for the decoupled optimal controller design of the biomechanical sit-to-stand maneuver. *International Design Engineering Technical Conferences and Computers and Information in Engineering Conference*, 2010.

[280] Burak Ozsoy and James Yang. Simulation-based unassisted sit-to-stand motion prediction for healthy young individuals. *International Design Engineering Technical Conferences and Computers and Information in Engineering Conference*, 46391:V006T10A001, 2014.

[281] Hiroshi R Yamasaki, Hiroyuki Kambara, and Yasuharu Koike. Dynamic optimization of the sit-to-stand movement. *Journal of applied biomechanics*, 27(4):306–313, 2011.

[282] Shunsaku Nishihara, Nobuhiko Sugano, Takashi Nishii, Kenji Ohzono, and Hideki Yoshikawa. Measurements of pelvic flexion angle using three-dimensional computed tomography. *Clinical Orthopaedics and Related Research®*, 411:140–151, 2003.

[283] Alma B Pedersen, Søren P Johnsen, Søren Overgaard, Kjeld Søballe, Henrik T Sørensen, and Ulf Lucht. Total hip arthroplasty in denmark: incidence of primary operations and revisions during 1996–2002 and estimated future demands. *Acta Orthopaedica*, 76(2):182–189, 2005.

[284] Jacob M Elkins, Megan K O'Brien, Nicholas J Stroud, Douglas R Pedersen, John J Callaghan, and Thomas D Brown. Hard-on-hard total hip impingement causes extreme contact stress concentrations. *Clinical Orthopaedics and Related Research®*, 469:454–463, 2011.

APPENDICES

Appendix A

Motion Capture Experiment Data Processing

A.1 Calibration

Two major steps are required for the calibration of the setup. The first step is the system calibration and the second step is for subject calibration. The system calibration starts with the swinging of a calibration tool that has some labels to identify the environment. During this step, the person who is doing the swing should be cautious not to be in front of the cameras. This process should be done in all volume space in which the activities would take place. After that, the global coordinate system should be specified. For this purpose, an origin is considered and the direction of positive x and positive z have been determined by a probe.

After the calibration of the system, subject calibration is essential. Two criteria are important for landmarks on the body. The attachment area should target bony

surfaces rather than soft tissue and be in the most visible location according to the camera locations. To digitize anatomical landmarks, after getting permission from the subject to touch, the appropriate position on the body could be determined with a palpate procedure. For this purpose, markers were placed on the shank, thigh, pelvis, spine, and head. For the shank, markers were attached to the medial-lateral tibial condyle and medial-lateral malleus. The markers for the thigh were attached to the medial-lateral femoral condyle. Four markers were attached to the pelvis on the right and left anterior superior iliac spine (ASIS) and posterior superior iliac spine (PSIS). Eight markers were used for the spine. In the lumbar part, 5 markers were used where two markers are placed on L3 and L1 and one placed on L5. Two markers on the thoracic part were considered on the T6 and 1 marker for the cervical part which is placed on the C7. Four markers were used to evaluate the head position and orientation.

The position of each marker will be available after the experiment is completed. Due to noise and missing data, it is necessary to process the data before kinematic calculation. This process has been done with data filling and a low-pass frequency filtering. Because of dynamic experiment tasks, the cut-off frequency is set for 5Hz. The noise could be because of the motion type and sampling rate which is used for this experiment. These could have effects on the results according to derivative calculation in the optimization for the calculation of the velocity and acceleration of joints. The reason for missing data is mostly because of missed markers by the cameras, which is a problem when calculating the joint coordinate system for joint angles. This problem could be solved by using an interpolation as a spline between two missing points.

A.2 Standard Coordinate Systems

To calculate joint angles, it is needed to define local coordinate systems in each segment. The Standardization and Terminology Committee (STC) of the International Society of Biomechanics (ISB) proposed a general reporting standard for joint kinematics based on the Joint Coordinate System (JCS). The joint angle calculations here are based on the standard defined by the ISB [217].

A.2.1 Local Coordinate System Equations

Local coordinate system for the shank

There are two ways for describing the local coordinate system of the shank. One could be placed on the tibia-fibula and the other way is defined on the tibia, and we used the second definition. The z-axis is defined from the center of medial and lateral tibia condyle (ITC) to the lateral tibia condyle (LTC). The x-axis could be defined as the cross product of two vectors which are from the (ITC) to the medial (MM_{sh}) and lateral malleolus (LM_{sh}). The y-axis would be perpendicular to those as cross products of these two vectors. The unit vectors for each coordinate system were calculated:

$$\hat{k} = \frac{LTC - ITC}{\|(LTC - ITC)\|} \tag{A.1}$$

$$\hat{i} = \frac{(ITC - LM_{sh}) \times (ITC - MM_{sh})}{\|(ITC - LM_{sh}) \times (ITC - MM_{sh})\|} \tag{A.2}$$

$$\hat{j} = \hat{k} \times \hat{i} \tag{A.3}$$

Local coordinate system for the thigh

For the local coordinate system of the thigh, the y-axis is defined from the mid-point of medial and lateral femoral condyle (IFC) to the hip joint center (O_{hip}). The x-axis is defined as a cross product of two vectors, one from the lateral (LFC) to the medial femoral condyle (MFC) and the other is the y-axis. The z-axis could be calculated by cross product of these two vectors. The unit vectors for each coordinate system have been calculated. The hip joint center is calculated based on the method introduced by Bell [242].

$$\hat{j} = \frac{O_{hip} - IFC}{\|(O_{hip} - IFC)\|} \tag{A.4}$$

$$\hat{i} = \left(\hat{j}\right) \times (MFC - LFC\ )/\| \left(\hat{j}\right) \times (MFC - LFC\ )\| \tag{A.5}$$

$$\hat{k} = \hat{i} \times \hat{j} \tag{A.6}$$

Local coordinate system for the pelvis

The z-axis is defined from the left anterior superior iliac spine ($LASIS$) to the right anterior superior iliac spine ($RASIS$). The x-axis is defined as a cross product of a vector to the z-axis. This vector is calculated with the cross product of two vectors from the mid-point of the right and left PSIS ($MPSIS$) to the right and left ASIS. The y-axis would be the cross product of those two. The unit vectors for each coordinate system have been calculated.

$$\hat{k} = \frac{RASIS - LASIS}{\|RASIS - LASIS\|} \tag{A.7}$$

$$\hat{i} = \frac{\left[((RASIS - MPSIS) \times (RASIS - MPSIS\ )) \times \hat{k}\right]}{\|((RASIS - MPSIS) \times (RASIS - MPSIS\ )) \times k\|} \tag{A.8}$$

$$\hat{j} = \hat{k} \times \hat{i} \tag{A.9}$$

Local coordinate system for the spine

In the lumbar part of the spine, the y-axis is defined along each segment. The x-axis is defined using the cross product of two temporary vectors from the base point of each segment to the upper left and right marker. For example, for the L5-L3 segment.

$$\hat{j} = \frac{L3 - L5}{\|L3 - L5\|} \tag{A.10}$$

$$\hat{i} = \frac{[((L5 - L3_{left}) \times (L5 - L3_{right}))]}{\|((L5 - L3_{left}) \times (L5 - L3_{right})) \|} \tag{A.11}$$

$$\hat{k} = \hat{i} \times \hat{j} \tag{A.12}$$

A.2.2 Intersegmental Angles

To find intersegmental angles, inverse kinematics has been used. The rotational matrix with the Euler angles of Z,Y,X are defined as a function and for each adjacent segment by using the calculated local coordinate system for each segment:

$$R_b^g = R_x \times R_y \times R_z = \begin{bmatrix} C\beta C\gamma & C\beta S\gamma & -S\beta \\ S\alpha S\beta C\gamma - C\alpha S\gamma & S\alpha S\beta S\gamma C\beta C\gamma & S\alpha C\beta \\ C\alpha S\beta C\gamma S\alpha S\gamma & C\alpha S\beta S\gamma - S\alpha C\gamma & C\alpha C\beta \end{bmatrix} \tag{A.13}$$

Where:

$$C\alpha = cos(\alpha),\ S\alpha = sin(\alpha);$$

$$C\beta = cos(\beta),\ S\beta = sin(\beta);$$

$$C\gamma = cos(\gamma),\ S\gamma = sin(\gamma).$$

By putting this matrix equal to the direction cosine matrix, which contains the unit vectors of the two CSs, the intersegment angles can be calculated using the following equations:

$$R_b^g = \begin{bmatrix} c_{11} & c_{12} & c_{13} \\ c_{21} & c_{22} & c_{23} \\ c_{31} & c_{32} & c_{33} \end{bmatrix} \tag{A.14}$$

$$\beta = Atan2\left(-c_{13}, \pm\sqrt{{c_{11}}^2 + {c_{12}}^2}\right) \tag{A.15}$$

$$\alpha = Atan2\left(\frac{c_{23}}{cos\beta}, \frac{c_{33}}{cos\beta}\right) \tag{A.16}$$

$$\gamma = Atan2\left(\frac{c_{12}}{cos\beta}, \frac{c_{11}}{cos\beta}\right) \tag{A.17}$$